

Closed-Loop Feedback Control System for EXOhSPEC Development

Theses submitted in partial fulfilment for the degree

Msc Astrophysics With Advanced Research

by

Biswajit Jana

Student Id. - 21089205

Supervisor: Professor Hugh Jones,

2nd Supervisor: Professor William Martin

April, 2024

Declaration

I hereby declare that this research project, conducted at the Optics Labs of the University of Hertfordshire, was carried out under the guidance of Professor Hugh Jones and Professor William Martin. The thesis contains original work, and no part of it has been previously submitted for any other degree or diploma. While I acknowledge collaborative contributions, the experimental work is predominantly my own. Proper acknowledgements and references have been provided for all supporting literature and resources. The collected data remains confidential unless specifically requested to my supervisors. Furthermore, in accordance with copyright law, any use of information or quotations from this dissertation requires proper acknowledgment, and substantial extracts cannot be published without my written consent.

Biswajit Jana
26th April, 2024

Acknowledgements

I deeply appreciate the guidance and support provided by my first supervisor, Professor Hugh Jones. His unwavering commitment and encouragement have been a beacon of light throughout my academic journey. Our routine interactions via email and regular weekly meetings have been a source of motivation, helping me navigate through challenges. His profound knowledge and constructive feedback have played a pivotal role in molding my project and refining my academic prowess.

For my second supervisor, Professor William Martin, I hold immense gratitude. His persistent support, critical insights, and the countless hours we spent in the lab working with lasers and adjusting interferometers have been a source of inspiration. His affable nature and positive attitude have always pushed me to extend the boundaries of my project. His practical approach to teaching optics, especially during the alignment on the steel rail, has been an enriching learning experience.

I am also indebted to Thomas Wocial, who was instrumental during the initial stages of the project. His technical prowess and meticulous attention to detail accelerated the progress of the project. We had countless discussions, spent hours coding, and together we explored and overcame many technical challenges. Our goal was specific, but we ventured into many other areas, finding solutions to problems and enhancing the technical aspect of the project.

This thesis, I hope, will serve as a guide for those who will carry this project forward. The thorough system evolution documented here will save time and allow future researchers to focus on other objectives in building the spectrograph. It's crucial to consider these aspects as part of experimental projects, as they involve dealing with real-world practical problems. Lastly, I would like to express my deepest gratitude to my parents. Their unwavering love, constant encouragement, and endless support have been my driving force. Their faith in me and their belief in my abilities has been the backbone of my academic success. This thesis would not have been possible without them. And yes, Mom and Dad, I've finally completed this step, few more milestones to go. Your belief in me has made this journey worthwhile.

To all of you, I am forever grateful. Thank you.

- Biswajit Jana

Abstract

This master's thesis introduces a novel approach to high-resolution radial velocity spectroscopy, a critical tool in the quest for habitable Earth-like exoplanets. The research tackles challenges in instrument stability and wavelength calibration by proposing a closed-loop feedback control system as an alternative to traditional vacuum environments. The study zeroes in on environmental stability, with a particular emphasis on the refractive index of air as a tool for calibration and its role in correcting optical path length variations. The research found a direct proportionality between temperature, pressure, humidity, and the change in optical path length. Notably, a 1hpa change in pressure results in a $0.4\mu\text{m}$ change, and a 1-degree Celsius change results in a $6\mu\text{m}$ change. These values can be implemented as feedback parameters in the control system to stabilize the Optical Path Length (OPL) using the laser interferometer upto pm precision. The study also conducted diagnostic tests on individual components used in the project development, providing valuable insights for future improvements. Despite some limitations, the research paves the way for future advancements in spectroscopic measurements. By addressing these limitations and pursuing enhancements, we can further improve the accuracy, stability, and adaptability of these measurements, ultimately contributing to our understanding of the universe and the search for habitable exoplanets.

Keywords: Radial Velocity Spectrograph, IDS, Control System

Contents

Acknowledgments.....	4
Abstract.....	5
Contents.....	6
List of Figures.....	8
List of Tables.....	11
1. Introduction	
1.1. State of Art: High-Resolution RV Spectrograph	12
1.2. Importance of Environmental Stability	14
1.3. Need for Closed Loop Feedback Control System.....	15
1.4. Refractive Index of Air.....	16
2. System Overview	
2.1. Introduction to EXOhSPEC.....	18
2.2. Active Components Used for Close Loop Feedback Control.....	20
2.2.1. Interferometric Displacement Sensor (IDS3010)	20
2.2.2. Environmental Sensor: BME680 & ECU.....	27
2.2.3. Temperature Sensor (PT-104)	32
2.3. Environmental Control Boxes: Box1 and Box2.....	33
2.3.1 Box1: Small Temperature Control Box Housing Spectrograph.....	35
2.3.2 Box2: Modified Protective Temperature Control Box.....	37
2.3.3 Thermal Expansion and Contraction.....	43
3. Methodology	
3.1. Control System.....	45
3.2. Air Refraction Compensation.....	48
4. Experimental Data Analysis, Results and Discussion.....	49
5. Conclusion and Future Work	
5.1 Summary of Findings.....	60
5.2 Limitations and Areas for Improvement.....	61
5.3 Future Developments and Enhancements.....	61
Bibliography	
Appendix	
A. Arduino Code: Collecting data from BME680.....	64
B. Code: Implementation Details and Source Code.....	66
C. Experiment IDS 3010+BME680	66
D. Web Development.....	70

Acronyms

HPRV = High Precision Radial Velocity Spectrograph

HARPS = High Accuracy Radial Velocity Planet Searcher

IDS = Interferometric Displacement Sensor

CARMENES = Calar Alto high-Resolution search for M-Dwarfs with Exo-Earths with a Mear-Infrared Echelle Spectrograph.

ESPRESSO = Echelle Spectrograph for Rocky Exoplanets and Stable Spectroscopic Observations

ANDES = Echelle Spectrograph for Rocky Exoplanets and Stable Spectroscopic Observations

ECU = Environmental Compensation Unit

GPL = Geometric Optical Path Length

OPL = Optical Path Length

LASER = Light Amplification By Stimulated Emission Of Radiation

PID = Proportional Integral Derivative control

List of Figures

Fig. 1.1: (Left) Mass-period distribution of detected exoplanets with the corresponding detection method. (Right) No. of detected exoplanets per year. Credit: NASA Exoplanet Archive.....	10
Fig. 1.2 Diagram illustrating habitable zones within a temperature vs. orbital period plot. Highlighted is the critical swath indicating potential for planetary growth, with accessibility to HARPS instruments for further study. Image Credit: Chester Harman Planets, NASA/jpl/arizona/UPR at Arecibo.....	12
Fig. 2.1: Internal structure of the Modified EXOhSPEC along with IDS and BME680 integrated, kept inside Box1 on a carbon fibre breadboard.....	16
Fig. 2.2: First Calibration and Tuning of ExohSpec result shows Thorium Argon spectrum. The bright features at near infrared shows argon emissions. Caveat: Not tuned, as the pixels in the far-infrared shows elongated.....	17
Fig. 2.3: Illustration explaining constructive and destructive interference based on the amplitude of two waves.....	18
Fig. 2.4: Working principle of Laser Interferometer.....	19
Fig. 2.5: Experimental setup showing IDS location outside Box2 : (a) IDS3010, (b) Sensor head selection and alignment simplified with advanced mounting kits, (c) Optical items: retroreflector.....	20
Fig. 2.6: Change in optical path from IDS vs time, (b)Temperature, Pressure and Humidity vs Time. Clearly, shows pressure is correlated with change in optical path, hence a dominant term. However, notably also shows temperature dominance in path length change. Humidity decreases alongside pressure drops following Ideal Gas Law.....	21
Fig. 2.7: Close-up view of internal setup for robustness test, displaying thickness variations of slip 1 and slip 2 in the optical path, where slip1 is about 0.12mm – 0.16mm and slip2 is micrometer thickness....	23
Fig. 2.8: Plot displaying change in optical path with time, revealing altered self-interferometry properties due to glass slip 1 manipulation.....	23
Fig. 2.9: Plot depicting change in optical path length over time, highlighting calibration issues related to self-interferometry properties. I denotes when the slip was inserted and R denotes when the slip was removed from the optical path.....	24
Fig. 2.10: ECU and BME680 size comparison.....	25
Fig. 2.11: (a) Circuit Design of Nodemcu ESP8266 and BME680 sensor, (b) Temperature vs. Time, demonstrating resistivity-induced temperature increase with oversampling.....	26
Fig. 2.12: Plot showing correlation between ECU and BME, with a temperature difference of approximately 1.97 °C, humidity about 5% and Pressure curve of about 1.6hPa, which states about there precision and accuracy.....	28

Fig. 2.13: Plot of ECU and BME680 refractive indices over time, revealing a close relationship.....	29
Fig. 2.14: Regression analysis of refractive indices for BME and ECU sensors, displaying error bars indicating value discrepancies.....	29
Fig. 2.15: Plot of Geometrical Path Length over time, zoomed out plot showcasing a sinusoidal curve due to air conditioning effects.....	30
Fig. 2.16: Peltier-104 Temperature Sensor connected with a probe to computer. The temperature variation over time is observed using Pico Log Software.....	31
Fig. 2.17: PID loop Temperature vs. Time plot, highlighting temperature oscillation with too small P value.....	32
Fig. 2.18: PID loop Temperature vs. Time plot, demonstrating long-period oscillation with short I value.....	32
Fig. 2.19: PID loop Temperature vs. Time plot, demonstrating long-period oscillation large D value.....	32
Fig. 2.20: Side View of Box1 housing the spectrograph on a carbon fiber breadboard, depicting potential air leakage. Hence need for Box2.....	33
Fig. 2.21: Side View of Box2, a modified protective box focusing on temperature control.....	33
Fig. 2.22: Temperature characteristics of Box 1, revealing variations with stable internal components but fluctuating room temperatures.....	34
Fig. 2.23: Shows the setup in which IDS will be placed on the steel railing and the temperature sensors position in the box2, at centre placed the PT104, to conduct an experiment to study the temperature and improving the PID control loop.....	35
Fig. 2.24: Temperature data over 2 weeks from 4 probes, indicating stability with new PID values and room temperature variations.....	36
Fig. 2.25: Histograms depicting data distribution, crucial for understanding temperature variations....	37
Fig. 2.26: Shows the combined variation in data in form of histograms.....	38
Fig. 2.27: Region of focus: Region 1 and Region 2, to study system behavior during initial and final phases.....	38
Fig. 2.28: Region 1 analysis shows that approx 30 -60 h, the inside of the box maintained a constant temperature regardless of outside spike in room temperature of 2 degree celsius, this proves the temperature control system working well.....	39

Fig. 2.29: Region 2 shows at about 180 - 230 hrs, the temperature variation in the system suggesting the top left is temperature controlled, the middle and middle end is not with a difference 0.3 degree celsius approx, further inspection reveals the phenomenon of convection taking place in the box.....	40
Fig. 2.30: Matrix representation of temperature region relationships.....	41
Fig. 2.31: Region 1 of the experiment, in order to determine the thermal expansion coefficient of the carbon fibre breadboard.....	42
Fig. 3.1: Flow chart of Singular control system.....	44
Fig. 3.2: Overview of the multi-layered control systems implemented in the project, emphasizing temperature stabilization, environmental isolation, and feedback mechanisms for maintaining optical path length stability.....	45
Fig. 3.3: Algorithm to extract the residual signal, which will be implemented as a feedback signal in the control system.....	46
Fig. 4.1: Plot of T, H, P profile over time, highlighting constant temperature and humidity despite atmospheric pressure changes.....	48
Fig. 4.2: Plot of Measured optical path length vs. time, showcasing its direct proportionality to pressure changes and noise reduction with moving average.....	48
Fig. 4.3: Plot of Uncompensated path length and compensated path length with respect to time in hours, a smooth function of window size = 100 been used as a low pass filter, the compensated path is a flat getting rid of T,H,P components.....	49
Fig. 4.4: Experiment conducted in Box1, plot is change in OPL and GPL with respect to house, lower panel is the residual signal, however the region of focus is region1 and region 2, suggests two different nature/ behaviour of the system.....	50
Fig. 4.5: Plot showing the the GPL using the empirical model, has compensated the pressure term.....	50
Fig. 4.6: Extracted T, H, P changes using reverse model, potential feedback signal for control system implementation.....	52
Fig. 4.7: Plot showing Pressure dominates when the temperature is kept constant.....	53
Fig. 4.8: Plot showing Humidity Dominates when the T and P is constant.....	53
Fig. 4.9: Plot showing temperature dominates when pressure is constant	54
Fig. 4.10: Plot showing pressure dominates when humidity is at 0% while the T and P are varying....	54
Fig. 4.11: Plot showing pressure dominates when humidity is at 50% while the T and P are varying, hence the Model is not appropriate for RH greater than 50%, the GPL increases.....	55

Fig. 4.12: In Region 2, spanning from the 20th to the 140th hour, minimal fluctuations in path length measurements reveal system stability. The upper panel shows Optical Path Length (OPL) variation of 4 micrometers, while the Geometric Path Length (GPL) remains under 2 micrometers. Pressure experienced nominal change (~30 hPa) with constant temperature (~20.5°C) and slight humidity fluctuation (~20%).....57

List of Tables

Table. 2.1: Comparison of accuracy between BME680 and ECU components.....	28
Table. 2.2: Table showing a comparison between BME and ECU sensor readings, highlighting the differences in temperature, humidity, and pressure measurements.....	29
Table. 2.3: Statistical analysis of mean, mode, and standard deviation in different regions of the box...38	

Chapter 1

Introduction

The journey of exoplanet discovery began in earnest in 1953, when radial velocities were compiled for over 15,000 stars (Wilson et. al 1953). The precision of these measurements was typically around 750 m/s. It was during this time that Otto Struve proposed the idea of high-precision radial velocity work for planet hunting. Struve suggested that Jupiter-like planets could be as close as 0.02 AU to their host stars and that these close-in, massive planets could be detected with the Doppler precision available in the 1950s. Fast forward to 1995, and the first Jupiter-mass companion to a solar-type star was detected by Michael Mayor and Didier Queloz. Struve's prediction had come true. Since then, we have detected over 5500 exoplanets using various methods, with the majority being discovered through transit methods. Radial velocity is a crucial concept in this field. It refers to the change in distance and speed of a star or other celestial body along the line of sight of the observer. It is a key parameter in the search for exoplanets, as it allows us to detect the tiny wobble of a star caused by the gravitational pull of an orbiting planet. The Radial Velocity method, unlike the Transit method, can detect exoplanets irrespective of orbital plane orientation and star brightness. It directly measures a planet's minimum mass and is effective in identifying multi-planet systems. However, it faces challenges like stellar activity and the need for high-precision spectrographs. In the following section, we will delve into the evolution of High Precision Radial Velocity (HPRV) spectrographs.

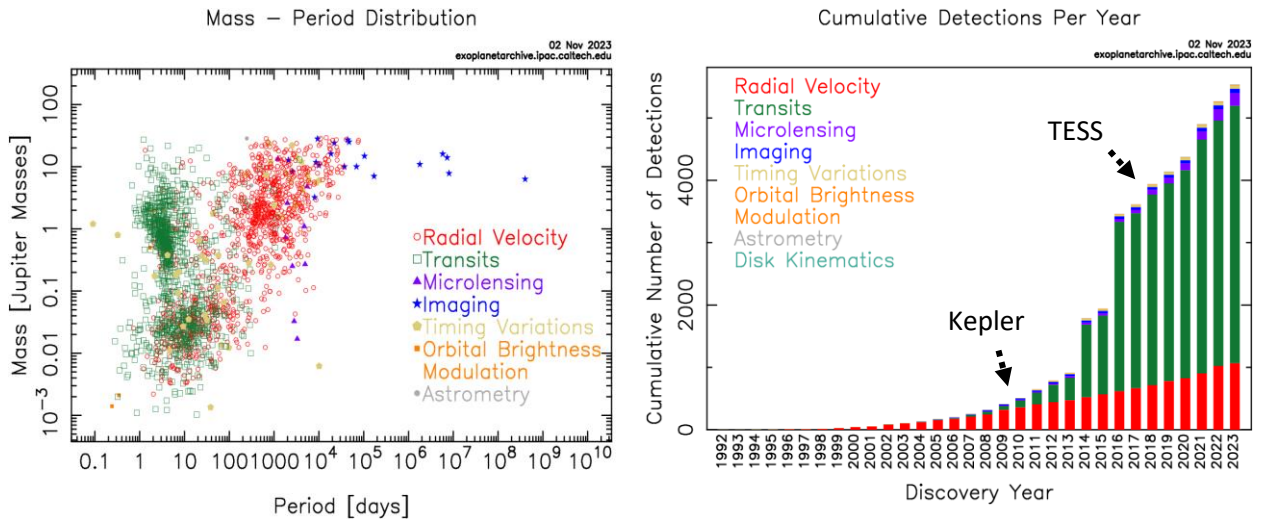


Fig 1.1: (Left) Mass-period distribution of detected exoplanets with the corresponding detection method.
(Right) No. of detected exoplanets per year. Credit: NASA Exoplanet Archive

1.1. State of Art: High-Resolution RV Spectrograph

Over the past two decades, there has been significant progress in the development of high-resolution spectrographs. The race to achieve unprecedented accuracy, with an ambitious goal of

CHAPTER 1: INTRODUCTION

approximately 10 cm/s, has been marked by intense competition. 10 cm/sec refers to a velocity of 10 centimeters per second. This measurement is typically achieved using spectrographs, which analyze the light emitted or absorbed by celestial objects. One significant reason for spectrographs worldwide aiming to achieve this precision is to detect Earth-like exoplanets around Sun-like stars. The radial velocity method relies on measuring the subtle Doppler shifts in a star's spectrum caused by the gravitational tug of an orbiting planet. For instance, the radial velocity of the Sun due to the gravitational influence of Earth is approximately 10 cm/sec. Detecting such minute variations in radial velocity requires highly precise spectrographs. Beyond exoplanet hunting, spectrographs have other applications. For example, the [Andes](#) Spectrograph project aims to observe the expansion of the universe. By analyzing the spectral lines of distant galaxies, researchers can measure their radial velocities and infer cosmic expansion rates. The Andes project plans to achieve a precision of 0.1 m/s over ten years, utilizing different wavelength calibrators and techniques to broaden its observational scope. This precision is crucial for accurately measuring the redshift of distant galaxies and understanding the dynamics of the cosmos. The quest for precision in radial velocity measurements has seen significant advancements since the early 2000s. Each instrument, while pushing the boundaries of precision and accuracy, has faced its unique set of challenges, particularly related to environmental stability.

The CHIRON spectrograph, designed in the early 2000s primarily to search for planets around Alpha Centauri A and B, demonstrated the advantage of a fiber-fed instrument and very high cadence Doppler observations. However, the survey suffered from increasing contamination as the separation of the two binary stars decreased, highlighting the challenge of maintaining precision in complex stellar environments. In 2003, the High Accuracy Radial velocity Planet Searcher (HARPS)(Mayor et al., 2003) marked a milestone in achieving extremely precise measurements of stellar radial velocities. HARPS, however, had to contend with the challenge of producing high fidelity spectra to reach higher precision. A near twin of HARPS, the vacuum-enclosed HARPS-N (Cosentino et al., 2012), was commissioned in 2012. It boasts temperature and pressure stabilization, a resolution of 115000, and a wavelength range from 383 to 693 nm. It was initially commissioned with thorium-argon simultaneous calibration, a method often used for wavelength calibration in spectroscopy. One of the challenges faced by HARPS-N was the accurate calibration of wavelengths, a critical factor in achieving precise measurements. Introduced in 2016, EXPRES (Jurgenson et al., 2016) utilizes advanced techniques to achieve unprecedented precision, capable of detecting Earth-size planets in the habitable zones of mid- to late-M dwarfs. The focus on M dwarfs, which are cooler and less massive than our Sun, due to their potential to host habitable exoplanets, presents its own set of challenges due to their inherent variability and magnetic activity. In 2018, the groundbreaking Echelle Spectrograph for Rocky Exoplanets and Stable Spectroscopic Observations (ESPRESSO) (Pepe et al., 2020) was introduced. Designed for Earth twin detection, ESPRESSO boasts a four-telescope feeding system and ultra-stabilized design. The challenge for ESPRESSO was maintaining stability with a thermally stabilized vacuum vessel at mK levels and low pressure, crucial for reliable and accurate radial velocity measurements. The 2020s saw the commissioning of NEID(Stefansson et al., 2020), an ultra-stabilized spectrograph designed to maintain stability with a thermally stabilized vacuum vessel at mK levels and low pressure. This design addresses the critical challenge of environmental stability, ensuring reliable and accurate radial velocity measurements. Moreover, Maroon X (Schwab et al., 2020), designed specifically for M dwarfs, aims to detect Earth-size planets in the habitable zones of mid- to late-M dwarfs. With unprecedented precision capable of achieving 1 m/s radial velocity precision, Maroon X operates in the 700-900 nm region for maximum radial velocity information. The

challenge for Maroon X lies in extracting precise radial velocity information from the near-infrared region where M dwarfs emit most of their light.

These advanced spectrographs push the boundaries of radial velocity precision and have diverse applications in exoplanet hunting. These advancements in radial velocity spectrographs have significantly contributed to our understanding of exoplanets and hold promise for future discoveries. However, they also underscore the importance of environmental stability in achieving precise measurements and the various challenges associated with it, such as temperature, pressure, wavelength calibration, detectors, signal-to-noise ratio, spectral resolution and sampling, analysis error, telluric contamination, extracting signals from noisy data, and astrophysical noise. In this project, our primary focus will be on environmental stability, a critical factor in the development and operation of these instruments.

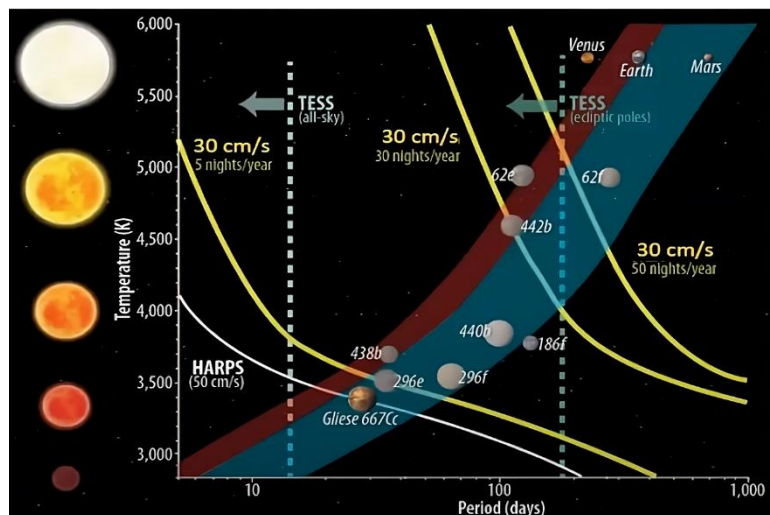


Fig 1.2 Diagram illustrating habitable zones within a temperature vs. orbital period plot. Highlighted is the critical swath indicating potential for planetary growth, with accessibility to HARPS instruments for further study. Image Credit: Chester Harman Planets, NASA/jpl/arizona/UPR at Arecibo.

1.2. Importance of Environmental Stability

Higher precision radial velocity measurements are crucial for discovering habitable worlds, confirming transit mission detections, and providing mass measurements for space-based missions such as the Transiting Exoplanet Survey Satellite (TESS) (Ricker et al., 2015). However, these instruments come with a high cost in terms of time and financial resources. Large spectrographs, such as HARPS (Mayor et al., 2003) and its equivalents like ESPRESSO (Pepe et al., 2020), ANDES (Marcantonio et al., 2022), etc, are typically housed in vacuum chambers.

A vacuum atmosphere is crucial for measuring gas rejection, as gas molecules can distort spectral observations. The absence of air in the vacuum ensures that the beam wavelength remains constant, reduces the impact of climate change on the spectrograph's performance, and prevents damage to the optical components through oxidation or contamination. However, vacuum chambers come with their own set of challenges. They have high manufacturing and maintenance costs, and their

complexity can hinder rapid development (Hernandez et al., 2024). Furthermore, the strict requirement for vacuum compatibility necessitates complex technology, making these spectrographs both complex and expensive such as for near infrared spectrograph, CARMENES, a strict temperature of -30 °C (Quirrenbach et al., 2014). Technological advances in precision radial velocity measurements have been centered around building stable instruments and improving the environmental control, detectors, and wavelength calibration (Lovis & Fischer, 2011).

Our project aims to provide an alternative. We are developing an environmental stable platform for our high-resolution radial velocity spectrograph, EXOhSpec (Jones et. al 2021). This approach provides a cost-effective solution that avoids the need for a vacuum chamber. Our design relies on environmental stability to overcome the challenges posed by expanding or contracting optical physical components due to environmental fluctuations. The main focus of our project is to develop a closed-loop feedback control system that uses IDS technology to compensate for environmental parameters such as temperature, pressure and humidity which been sensed by active sensors. Despite the seemingly minor effects of these variables, they can cause significant shifts in spectral monitoring accuracy.

1.3. Need for Closed Loop Feedback Control

As we have understood from the previous section, the three important factors that can affect the measurement of High-Resolution radial velocity (RV) Spectrographs are temperature, pressure, and humidity. We will delve deeper into these dependencies in the later chapters. However, for now, we know that these factors necessitate an alternative approach to the vacuum system, which is a closed-loop feedback control system.

A control feedback system, particularly a closed-loop feedback control system, is essential in the context of high-resolution spectrographs for several reasons:

- *Stability and Accuracy:* Environmental factors such as temperature, pressure, and humidity can cause variability in the optical path of a spectrograph, leading to inaccuracies in the spectral data. A closed-loop feedback control system can maintain a constant environment for the spectrograph, thereby enhancing the stability and accuracy of the measurements.
- *Real-time Adjustments:* The system contains active components such as sensors and actuators. The sensors monitor the environmental parameters and provide feedback to the control system. If any deviations from the desired conditions are detected, the control system activates the actuators to make necessary adjustments in real time. This ensures that the environmental conditions inside the spectrograph remain constant, regardless of external changes.
- *Cost-effectiveness and Reliability:* While vacuum systems are commonly used to achieve environmental stability, they are complex and expensive. A closed-loop feedback control system provides a cost-effective and reliable alternative. It contributes to the practicality of the system while ensuring high accuracy of the spectral data.

- *Flexibility:* Closed-loop systems are adaptable and can be fine-tuned based on the specific requirements of the application. This makes them suitable for a wide range of applications, including high-resolution spectrographs like EXOhSPEC.

In summary, the need for a closed-loop feedback control system in high-resolution spectrographs stems from its ability to maintain environmental stability, provide real-time adjustments, ensure cost-effectiveness and reliability, and offer flexibility for different applications. This is crucial for improving the stability of discrete measurements and enhancing the accuracy of high-resolution spectral data. Will be discussed in more detail in the follow-up chapters.

1.4. Refractive Index of Air

In our previous discussion, we highlighted the critical factors influencing high-resolution spectrographs, namely temperature, pressure, and humidity. These factors underscore the need for a closed-loop feedback control system to maintain stability and accuracy in spectral measurements. Expanding on this, we'll now delve into another crucial parameter: the refractive index of air. The refractive index of air plays a pivotal role in optical design and metrology, impacting various applications. Under standard conditions, in a vacuum, the refractive index of air is conventionally set to 1. However, in real-world scenarios characterized by atmospheric pressure, temperature, and humidity fluctuations, the refractive index deviates. This deviation becomes significant in our project due to our reliance on a geometric optical path length within the spectrograph. What exactly does this mean in the context of a spectrograph? Well, the geometric optical path length refers to the distance light travels within the instrument. It's a critical parameter for accurately capturing spectral data. Environmental factors like temperature, pressure, and humidity induce micro to picometer-level changes in this optical path. Consequently, the data output from the instrument represents an uncompensated path length. By modified empirical Edlen equation(Edlen 1966),

$$\text{Refractive Index, } \eta = 1 + 7.86 \times 10^{-4} \frac{P}{273.15+T} - 1.5 \times 10^{-11} RH(T^2 + 160)^1$$

where, T (0 to 35°C) is temperature, P (50kPa to 120 kPa) is pressure, H (0 to 100%) is relative humidity . Now using the values and plugging into the equation.

$$\begin{aligned}\eta_{\text{sa}} &= \eta_{\text{standard air}} = 1 + 7.86 \times 10^{-4} \frac{101.325}{273.15+T} - 1.5 \times 10^{-11} \times 50(20^2 + 160) \\ &= 1.00027139838\end{aligned}$$

To address this issue, our project requires meticulous calibration techniques to rectify these variations. Understanding the variations in the refractive index of air is paramount for ensuring the reliability and accuracy of our measurements. Moreover, in our setup, the refractive index serves as a fundamental tool for extracting feedback signals within the closed-loop control system.

In essence, considering the refractive index of air is essential for optimizing the performance of our high-resolution spectrograph. It allows us to account for environmental fluctuations and calibrate our measurements accurately, ultimately enhancing the precision and reliability of our spectral data.

¹ [NIST: Index of Refraction of Air](#)

CHAPTER 1: INTRODUCTION

The report documents the development of a closed feedback loop control system for the EXOhSPEC project. It is divided into several chapters, each focusing on different aspects of the work. In the first chapter, we studied the state of the art of radial velocity spectrographs and why environmental stability is important. In Chapter 2, we provide an overview of the system, look briefly at some of the principle components we are using for the development of EXOhSPEC, and discuss some of the preliminary results or system diagnostics as part of experimental results. In Chapter 3, we will learn about the methodology, discussing briefly how these different data have been collected, and will look into some of the algorithms that have been developed based on the requirement. In Chapter 4, we will look into some of the important experimental results and discuss in detail some of the important analyses and how good our system performance is. Finally, in Chapter 5, we will conclude and list some of the future work essential as a follow-up of the project. The EXOhSPEC project is a significant step towards advancing our understanding of exoplanets and their properties. By using a compact, low-cost, and efficient high-resolution spectrograph, state-of-the-art technology, and innovative techniques, this project has the potential to make unprecedented discoveries in astrophysics.

Chapter 2

System Overview

In this chapter, we will be discussing the EXOhSPEC. The system is designed with a focus on precision and control, employing a range of active components for close loop feedback control. These include the Interferometric Displacement Sensor (IDS3010), an Environmental Sensor such as BME680 by Bosch & Environmental Compensation Unit (ECU) by Attocube, and a Peltier based 4 channel Temperature Sensor (PT-104). The system also incorporates two environmental control boxes, Box1 and Box2, each with its unique function. Box1 is a small temperature control box that houses the spectrograph, while Box2 is a modified protective temperature control box. Through this chapter, we aim to provide a comprehensive overview of the system's components and their roles in ensuring optimal performance.

2.1. Introduction to EXOhSPEC

The **Exoplanet High-Resolution Spectrograph (EXOhSPEC)**, a project of the University of Hertfordshire, is a specialized instrument designed for the detailed study of exoplanet radial velocities. This instrument, depicted in Figure 2.1, is equipped with a suite of features that enhance its performance and functionality. Central to EXOhSPEC is the **IDS3010 Displacement Measuring Interferometer**, a key component that provides displacement measurements at the picometer level. Given the minimal number of optical components, an optical path is present. To measure this optical path length, an Interferometric Laser Displacement sensor is employed. The operation of this sensor will be elaborated in section 2.2.1.

The IDS is complemented by the integration of the **BME680** and **PT104** sensors for monitoring pressure, humidity, and temperature, respectively.

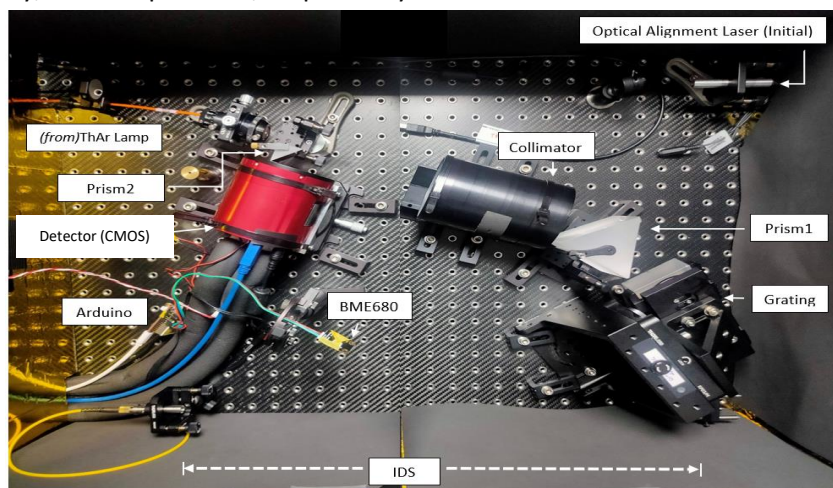


Fig. 2.1: Internal structure of the Modified EXOhSPEC along with IDS and BME680 integrated, kept inside Box1 on a carbon fibre breadboard.

CHAPTER 2: SYSTEM OVERVIEW

These components work in unison to ensure a comprehensive environmental monitoring system within the instrument. The spectrograph, with its resolution of $\geq 70,000$ (an estimated value based on previous calculations, the actual value will be known once the overall system is deployed), is a testament to the advancements in stability optimization. Its design is compact, cost-effective, and efficient, making it a valuable tool in the field of high-resolution spectrometry. Please note that the bifurcated fiber for simultaneous telescope and Thorium Argon input is not currently deployed in the system, which will be used as wavelength calibration. The operation of the spectrograph is as follows: The Thorium Argon lamp serves as the light source, with the emitted light being channeled through a multimode fiber. This fiber allows multiple light paths or modes to propagate, which can increase the amount of light delivered. The collimator, a device that narrows a beam of particles or waves, then directs this light to Prism 1, which disperses the light spectrum onto the grating. The collimator lens then focuses the dispersed light. Prism 2 subsequently focuses the spectrum onto the CMOS detector. The advantage of a CMOS detector is that it is generally more efficient and faster than other types of detectors, and it captures the spectral characteristics of the incoming light.

Preliminary Spectrograph Tuning Results:

In the initial phase of the project, the primary focus was on fine-tuning the optical components of the spectrograph to ensure optimal performance. This was crucial as it provided a fundamental understanding of the spectrograph's operation and the role of individual optical components. The spectral data captured, as shown in the referenced image, reveals bright lines indicating Argon emission lines in the near-infrared spectrum. The exposure time for this spectrum was set at 1 minute, enabling a detailed and comprehensive analysis of the lamp's emission characteristics. Although the spectrum shows some of the features.

It's important to note that variations in temperature, pressure, and volume affect the spectrum. This is where the Ideal Gas Law comes into play. The Ideal Gas Law, given by the equation, $PV = nRT$, where P is pressure, V is volume, n is the number of moles of gas, R is the gas constant, and T is temperature, illustrates the relationship between these three parameters.

If the temperature increases, the pressure increases, assuming the volume remains constant. Similarly, if the pressure increases, the volume increases, assuming the temperature remains constant. These changes can affect the refractive index of the air in the spectrograph, leading to inaccuracies in the spectral data. Humidity also plays a role as it can change the air density, which in turn affects the refractive index. High humidity can increase the air density, leading to a higher refractive index. Conversely, low humidity can decrease the air density, leading to a lower refractive index. These factors are particularly important when using a high-resolution spectrograph, as even minor changes in these parameters can lead to significant variations in the spectrum. Therefore, calibration becomes imperative to obtain accurate and reliable spectra under changing environmental conditions. This will be discussed in more detail in the subsequent chapters.

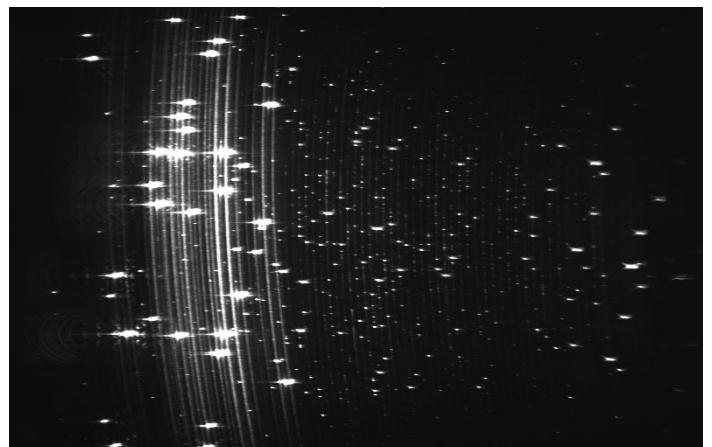


Fig. 2.2: First Calibration and Tuning of ExohSpec result shows Thorium Argon spectrum. The bright features at near infrared shows argon emissions. Caveat: Not tuned, as the pixels in the far infrared shows elongated.

2.2. Active Components Used for Close Loop Feedback Control

Active components are electronic elements that have the ability to control voltage or current, unlike passive components. In our project, active components are sensors that measure temperature, pressure, and humidity, as well as a laser interferometer for displacement in path length measuring device. In the development of our environmentally stable spectrograph, we encounter three critical variables: temperature, humidity, and pressure. Given the intrinsic sensitivity of the spectrograph's optical components to various environmental conditions, we sought a comprehensive solution. The laser displacement interferometer emerged as the most suitable instrument for measuring optical path differences caused by these environmental factors. For measuring pressure and humidity, we selected the BME680 sensor. While there are other sensors available, such as the DHT22, they do not meet our requirements in terms of precision and sensitivity. To manage temperature changes, we opted for a Peltier-based module, which ensures accurate and reliable temperature readings. One of the key components in our setup is the IDS 3010 Displacement Sensor, which is vital for precise interferometric sensing. We also use the BME680 sensor in conjunction with the NODEMCU ESP8266, an alternative to the Arduino Uno, and the PT-104 Temperature Sensor for environmental monitoring. The NODEMCU ESP8266, which we plan to implement in the future, offers a higher data transfer rate over the web and has built-in Wi-Fi, enabling real-time data transfer. Currently, we use an Arduino nano microcontroller to collect data from the BME680. However, we plan to transition to the NODEMCU in the future to facilitate real-time data collection via the Internet of Things (IoT). This change will enhance our ability to dynamically receive and process data over a network, aligning with the evolving requirements of our spectrograph development.

2.2.1. Interferometric Displacement Sensor (IDS3010)

Before we delve into the specifics of the IDS3010 by attocube, it's crucial to understand the concept of interferometry and its significance in our project. Interferometry is a measurement technique that uses wave interference, typically with light, radio, or sound waves. It's employed to evaluate the characteristics of waves and the materials they interact with. Displacement Measuring Interferometry, a specific type of interferometry, uses light waves to study displacement changes. This technique is widely used for calibration and mechanical stage motion control in precision machining ([Wana C. 2013](#)).

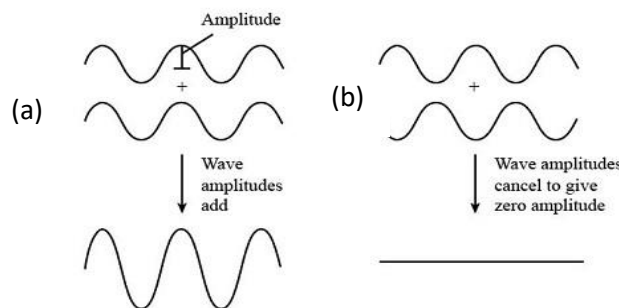


Fig. 2.3: Illustration explaining constructive and destructive interference based on the amplitude of two waves.

CHAPTER 2: SYSTEM OVERVIEW

Interferometers come in various types, such as the Michelson Interferometer and Fabry Perot interferometer. However, they all operate on the same fundamental principle of producing interference. In our project, we focus on Laser Interferometry due to its superior precision and

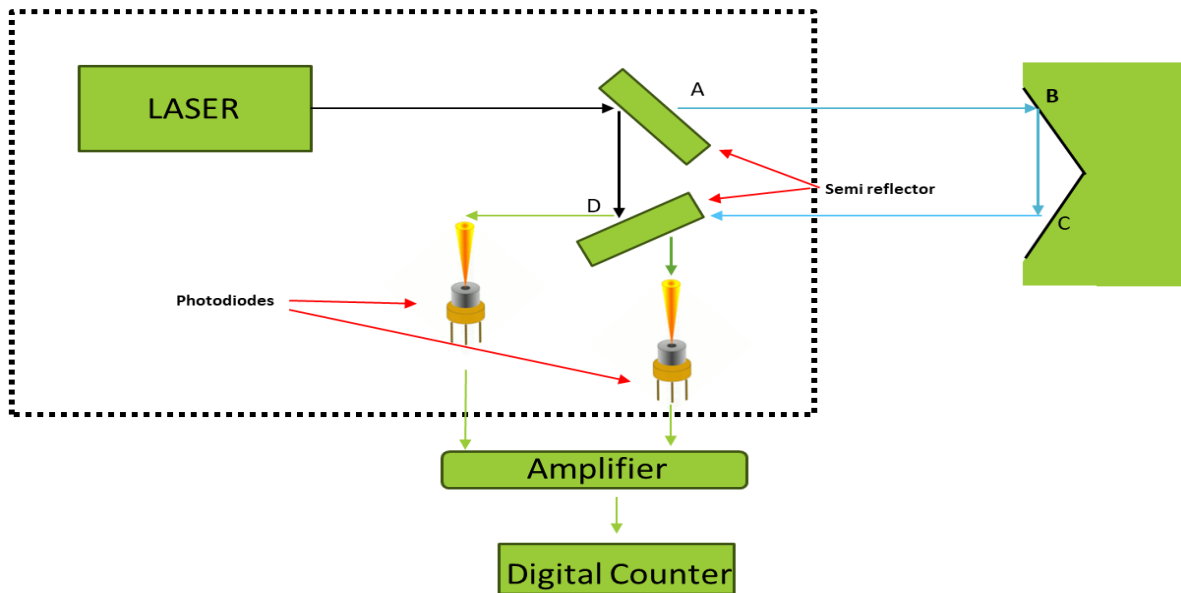


Fig. 2.4: Working principle of Laser Interferometer

accuracy compared to other types of interferometers. Laser interferometers utilize a laser as a coherent and monochromatic light source. The laser beams are directed to semi-reflectors, splitting them into two perpendicular paths. These paths rejoin to create an interference pattern, which changes with variations in optical path lengths. A photodetector captures these shifts in the interference pattern due to mirror displacement, and the amplified signal is sent to a digital counter for precise displacement measurements. Laser interferometers stand out due to their unique properties. Unlike ordinary light, laser light is monochromatic, with a stable wavelength and a bandwidth of 0.4 to 0.5 micrometers. This eliminates the need for light filters. Lasers also have coherence, with rays perfectly in phase, creating a beam of light free from random phases and partial interference.

In our project, we have implemented the IDS3010 by attocube. This instrument, designed for industrial applications like beamline, calibration, closed-loop motion control, and machine vibrometry analysis,

CHAPTER 2: SYSTEM OVERVIEW

has been repurposed for astrophysics. It's used to build a spectrograph, demonstrating its adaptability and widespread use. The IDS3010² boasts a high bandwidth of up to 10 MHz, allowing for vibration detection even at high distances. Its specifications include fibre-coupled laser diodes, a compact modular design, three sensor axes, a sensor resolution of 1 pm, and a distance coverage of mm to 30 metres. The IDS3010 utilizes a Distributed Feedback (DFB) laser, operating at a power of 400µW and a



Fig. 2.5: Experimental setup showing IDS location outside Box2 : (a) IDS3010, (b) Sensor head selection and alignment simplified with advanced mounting kits, (c) Optical items: retroreflector

wavelength of 1530nm. Functioning as a laser displacement measuring interferometer, it measures the displacements in the optical path at the picometer level which we will be using for environmental compensation. This technology ensures accurate and sensitive detection, crucial for maintaining stability in the system amid environmental fluctuations.

IDS Diagonistic:

(i) Positional Displacement Analysis

Retrieving positional displacement data is essential for accurate measurements. The python function `ids.displacement()` is employed to obtain the positional displacement values. Utilizing the fundamental equation(1) for linear displacement laser interferometers –

2 IDS3010

CHAPTER 2: SYSTEM OVERVIEW

where, N is the number of fringes within the interferometer detectors - initial testing involved plotting raw positional data over time. To enhance the data quality, a moving average, acting as a low-pass filter, was applied to eliminate high-frequency components, resulting in extracted data points for subsequent calibration.

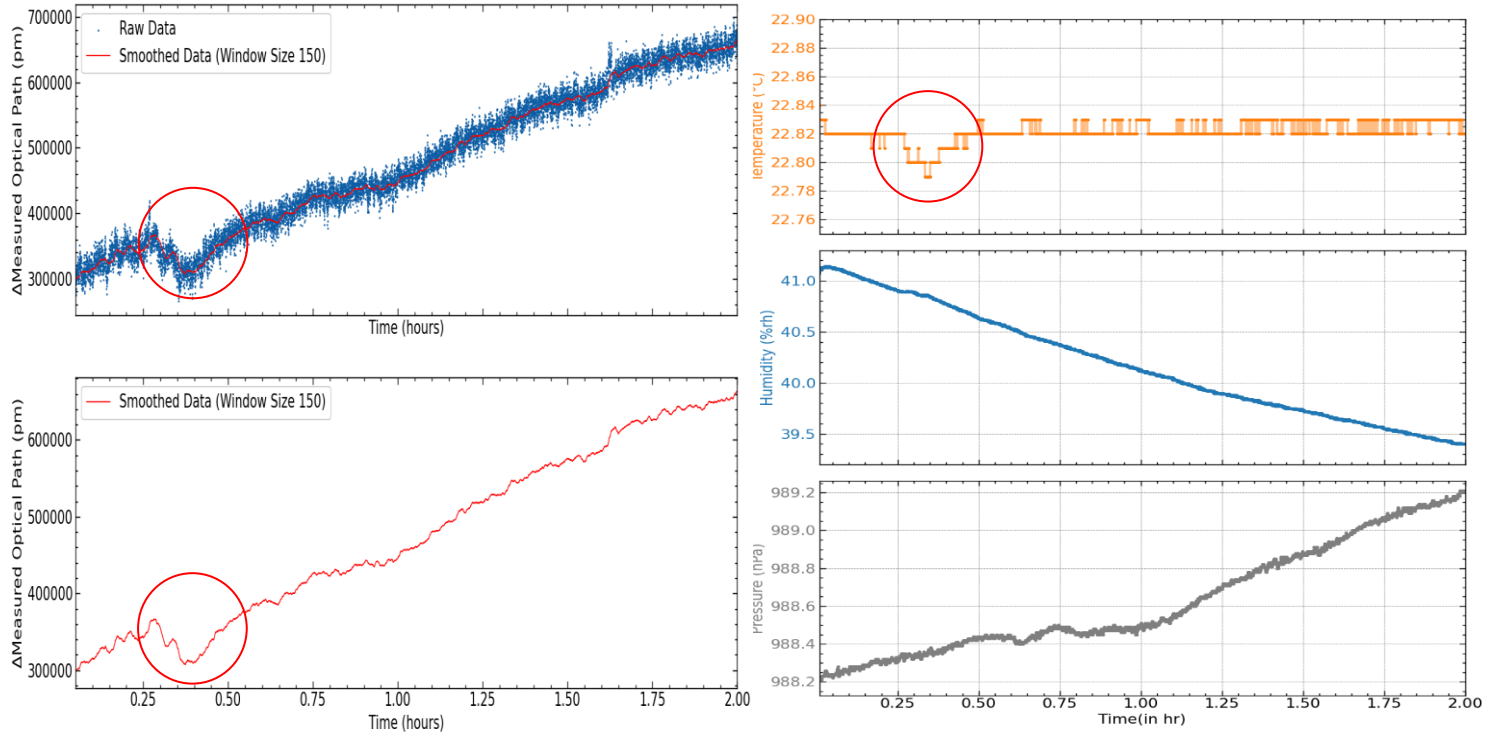


Fig. 2.6: Change in optical path from IDS vs time, (b)Temperature, Pressure and Humidity vs Time. Clearly, shows pressure is correlated with change in optical path, hence a dominant term. However, notably also shows temperature dominance in path length change. Humidity decreases alongside pressure drops following Ideal Gas Law.

The IDS3010, which can be controlled using either the Wave software developed by attocube or via any Python terminal, is a key component of our project. This laser interferometer comes with comprehensive technical documentation, including a specific Python library called IDS. We import this library and call its functions to control the IDS3010. A detailed version of the developed code is available in the GitHub repository, the link to which is shared in the Appendix section.

The first step in using the IDS3010 is to connect it using an IP address. Once connected, we specify the axis number. The IDS3010 has three axes, allowing it to measure displacement in three different directions: x, y, and z. For our current project, we are focusing on one direction, say x. However, in the future, we plan to explore 3D space, which will enable us to evaluate not only the unidirectional measurement of the optical path affected by environmental factors but also other directions.

Once the initial settings are configured, we start the operation at a specific sampling frequency. For instance, in the experiment depicted in Figure 2(a), we measured the change in displacement at a sampling frequency rate of 1kHz over a period of 2 hours. In addition, we measured three environmental parameters - temperature, pressure, and humidity - using the BME680 sensor. This experiment was conducted in Box1 with the temperature control turned on.

CHAPTER 2: SYSTEM OVERVIEW

The left plot in Figure 2(a) shows the measurement of the uncompensated optical path length, which is raw data without any calibration. To process this data, we implemented a smoothing function, taking an average of 150 data points across the time axis. This tool helps us eliminate high-frequency noise in the data, providing a good quality of raw data. This noise is often a result of various acoustic disturbances from the surroundings, such as air conditioners. Given that we are looking at the picometer level, our laser interferometer is quite sensitive and susceptible to picking up noise from the surroundings. The right plot in Figure 2(a) shows a graph of temperature, pressure, and humidity. Comparing these plots side by side, we can observe a coherent relationship between the two. For instance, at about 0.25-0.5h, a temperature spike (a decrease in temperature of about 0.03 degrees Celsius) led to a decrease in the optical path length by a certain factor. Also, the change in the optical path length (OPL) seems to follow the trend of the pressure. We have repeated the experiment many times, and every time it's the pressure that gives the trend to the optical path length. The temperature spikes (increase/decrease) influence the OPL (increase/decrease). The relationship between humidity and pressure, as seen from the graph as the pressure increases the humidity decreases, note the pressure here is an atmospheric pressure which is uncontrollable, but in Future work section we came up with a explanation of how this can be controlled for optimal stability of the system.

(ii) Robustness Testing: Slip Width Variation Experiment

The conducted experiment aimed to simulate microscope glass slip conditions, providing insight into the system's robustness and its response under such scenarios. The idea of the slip here is to implement on the optical path of the laser, which will obviously. The collected data will undergo thorough examination, and implications for the performance of EXOhSPEC will be discussed. The experimental setup involved manually opening the box after a specific duration, introducing a slip, and later removing it to assess whether the system would revert to the initial optical path.

Observing the plotted data below, it is evident that the introduction of the slip resulted in a noticeable change in the optical path. However, intriguingly, the optical path did not fully return to its initial position. To comprehend this behavior, it is essential to delve into the concept of self-mixing interferometry employed in the IDS3010. Self-mixing interferometry is a laser-based technique integral to the IDS operation. This method involves the laser not only emitting light but also functioning as a sensor. When the emitted laser light reflects off a surface, a portion of it is scattered back to the laser cavity. This returning light interferes with the light generated by the laser, creating an interference pattern. The interference pattern encodes information about the target's distance or displacement. In the context of the IDS3010, the initial startup sequence is crucial. At the device's commencement, specific commands are executed to perform optical alignment. This alignment process ensures that the laser beam is correctly directed and focused on the target. Subsequently, the IDS can provide accurate positional displacement data based on the interference pattern created during its operation. The observed deviation in the optical path following the introduction of the slip suggests that the initial optical alignment, crucial for accurate measurements, might have been perturbed. This deviation highlights the sensitivity of the IDS to changes in the optical path and underscores the significance of precise optical alignment during the device's startup for reliable positional displacement data. The self interferometry Outcome: Not Robust in extreme, found undocumented feature as per the manufacturer documentation.



Fig. 2.7: Close-up view of internal setup for robustness test, displaying thickness variations of slip 1 and slip 2 in the optical path, where slip1 is about 0.12mm – 0.16mm and slip2 is micrometer thickness

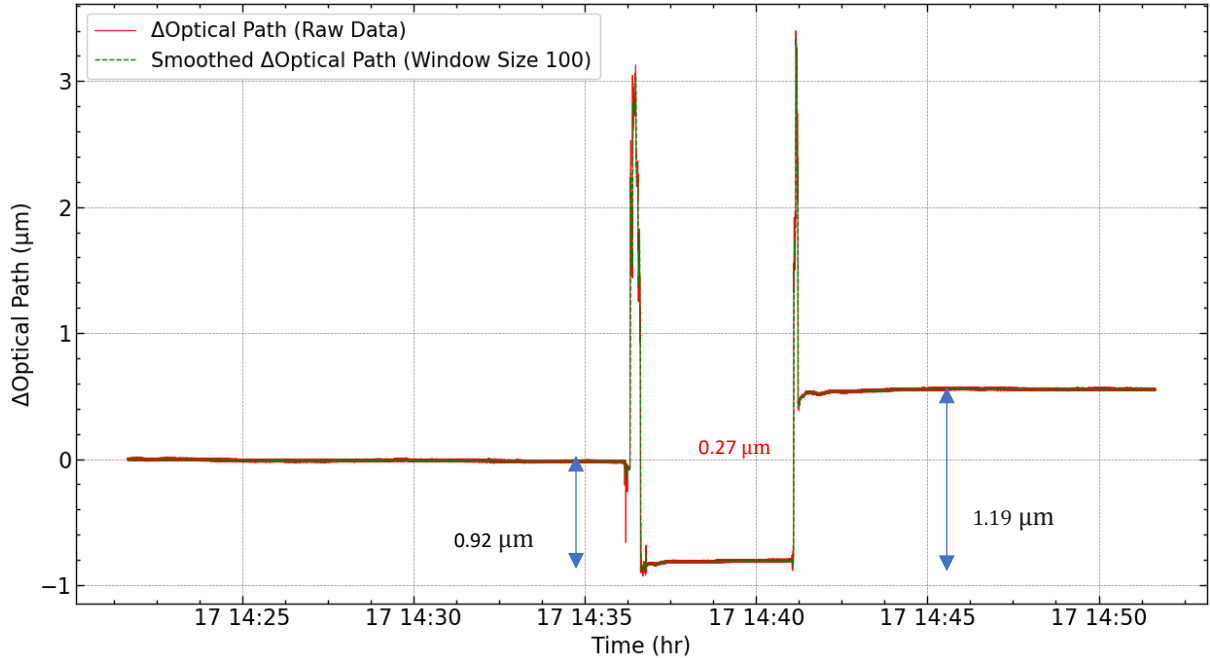


Fig. 2.8: Plot displaying change in optical path with time, revealing altered self-interferometry properties due to glass slip 1 manipulation.

Next, To introduce additional complexity, two slips of different sizes were employed, yielding specific outcomes. The observed discrepancies in the optical path raise questions about the system's behavior under varying slip conditions.

Possible Explanations:

- **Hysteresis:** The sensor may exhibit hysteresis, wherein its output depends not only on the current input but also on its previous input history. This behavior may cause a delay or non-reversibility in the response after a change in the optical path.
- **Environmental Effects:** Changes in temperature, humidity, or other environmental factors during the experiment could influence the sensor's behavior, contributing to variations in the optical path.

CHAPTER 2: SYSTEM OVERVIEW

- Mechanical Effects: The introduction and removal of the glass slip may have induced mechanical changes or stresses in the experimental setup, impacting the sensor's alignment or calibration.

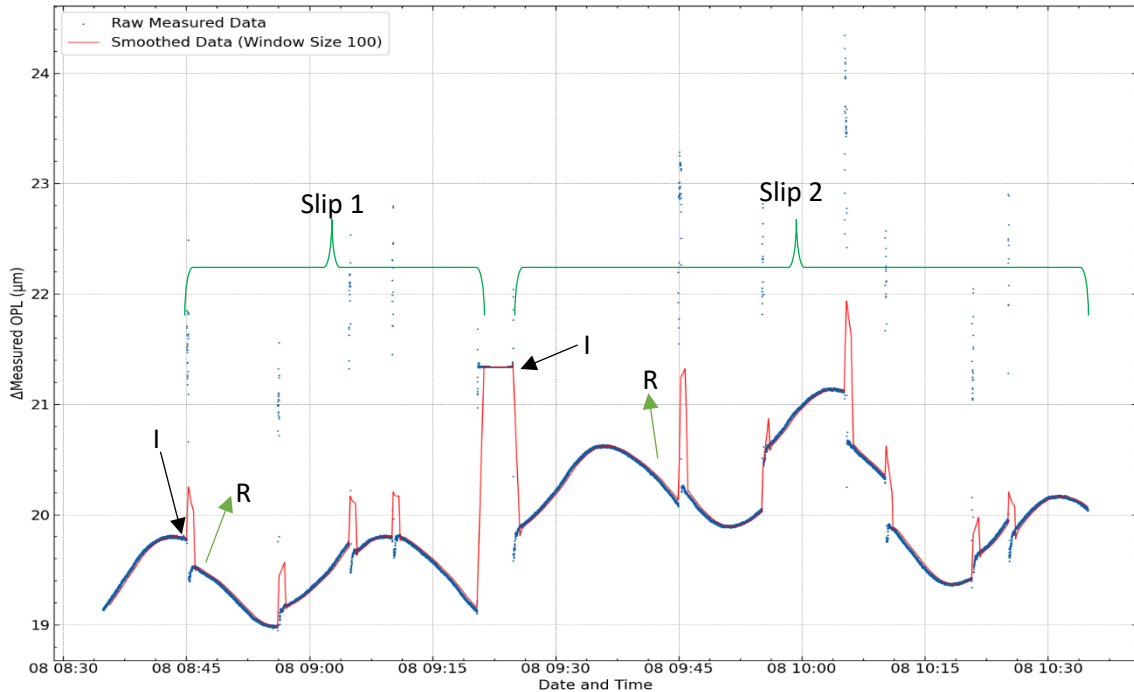


Fig. 2.9: Plot depicting change in optical path length over time, highlighting calibration issues related to self-interferometry properties. I denotes when the slip was inserted and R denotes when the slip was removed from the optical path.

Potential Solutions:

- Further Experiment with Long Exposures: Conduct experiments with extended exposure times to observe the sensor's response over prolonged periods, potentially capturing hysteresis effects.
- Recalibrate the Sensor: After introducing and removing the glass slip, recalibrate the sensor to account for any changes in alignment or calibration.
- Investigate Potential Hysteresis: Systematically investigate and analyze the sensor's response to detect and understand any hysteresis effects.
- Monitor and Control Environmental Conditions: Implement rigorous monitoring and control of environmental conditions during experiments to minimize external influences on the sensor.
- Check for Mechanical Changes: Examine the experimental setup for any mechanical changes and ensure stability to eliminate potential sources of variation in the optical path.

Two of our experiments suggested and proven the fact about the self interferometry property, hence we must be aware of the fact once the IDS is been initiated or started, it goes through optical alignment for few minutes and then it starts taking reading of displacement hence, we must take care about any kind of mechanical potential which can add a noise to our data and get rid of them.

CHAPTER 2: SYSTEM OVERVIEW

In conclusion, interferometry, and more specifically, laser interferometry, plays a crucial role in our project. It provides the precision and accuracy, thus a robustness testing was important to understand the equipment as a whole.

2.2.2. Environmental Sensor: BME680 & ECU

Environmental sensors play a pivotal role in our project, as they help maintain the optimal conditions necessary for precise measurements. These sensors monitor parameters such as temperature, pressure, and humidity, which can significantly influence the performance of the spectrograph and the accuracy of the data collected. In a closed, compact system filled with air, as opposed to a vacuum,



Fig. 2.10: ECU and BME680 size comparison

variations in pressure, temperature, and humidity can alter the refractive index of the medium and the air density. In our work, we primarily focus on the real component of the refractive index of materials. The imaginary component represents losses in the material, but for the materials we are using, these losses are negligible. Specifically, when working with air, the loss coefficient is extremely small. Even over a significant distance, such as several kilometers, the loss in air is minimal and difficult to measure accurately. Therefore, we can safely ignore the imaginary component of the refractive index in our calculations. These changes can, in turn, impact the measurements and observations made by the spectrograph. This is where the need for environmental sensors comes into the picture. Acting as active sensing components, these sensors provide real-time variations of the aforementioned parameters, thereby enabling us to continuously track these environmental factors. This continuous monitoring ensures the stability of the system, enhancing the reliability of our observations and findings. In this section, we will be discussing two such sensors that we have incorporated into our project. These sensors not only help us maintain the necessary environmental conditions but also contribute to the overall accuracy and reliability of our system.

(i) BME680³

The BME680 is a versatile 4-in-1 digital sensor measuring temperature, humidity, barometric pressure, and gas concentrations like Volatile Organic Compounds (VOC). However, we are not interested in measuring the gas concentrations at the current stage of the experiment. We use Arduino Software to collect the data from the sensor, then using the serial monitor of the software, strategically send the data into python terminal (jupyter Notebook, in our case). Then, the data collected is been saved in a csv file for further analysis.

³ [BME680](#)

BME680 Diagnostic

The subsequent testing phase focused on the BME680 sensor, revealing an intriguing finding: the temperature readings exhibited fluctuations over time as seen in fig. 2.11. Further exploration uncovered that the gas element within the BME680 chip operates as a resistor element. This phenomenon can be explained by the fact that the resistivity of conductors increases with rising temperatures. As atoms vibrate more rapidly and over larger distances at higher temperatures, electrons moving through a metal experience more collisions, effectively raising the resistivity. Expressed mathematically, this relationship is captured by the equation $\rho = \rho_0 (1 + \alpha \Delta T)$, where ρ_0 represents the original resistivity, α is the temperature coefficient of resistivity, and ΔT is the temperature change. In simpler terms, the resistance of the gas element changes proportionally with temperature fluctuations. Consequently, the decision was made not to rely on the temperature readings obtained from the BME680 sensor. The reason is that these readings constitute a combination of internal and environmental temperatures from the surrounding environment. Instead, the focus will be on utilizing pressure and humidity readings, which remain reliable. Additionally, it's noteworthy that the accuracy of the BME680 temperature readings is within a range of ± 1 degree Celsius.

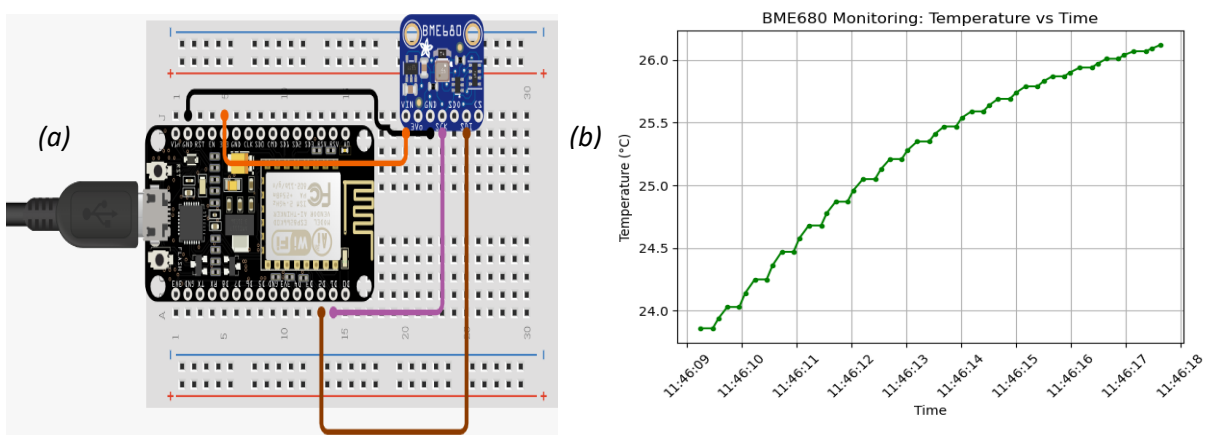


Fig. 2.11: (a) Circuit Design of Nodemcu ESP8266 and BME680 sensor, (b) Temperature vs. Time, demonstrating resistivity-induced temperature increase with oversampling.

(ii) ECU

To mitigate positional inaccuracies caused by variations in the refractive index due to air, attocube provides an Environmental Compensation Unit (ECU). The ECU measures local environmental parameters, enabling an accuracy typically better than ± 1 ppm in air. This unit is designed to be plug-and-play compatible with all IDS models.

(iii) Comparison Diagnostic Test: BME680 vs ECU

Now, in order to understand both these two components, we did a testing and compared the results.

Parameters	BME Accuracy	ECU Accuracy
Temperature (°C)	± 1	± 0.1
Humidity (%rh)	$\pm 3\%$	$\pm 2\%$
Pressure (hPa)	± 1	± 1

Table 2.1: Comparison of accuracy between BME680 and ECU components.

CHAPTER 2: SYSTEM OVERVIEW

During our 160-hour experiment conducted in Box1, we aimed to compare results between ECU and BME680, shedding light on ECU's functionality, particularly its compensation of optical depth, which was undocumented initially. The ECU offers two modes: one with compensation and one without. We

The collected data includes timestamps, measured Optical Path Length (OPL), ECU readings of temperature, humidity, pressure, and its calculated refractive index. The refractive index calculation by ECU was unknown(undocumented), but likely employed empirical equations involving temperature, humidity, and pressure coefficients.

The Geometric Path Length (GPL), calculated from the measured OPL and refractive index, provides an actual expected path length. For ECU and BME680 measurements, refractive indices were determined using Ciddor and Edlen equations. The difference between OPL and calculated GPL for both ECU and BME680 revealed path length changes.

```
DateTime: 2024-03-06, 18:24:54.034582,  
OPL: 589671273772 (Uncompensated, position reading, measured optical path length)  
ECU_Temperature, ECU_Humidity, ECU_Pressure, ECU_rIndex:  
20.63627,35.04,1011.87,1.0002673277916674  
GPL: 589513680381.6659 (Geometric Path Length/compensated = OPL/ECU_rIndex)  
BME_Temperature, BME_Humidity, BME_Pressure:  
22.61,40.11,1013.47  
BME_Ciddor, BME_Edlen:  
1.0002658741607788,1.0002658811361596 (Refractive Index using NIST model – empirical formula)  
BME_GPL_Ciddor, BME_GPL_Edlen:  
589514537089.1844, 589514532978.1892 (GPL = OPL/BME_ciddor_rIndex, BME_edlen_rIndex)
```

Fig, Snippet of the data for a specific time stamp for analysis purpose

Results indicate a very small discrepancy between the ECU and BME680 measurements, with the refractive index difference being negligible. Path length changes for both devices were also minimal, suggesting reasonable accuracy and consistency in the measurements.

Parameters	BME	ECU	Δ change
Temperature (°C)	22.61	20.63627	1.97373
Humidity (%rh)	40.11	35.04	5.07
Pressure (hPa)	1013.47	1011.87	1.6

Table. 2.2: Table showing a comparison between BME and ECU sensor readings, highlighting the differences in temperature, humidity, and pressure measurements.

Difference in Refractive Index (BME_Edlen - BME_Ciddor) = 6.97538072e-9

Will be using Ciddor equation for our system, Edlen is used in more robust system.

Path length change -> Δ_{ECU} : $OPL - GPL = 157593390.334 \text{ pm} \cong 0.1576 \text{ mm}$

Path length change -> Δ_{BME} : $OPL - BME_GPL_Edlen = 156740793.811 \text{ pm} \cong 0.1567 \text{ mm}$

$\therefore \Delta = |\Delta_{\text{ECU}} - \Delta_{\text{BME}}| = 852596.523 \text{ pm} \cong 0.00085 \text{ mm.}$

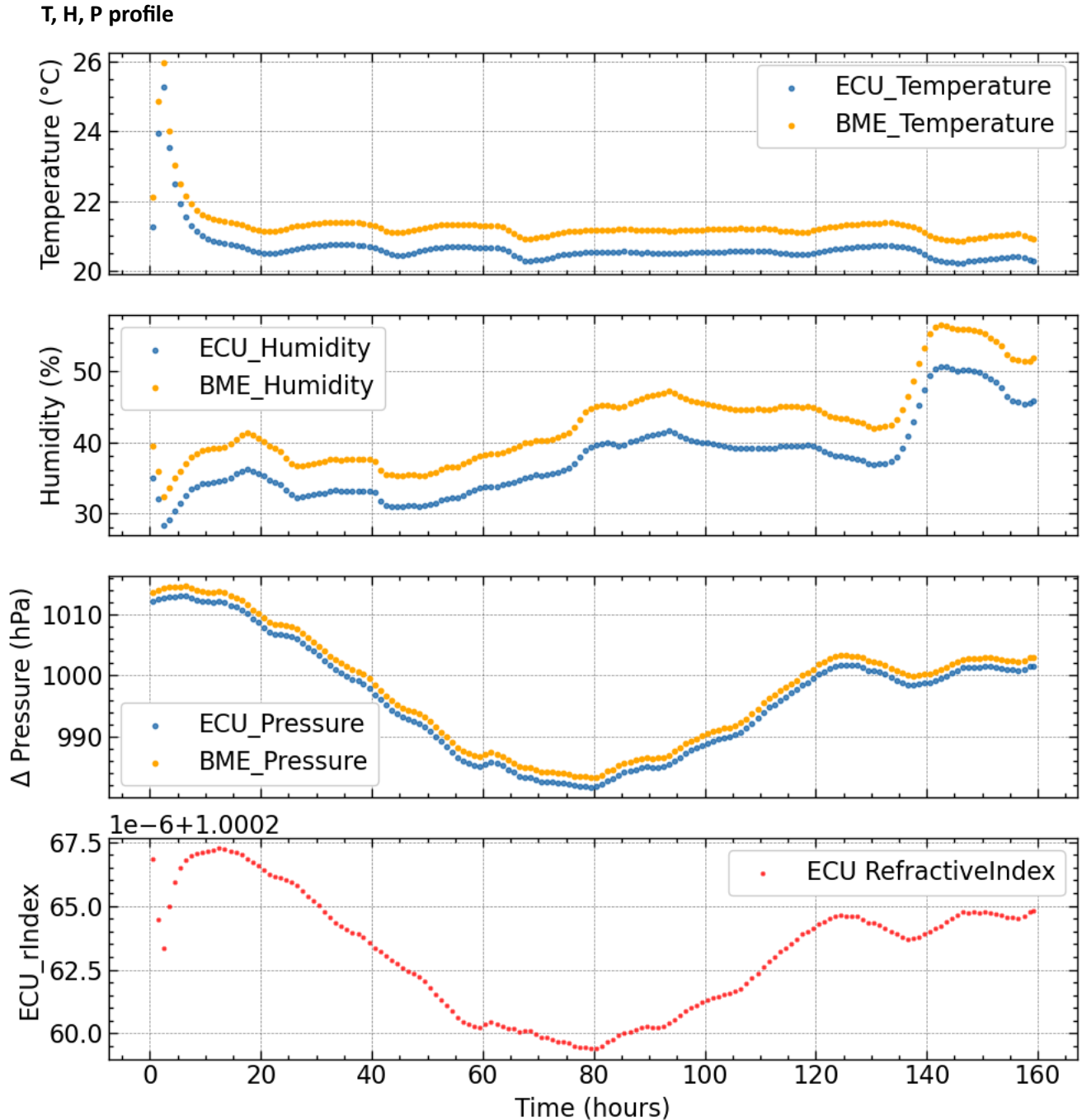


Fig. 2.12: Plot showing correlation between ECU and BME, with a temperature difference of approximately 1.97 $^{\circ}\text{C}$, humidity about 5% and Pressure curve of about 1.6hPa, which states about there precision and accuracy.

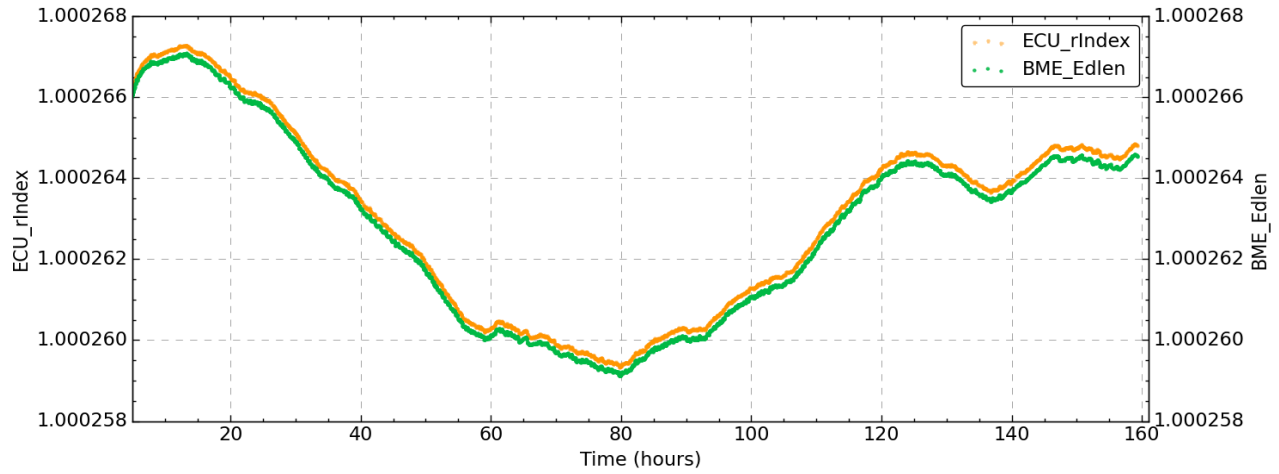
Comparison of ECU rIndex with BME_Edlen rIndex (Model)


Fig. 2.13: Plot of ECU and BME refractive indices over time, revealing a close relationship.

Correlation between BME_Edlen and ECU_rIndex: $99.78 \pm 0.06\%$

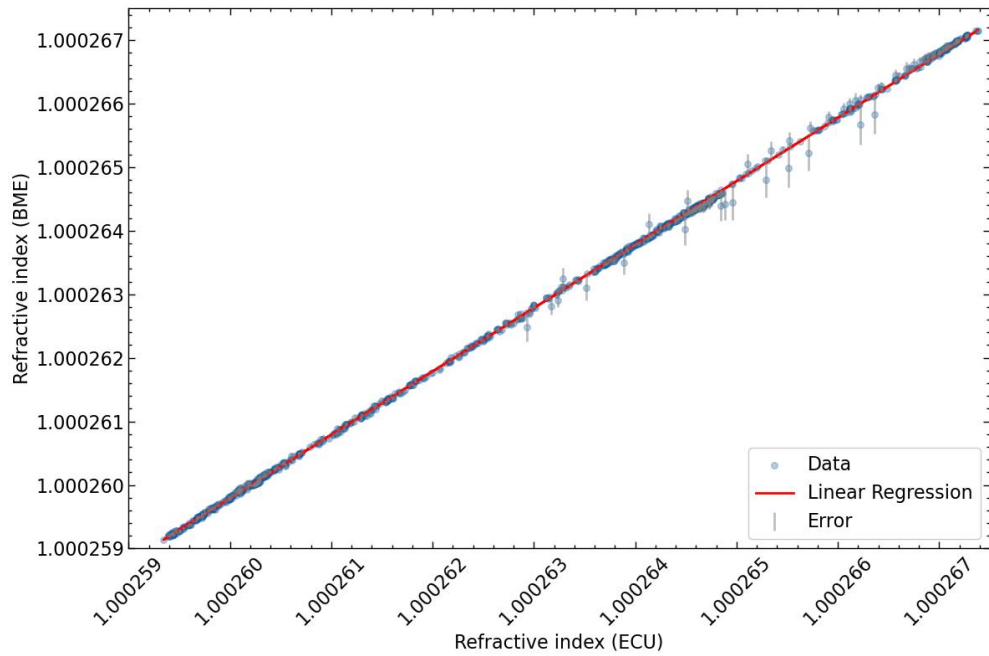


Fig. 2.14: Regression analysis of refractive indices for BME and ECU sensors, displaying error bars indicating value discrepancies.

We conducted a correlation analysis between the refractive indices obtained from both devices to assess their consistency. The correlation between BME_Edlen and ECU_rIndex was found to be $99.78 \pm 0.06\%$, indicating a strong correlation between the measurements. One thing to notice here again is that the refractive index curve follows the pressure trend. This suggests that regardless of whether we use the BME680 or ECU, we can expect to obtain similar results. Such high correlation values are deemed acceptable for our intended purposes. Subsequently, we generated a scatter plot of the refractive indices and applied linear regression to fit a linear curve to the data. Additionally, error bars were incorporated to identify any significant deviations between the measurements.

In the Fig 2.15, we observe the GPL of ECU and BME, overplotted on each other a zoom out version is overplotted to show what actually happening, a 7.2mins rise and fall constant fluctuation is noted, this is due to the air conditioner.

The time constant evaluated using model fit approximately 1 hour. In the conducted experiment, the time

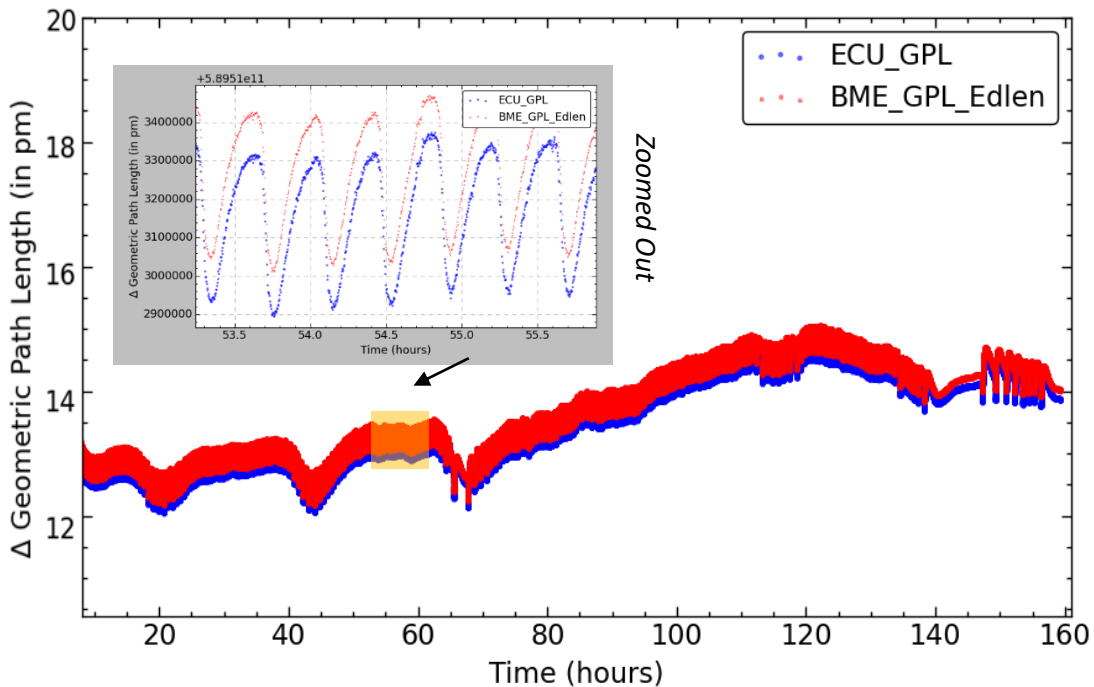


Fig. 2.15: Plot of Geometrical Path Length over time, zoomed out plot showcasing a sinusoidal curve due to air conditioning effects.

constant was calculated for a system exhibiting exponential decay. The data, representing change in geometric path length over time, was analyzed between the time interval of 38 to 38.120 hours. The initial position was recorded as $5.89513244\text{e+}11$ pm and the final position as $5.89512874\text{e+}11$ pm. A curve fitting method was employed to estimate the time constant using a model function for exponential decay. The time constant, denoted by τ , represents the time it takes for the system to decay to about 36.8% of its initial value. Upon computation, the time constant for the given data was found to be approximately 1.0 hours. This suggests that the system takes about 1 hour to decay to 36.8% of its initial geometric path length, under the assumption of an exponential decay model.

2.2.3. Temperature Sensor (PT-104)

Addressing the temperature variability issue, a Peltier-based temperature 4-channel module (PT104) was introduced, with resolution (0.001°C) and accuracy (0.015°C). Utilizing Pico log software for data recording, the information is later processed in Python for calibration purposes. Initial testing in Box2 illustrated temperature changes at different locations inside the box as seen in Appendix C.

CHAPTER 2: SYSTEM OVERVIEW

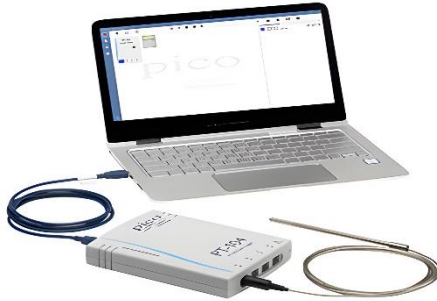


Fig. 2.16: Peltier-104 Temperature Sensor connected with a probe to computer. The temperature variation over time is observed using Pico Log Software

To address the temperature accuracy concerns, the project adopted a Peltier-based temperature 4-channel module known as PT104⁴. This module provides significantly more accurate temperature readings compared to the BME680. During the initial testing phase in Box2, a plot was generated, illustrating temperature changes. The experiment involved three probes strategically placed inside the box at different locations, and an additional probe outside the box for reference. Throughout the two-day experiment, the box remained active while the temperature control was turned off. The results revealed crucial insights. Firstly, the temperature within the entire box exhibited non-constant behavior. Secondly, a noticeable change of 2 degrees Celsius from the room temperature was observed. This change was attributed to the internal system operations, leading to the dissipation of heat within the box and, consequently, a rise in temperature. These findings underscore the significance of monitoring and understanding the thermal dynamics within the experimental setup for accurate environmental control. A brief explanation about the experiment and its finding is discussed in the section 2.3.2.

2.3. Environmental Control Boxes: Box1 and Box2

The **necessity of environmental control boxes** arises primarily from the need to safeguard our high-resolution spectrograph. This spectrograph, equipped with numerous optical components, is susceptible to environmental fluctuations, particularly temperature changes. These temperature variations can lead to thermal expansion and contraction of the materials, potentially compromising the spectrograph's performance. Before we delve into the subsequent sections, it's crucial to understand the significance of the **PID loop**. This control loop feedback mechanism, standing for Proportional, Integral, and Derivative, is an integral part of our system, tasked with controlling the temperatures of the two boxes.

⁴ [PT104](#)

In the project, we employ a PID loop to regulate the temperature of the box that houses the spectrograph. This control mechanism also serves to adjust the optical path by varying the temperature. As we know, an increase in temperature extends the path length, while a decrease contracts it. This principle allows us to achieve the desired geometric length

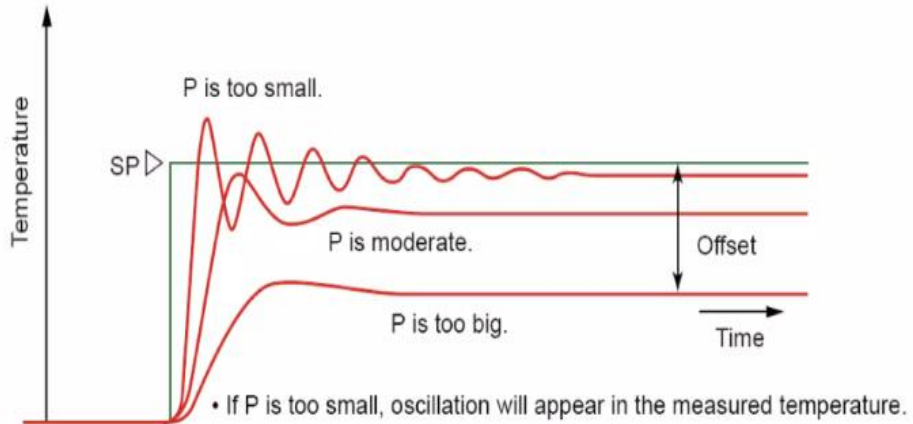


Fig. 2.17: PID⁵ loop Temperature vs. Time plot, highlighting temperature oscillation with too small P value.

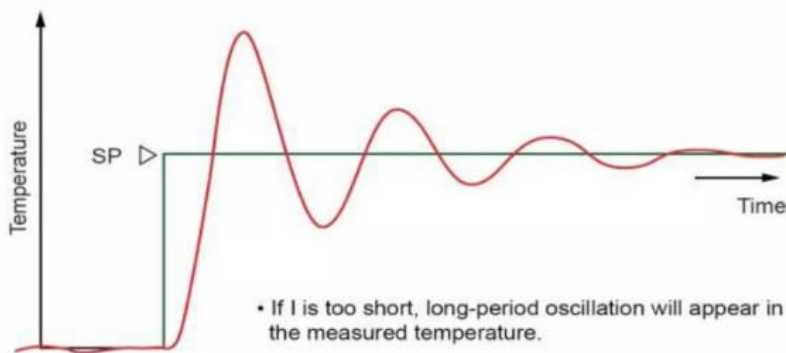


Fig. 2.18: PID loop Temperature vs. Time plot, demonstrating long-period oscillation with short I value.

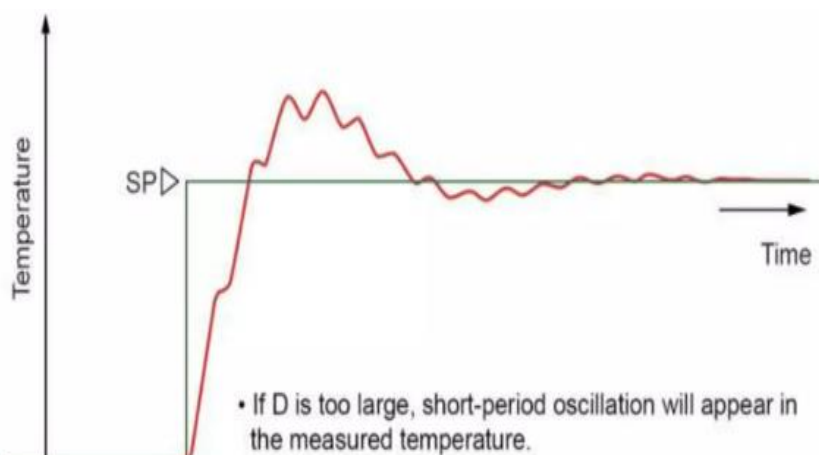


Fig. 2.19: PID loop Temperature vs. Time plot, demonstrating long-period oscillation large D value.

⁵ [Proportional Integral Derivative \(PID\) control](#)

CHAPTER 2: SYSTEM OVERVIEW

The PID controller equation is as follows:

$$u(t) = K_p e(t) + K_i \int_0^t e(\tau) d\tau + K_d \frac{d}{dt} e(t)$$

Proportional
 Integral
 Derivative

where:

- $u(t)$ represents the controller output,
- $e(t)$ denotes the error, calculated as the difference between the desired setpoint and the actual output,

K_p , K_i , and K_d are the proportional, integral, and derivative gain parameters, respectively.

The **Proportional Band** adjusts the output amplitude (reciprocal of gain), the **Integral** eliminates offset error (also known as automatic Reset or simply Reset), and the **Derivative** considers the rate of change of the error. The primary objective is to reduce the offset, adjusting from longer to shorter time. The larger the Derivative, the stronger the corrective action, and the more likely the output will oscillate. After continuous manual adjustment, we were able to fine-tune the values to achieve optimal performance. This brief explanation should provide a basic understanding of the PID control mechanism and its importance in our project, the recommended PID values given in Appendix C.

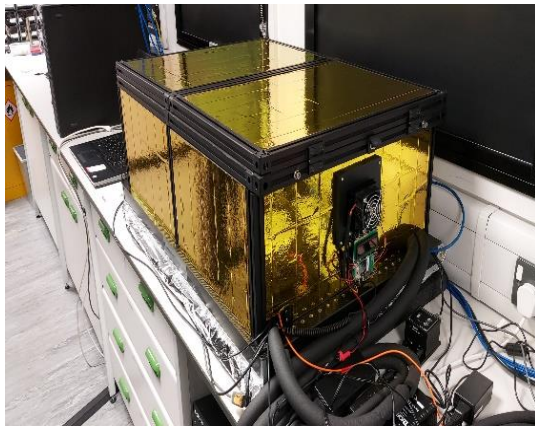


Fig. 2.20: Side View of Box1 housing the spectrograph on a carbon fiber breadboard, depicting potential air leakage. Hence need for Box2.



Fig. 2.21: Side View of Box2, a modified protective box focusing on temperature control.

2.3.1 Box1: Small Temperature Control Box Housing Spectrograph

Box1 as shown in Figure 7 serves as an efficient and effective environmental control unit, placing strong emphasis on maintaining stability. It works hand in hand with EXOhSPEC to play a vital role in achieving and maintaining the desired environmental conditions. Enclosed within the box is a

CHAPTER 2: SYSTEM OVERVIEW

spectrograph, securely mounted on a carbon fiber board that ensures thermal stability. The accompanying figure showcases the box, complete with a convenient top lid for effortless configuration adjustments. While it offers precise temperature control, it also allows for airflow, influenced by any temperature changes in the lab setting, which is a challenge for us and thus the need of another box, however we control the temperature of the Box using a PID loop values(first control system)

Box1 Diagonisitic:

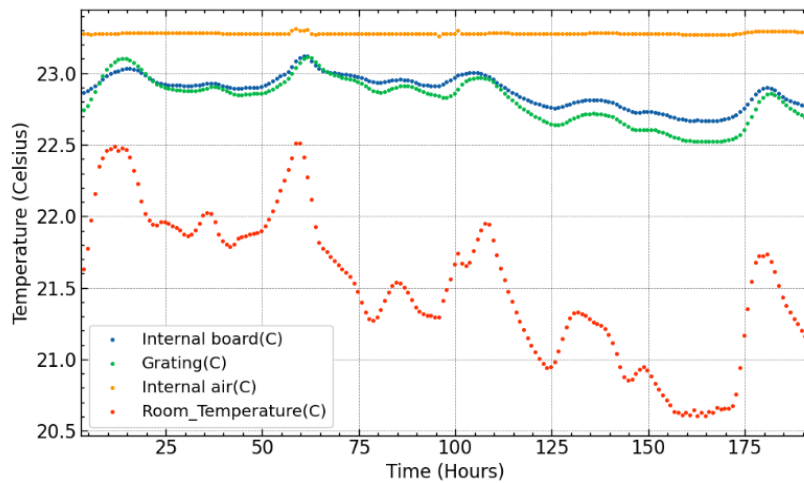
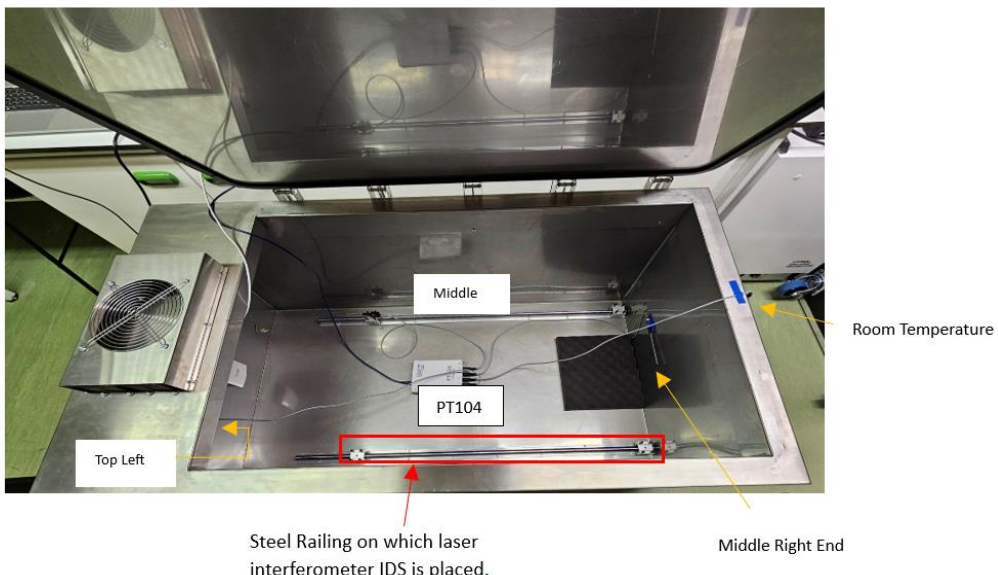


Fig. 2.22: Temperature characteristics of Box 1, revealing variations with stable internal components but fluctuating room temperatures.

Temperature characteristics of Box 1: PT104 is used to collect temperature reading from 4 crucial points in the box - internal carbon fibre breadboard, the grating element, internal air and outside room temperature, the temperature control was on during this experiment. The plot shows variations in room temperature, however the internal board and grating are quite stable comparing to room temperature, but there are lot of wiggles in curve due to constant change in temperature which is not good for our optical components as a result thermal expansion and contraction, however the internal air, a region where the thermocouple was kept close to the temperature control unit, shows that the temperature control is working well maintaining a constant temperature .

2.3.2 Box2: Modified Protective Temperature Control Box

Box2 is a versatile and innovative mechanism engineered to protect Box1 and the enclosed spectrograph from external factors. With its advanced temperature regulation and protective features, it ensures the optimal performance and durability of the equipment. Constructed with stainless steel 304, chosen for its excellent corrosion resistance and durability, it employs a Peltier-based 100 sensor to maintain the interior temperature of the box. A PID loop is used to control the temperature of the box, forming our second control system. Unlike its smaller counterpart, Box1, Box2, as shown in Figure 8, has a larger capacity and can house a significant volume of air. It's important to note that some temperature fluctuations may occur within the enclosure due to the placement of the temperature probe at one end. In future iterations, Box1 will be housed within Box2.



| Fig. 2.23: Shows the setup in which IDS will be placed on the steel railing and the temperature sensors position in the box2, at centre placed the PT104, to conduct an experiment to study the temperature and improving the PID control loop

for enhanced protection. Additionally, an internal fan will be integrated to facilitate proper air circulation, ensuring a consistent temperature throughout the enclosure. This forms part of our future work and continuous improvement efforts.

Box2 Diagnostic: The temperature profiles obtained from four sensors, namely Top Left (Temp1), Room Temperature (Temp2), Middle Right End (Temp3), and Middle (Temp4), provide valuable insights into the thermal dynamics of a controlled environment, presumably inside a large box. The statistical summaries and correlation matrix offer a detailed understanding of temperature variations within and outside the box. The experimental observation was done for over 330 hours or 13.75 days which is roughly 2 weeks. This was tested using new PID values, by varying the damping factor to achieve a desirable output. The overall objective was to test the new PID values and see how efficient the system's maintaining temperature inside with respect to fluctuations in room temperature.

CHAPTER 2: SYSTEM OVERVIEW

Regions	Mean (°C)	Mode (°C)	Standard Deviation (°C)
Temp1 (Top Left)	20.82	20.833	0.15
Temp2 (Room Temperature)	19.67	20.008	0.49
Temp3(Middle Right End)	20.55	20.477	0.22
Temp4(Middle)	20.58	20.532	0.16

Table 2.3: Statistical analysis of mean, mode, and standard deviation in different regions of the box.

The Fig 2. reveals the trend of temperature variations, one of the major fluctuations we can see in the range 50-60h, the box temperature control (Top Left) however maintains a constant, but a slight variation in change of about 0.15°C at 50th hour of Top Left with respect to the middle of the box. Let's discuss in brief below.

The analysis of temperature data obtained from the four sensors—Top Left (Temp1), Room Temperature (Temp2), Middle Right End (Temp3), and Middle (Temp4)—revealed insightful distribution characteristics. Figure 3 showcases histograms providing a visual representation of the frequency distribution for each temperature profile. These histograms include kernel density estimates (KDE) to offer a smoother depiction of the distribution patterns. A notable observation is the distinct distribution of room temperature fluctuations, evident in Temp2, which displays more bins compared to other temperature profiles. Temp1, representing the top-left sensor, demonstrates a single bin, indicating a relatively constant temperature—a desirable characteristic for the intended purpose. However, a subtle variation is observed in Temp3 and Temp4, each showing two bins in their histograms. This visual analysis contributes to a understanding of temperature variations across different sensors, emphasizing the effectiveness of maintaining a consistent temperature in the top-left region while highlighting slight fluctuations in other areas.

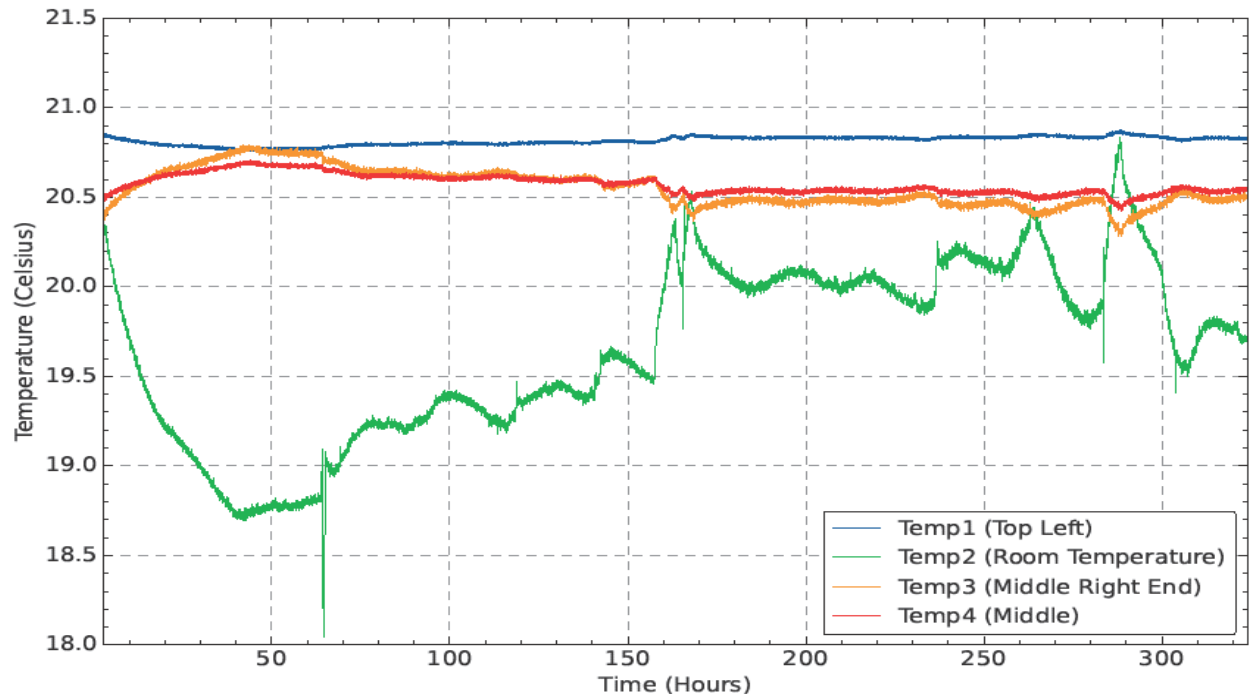


Fig. 2.24: Temperature data over 2 weeks from 4 probes, indicating stability with new PID values and room temperature variations.

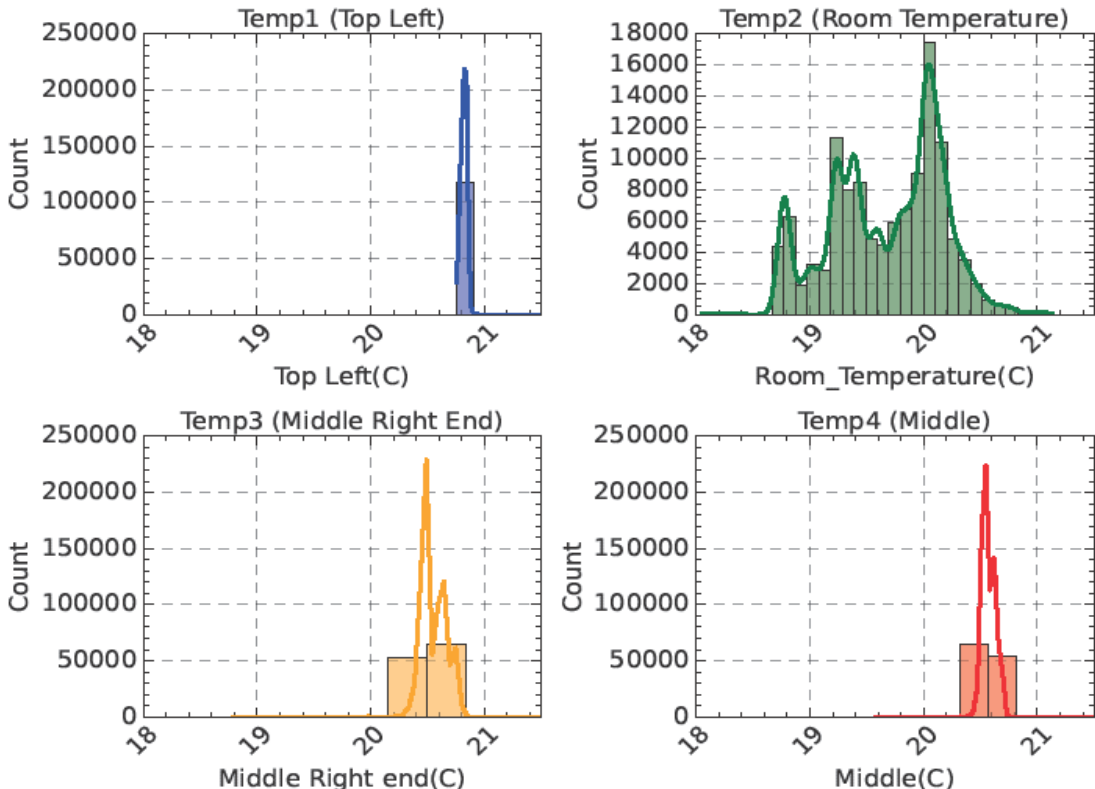


Fig. 2.25: Histograms depicting data distribution, crucial for understanding temperature variations.

For better understanding, I combined each of the different histograms (fig 4) into a single representation in the next section. This combined perspective offers a more understandable understanding of how room temperature varies. Temp1 displays the intended consistent temperature as expected. Inside the box, there is space for development, especially when it comes to maximizing air circulation. This enhancement is necessary to lessen the minor temperature swings that Temp3 and Temp4 show, finally bringing them closer to the constant temperature that Temp1 displays. By taking care of this, the box's temperature environment can be made more consistent and under control.

Now, let's delve deeper into these two regions of interest:

Region 1: This region is particularly intriguing due to the significant spike in room temperature, about 2 degrees Celsius, relative to temp1. Despite this substantial fluctuation, the internal temperature remarkably remains constant for a duration of 40 hours. This stability demonstrates the effectiveness of our environmental control system in maintaining a consistent internal temperature, even when faced with considerable external temperature changes.

Region 2: In contrast to Region 1, this region exhibits a correlation between the room temperature and the temperature inside the box. As the room temperature varies, so does the internal temperature of the box. However, temp1 remains constant as expected, and temp3 and temp4 are not only correlated but also remain constant. This suggests that our system is capable of maintaining certain temperatures constant, despite changes in other variables.

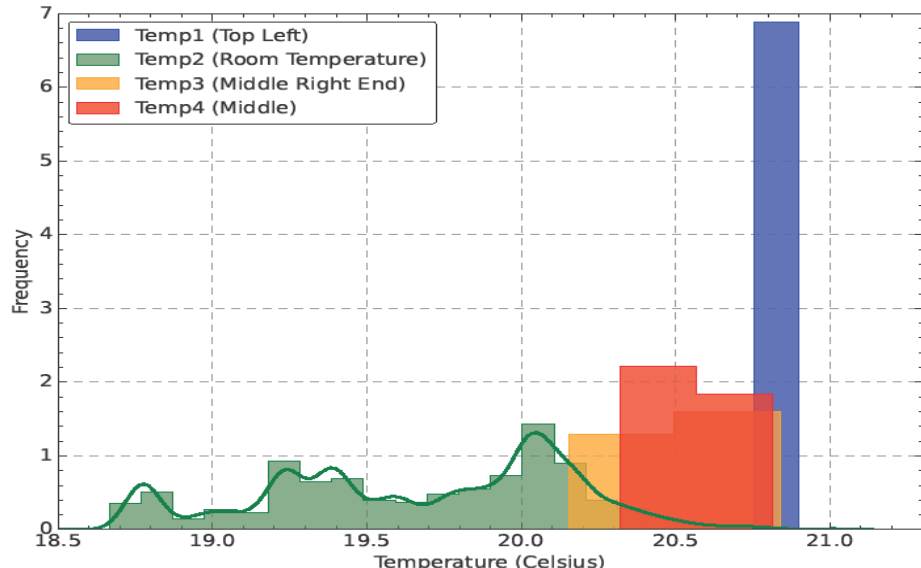


Fig. 2.26: Shows the combined variation in data in form of histograms, bin size = 30.

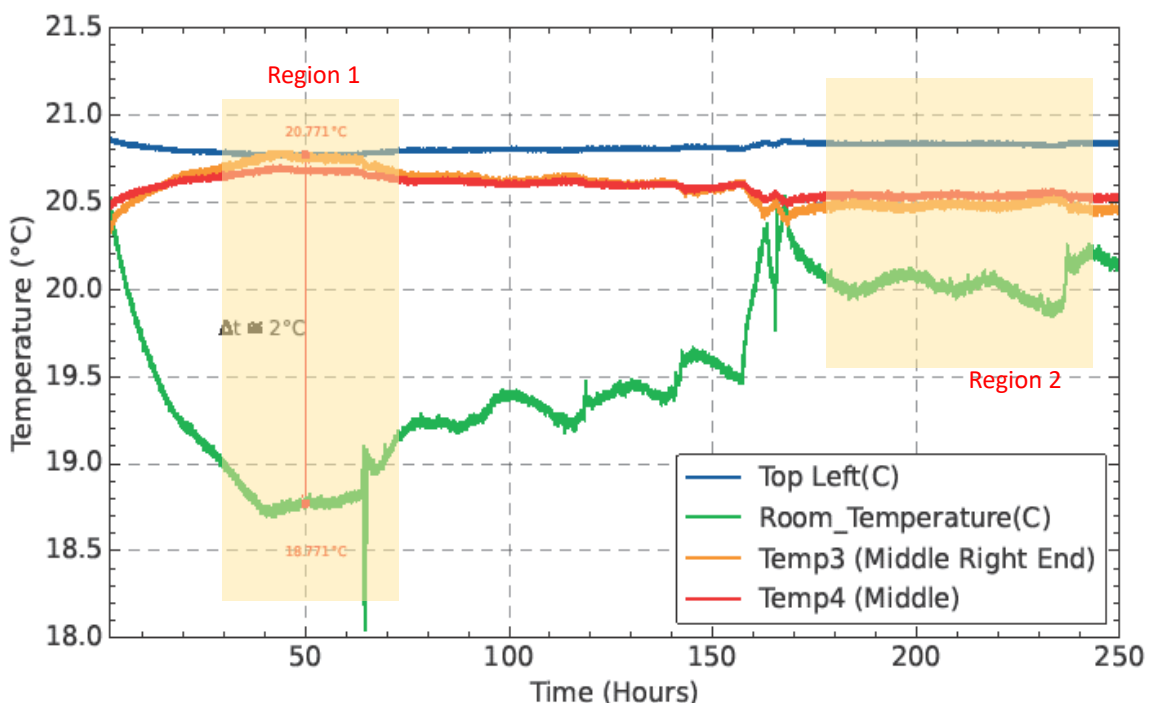


Fig. 2.27: Region of focus: Region 1 and Region 2, to study system behavior during initial and final phases.

The selection of these two specific regions provides valuable insights into the system's behavior during its initial and final stages. It allows us to understand how the system responds to external temperature changes and how it manages to maintain certain internal temperatures constant. These observations are crucial in further optimizing our temperature control mechanisms and ensuring the longevity and performance of our spectrograph.

Next, evaluated the time variations in Figure 2.27, which shows that the box's inside temperature remained constant over the observation period. The temperature differential of the interior environment (20.77 degrees Celsius) and the room (18.721 degrees Celsius) is roughly 2.049 degrees Celsius. This data is consistent with our hypothesis, confirming that the box can maintain a steady temperature even when there is an outside temperature surge of two degrees Celsius. It's important to keep in mind that although if the box can handle an external temperature change of two degrees, larger outside temperature variations may cause the reaction time to increase. Since it would probably take longer to reach and sustain, more research is needed to see how the box reacts to greater temperature fluctuations. Similarly, in Region 2, we conducted an analysis where we calculated the following temperature differences:

Δt_{12} (difference between Temp1 and Temp2): 0.928°C

Δt_{234} (difference between the average of Temp3 and Temp4 and Temp2): 0.65°C

Δt_{134} (difference between Temp1 and the average of Temp3 and Temp4): 0.278°C.

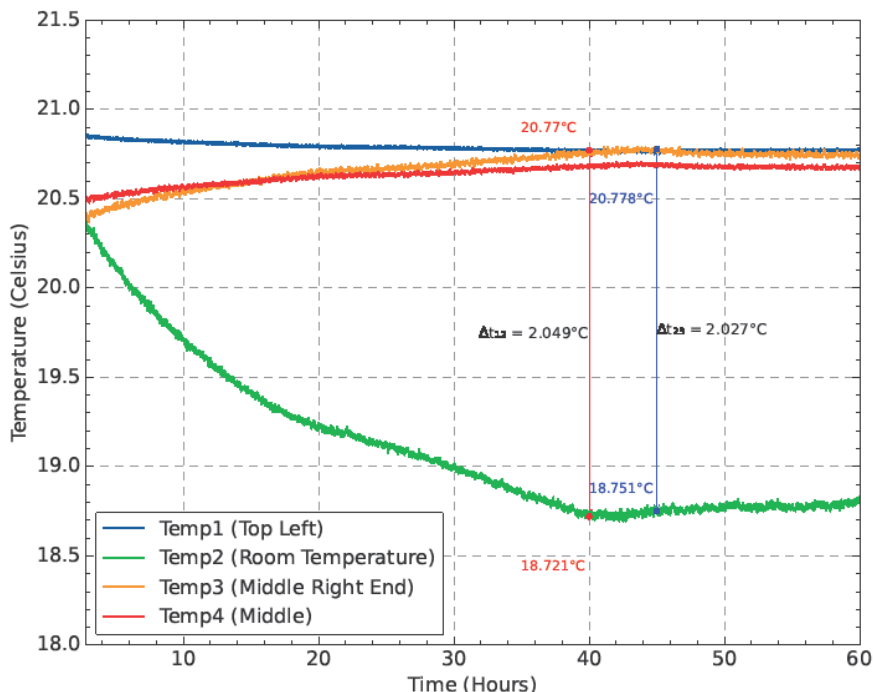


Fig. 2.28: Region 1 analysis shows that approx 30 -60 h, the inside of the box maintained a constant temperature regardless of outside spike in room temperature of 2 degree celsius, this proves the temperature control system working well.

These calculations provide insights into the temperature variations between different sensors, highlighting specific differences within Region 2. Next, performed an overall statistical analysis on the overall data of the room temperature vs the box temp1.

Mean Temperature Difference: -1.1497183283864267

Standard Deviation of Temperature Difference: 0.47327475586196827

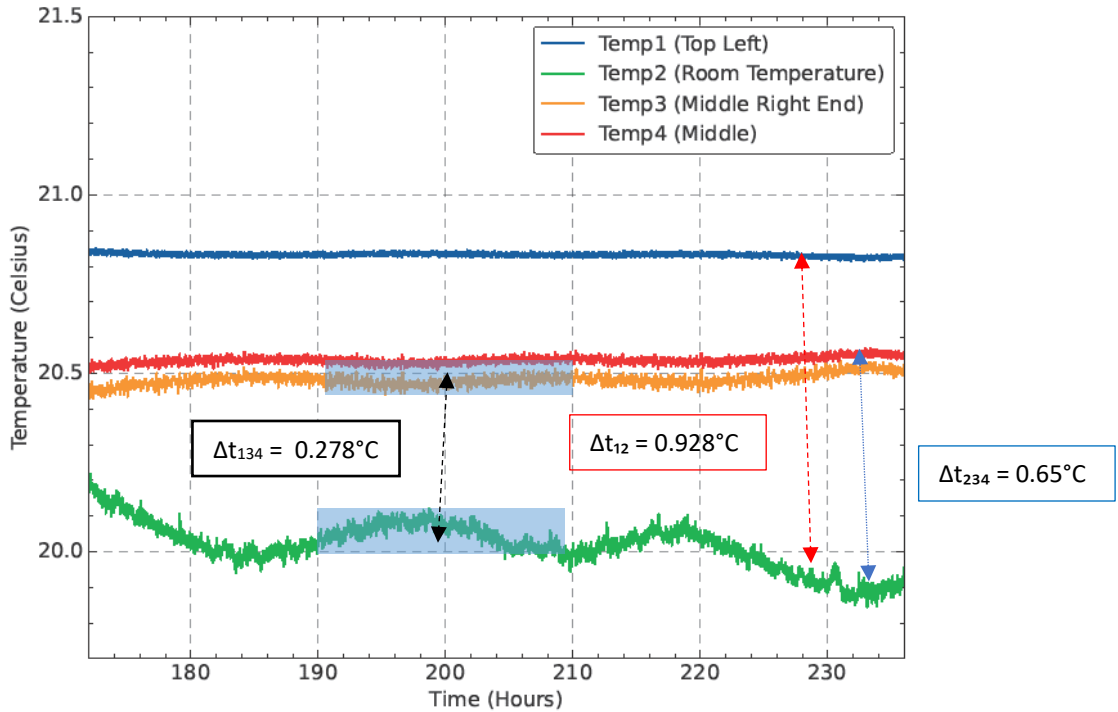


Fig. 2.29: Region 2 shows at about 180 - 230 hrs, the temperature variation in the system suggesting the top left is temperature controlled, the middle and middle end is not with a difference 0.3 degree celsius approx, further inspection reveals the phenomenon of convection taking place in the box.

In the conducted analysis, the mean temperature difference between the observed temperatures was found to be -1.1497°C . This negative value suggests an overall decrease in temperature. Additionally, the standard deviation of the temperature difference was calculated to be 0.4733°C , indicating a certain degree of variability or dispersion in the temperature differences. These statistical measures provide insights of the central tendency and spread of temperature differences within the dataset. The negative mean implies a consistent cooling trend, while the standard deviation quantifies the extent to which individual temperature variations deviate from this average change. This information is instrumental in characterizing and understanding the thermal dynamics captured by the collected data.

Correlation Matrix Results:

- Temp1 vs. Temp2 (0.29):**
Weak positive correlation, indicating some influence of room temperature changes on the Top Left area.
- Temp1 vs. Temp3 (0.50):**
Moderate positive correlation, suggesting a connected thermal response between Top Left and Middle Right End.
- Temp1 vs. Temp4 (0.72):**
Strong positive correlation, indicating a consistent temperature pattern between Top Left and Middle.

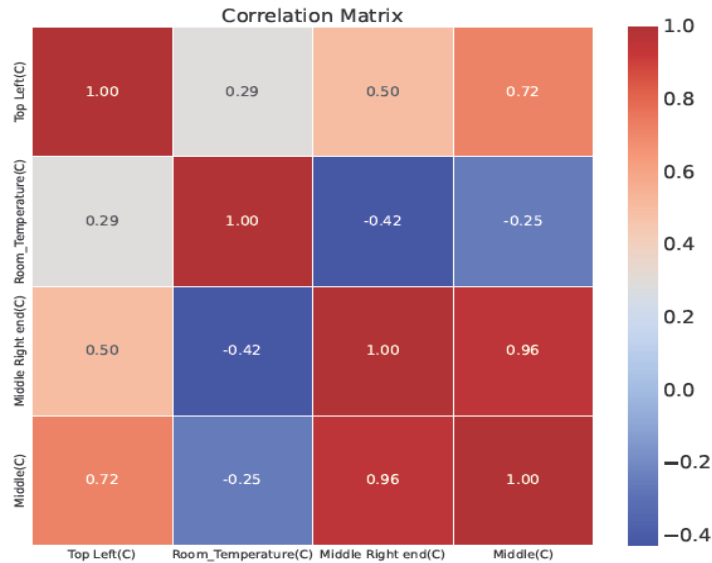


Fig. 2.30: Matrix representation of temperature region relationships.

- **Temp2 vs. Temp3 (-0.42):**

Moderate negative correlation, implying differential responses to external changes in Room Temperature and Middle Right End.

- **Temp3 vs. Temp4 (0.96):**

Very strong positive correlation, revealing a synchronized thermal behavior between the Middle Right End and Middle.

The results suggest that the box effectively maintains a constant temperature, especially in the region close to the Top Left probe. However, variations are observed in the Middle and Middle Right End areas. The correlation matrix indicates intricate relationships between the temperature profiles, with a significant influence of external changes on certain internal regions. Some interpretation from the results of the experiment –

- The Top Left probe, strategically placed for control, shows stable and consistent temperatures.
- Variations in the Middle and Middle Right End areas suggest potential challenges in achieving rapid temperature stabilization.
- The strong positive correlation between Temp3 and Temp4 indicates a synchronized response in maintaining a constant temperature in these two areas.

While the box demonstrates effective temperature control, further optimization may be considered for achieving quicker stability in all internal areas. Understanding the correlations helps identify areas with shared thermal behaviour and informs potential adjustments to enhance overall performance. In summary, the analysis provides a comprehensive overview of the temperature dynamics within the controlled environment, offering insights for fine-tuning the temperature control system.

2.3.3. Thermal expansion/contraction

We can also, find the coefficients –

The thermal coefficient of expansion (or contraction) can be calculated using the formula:

$$\text{Thermal Coefficient}(\alpha) = \frac{\text{Final Path Length} - \text{Initial Path Length}}{\text{Initial Path Length} \times (\text{Final Temperature} - \text{Initial Temperature})}$$

CHAPTER 2: SYSTEM OVERVIEW

i. For Stainless Steel 304

From the data collected, we have,

$$\text{Uncompensated or Initial Path Length(L1)} = 1.01375730\text{e+12 pm}$$

$$\text{Compensated or Final Path Length(L2)} = 1.01375583\text{e+12 pm}$$

$$\text{Initial Temperature(T1)} = 20.7 \text{ }^{\circ}\text{C}; \text{Final Temperature(T2)} = 20.5 \text{ }^{\circ}\text{C}$$

Plugging the values, we get, $\alpha = 7.25\text{e-06 K}^{-1}$. The mean coefficient of thermal expansion of Stainless Steel 304, the material used for Box2, is $17.25\text{e-06 }^{\circ}\text{C}$. This discrepancy could be due to the fact that we haven't taken into consideration the mounting materials. However, the values we obtained are reasonable and within the expected range given the complexity of our system.

ii. For Carbon Fibre Breadboard

From the data collected, we have,

$$\text{Uncompensated or Initial Path Length(L1)} = 5.896711\text{e+11 pm}$$

$$\text{Compensated or Final Path Length(L2)} = 5.869682\text{e+11 pm}$$

$$\text{Initial Temperature(T1)} = 26 \text{ }^{\circ}\text{C}; \text{Final Temperature(T2)} = 21 \text{ }^{\circ}\text{C}$$

Plugging these values into the formula, we get $\alpha = 0.12\text{e-06 }^{\circ}\text{C}$. This is not close to the mean coefficient of thermal expansion of [Carbon Fibre Breadboard](#), which is $-1\text{e-06 }^{\circ}\text{C}$. There are many types of carbon fibre available in the market, and their thermal expansion coefficients can range from -1 to 8, depending on how they are made. The manufacturer of our carbon fibre board claims a thermal expansion of 2.5×10^{-6} (mm/mm.K) at 273 K for a plane plate. One of the main caveats of these measurement results is that we have only considered the measurement in one direction. But the values obtained are reasonable as our system is quite complex.

This chapter provides a comprehensive overview of each system. It's crucial, especially for instrumentation projects, to understand the physical principles and practical results. In this chapter, we not only covered the technicalities of the system, but we also explored some of the diagnostic results, revealing insights into some of the undocumented features by the manufacturer. In the next chapter, we will discuss how these data were collected, what approach was used, and what algorithms were employed to obtain this data.

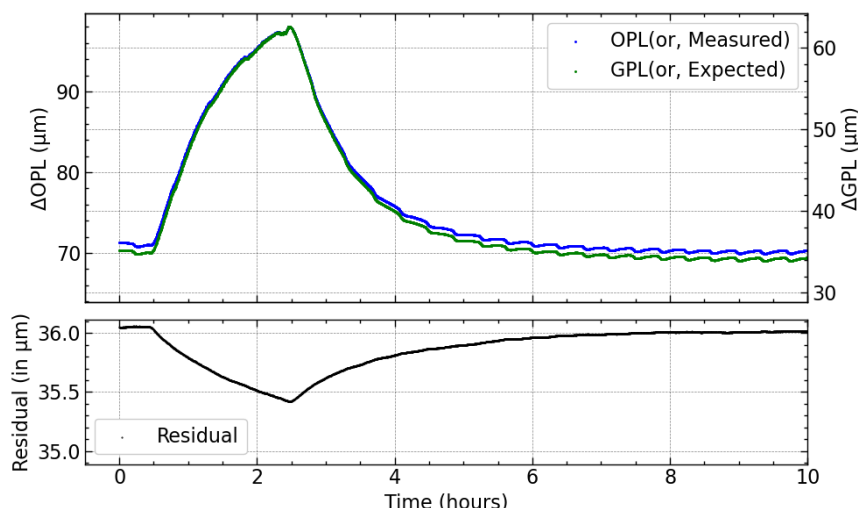


Fig. 2.31: Region 1 of the experiment, in order to determine the thermal expansion coefficient of the carbon fibre breadboard

Chapter 3

Methodology

This Chapter delves into the data collection methods used for the project. We explore the functionality of a singular control system, we will understand how our nested control system work and followed by air refraction compensation technique used as part of the project.

3.1. Control Systems

Single control system

The block diagram in Fig. showcases a closed-loop feedback control system, which is affected by external interferences such as temperature, pressure, and humidity. These factors have a direct impact on the optical path length within the system, specifically the distance between the IDS laser head and the retroreflector. Despite a defined expected path length, it is prone to changes due to environmental influences. The closed-loop feedback control system utilizes a structured approach in its data collection methodology to ensure optimum functionality. Its systematic process begins with the initiation phase, where commands are sent through the web interface to activate the system. The data acquisition stage utilizes various light sources such as the Thorium Argon Lamp, Sun, or a Star. Accurate measurements of displacement and environmental parameters are carried out using the Interferometer and BME680, respectively, with Python used for data processing. Following acquisition, the sensor data undergoes thorough processing, seamlessly integrating the Interferometer and BME680 data before being transmitted to the Control Unit. Next, the crucial step of spectrograph calibration takes place, involving precise adjustments to the Spectrograph. The calibration process for EXOhSPEC is tightly linked to its feedback loop, which operates at a rapid pace. Periodic evaluations are necessary to ensure the accuracy and functionality of the system. The outcome of calibration has a significant impact on the next steps taken. In the event of a successful calibration, the system proceeds with data acquisition. On the other hand, if calibration falls short, adjustments are promptly made, and the process is repeated. This rigorous methodology is followed for the desired number of iterations, resulting in a robust and well-calibrated closed-loop feedback system for EXOhSPEC. Important thing to note here, we haven't implemented the calibration of the spectrograph with respect to feedback signal, which is a part of future work.

The summary or the key steps in the closed-loop feedback control system:

- Initiation - Here we start the data collection process to brief we have temperature sensor BME680 which will collect raw data from the Arduino IDE and send it to our Jupyter notebook, a Python interpreter at 9600 baud rate. A code is provided in the Appendix. We use a delay of about 10 seconds within the code to avoid collecting bad data(meaning, unsynchronous data). According to the datasheet of BME680, the response time of the humidity sensor is 8 seconds, however, the response time for other sensors is less than 1 second. This buffer delay helps us to collect.
- Data Acquisition - We use the PT104, a 4-channel temperature sensor module. This uses PicoLog software which collects data that is temperature in degrees Celsius at 1Hz and stores it in a CSV file.

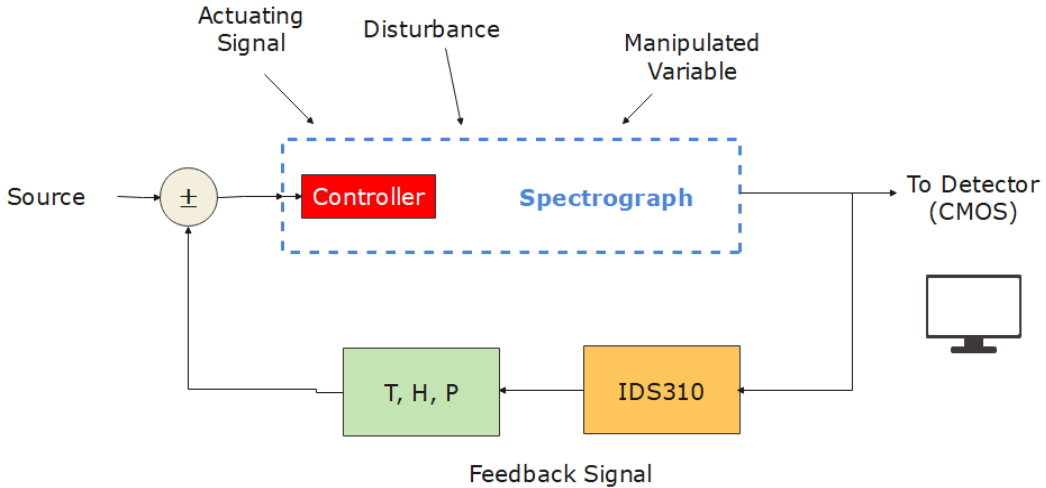


Fig. 3.1: Flow chart of Singular control system

- Sensor Data Processing - We collect data from the laser interferometer using Python Jupyter notebook with a set of code. We make sure once the IDS is connected with an IP address, the first step is optical alignment for the laser system before starting taking readings. We took the data at different sampling frequency during the initial phase, but now we will use the lowest sampling frequency rate, as radial velocity methods are a long-term observation, hence we do not need to take data from these components in the control system at a higher frequency sampling rate, as it will give anomalies in the data adding noise. As it's a complex instrument due to different components present, we need to take care of the internal heating issues, so a better sampling rate will give us better quality of data and the overall system would work in an efficient condition. The current sampling rate setting is we are collecting data every 10 seconds.
- Feedback Loop - We use a multiprocessing tool package of Python. The idea is to collect data from all the individual proprietary software at one particular time. What we found is that there was a buffer of roughly about 2 seconds to get data from all the components, therefore, a 10-second delay is appropriate for our case. A details about feedback loop, its need has been discussed in chapter 4 with experimental results.

Nested Control system

In the preceding section, we elucidated the fundamental operations of a singular control system. This system operates by meticulously collecting data from every potential source that could introduce disturbances in the optical path. Once we receive a signal indicative of such a disturbance, we utilize this as a feedback mechanism to our system, enabling us to retrieve the geometric path length. This process is a testament to the principles of feedback control systems, a cornerstone in the field of control engineering. However, the reality of our project is more complex, involving not just one, but three interrelated control systems that work in unison. The first control system is associated with the outer box, or Box 2. This box is ingeniously designed to isolate the system from the room temperature or the external environment. Its primary purpose is to maintain a constant temperature inside the box, a critical factor in ensuring the stability and accuracy of our spectrograph readings. The second control system is associated with the smaller box, which will be placed inside the larger box. The main consideration here is again the temperature control unit, which will regulate the temperature to our further requirements and minimize temperature fluctuation in the overall system. This nested

approach to temperature control is a novel method to ensure the stability of our system, even in the face of significant external temperature variations. The third control system is the most crucial one. As we have seen in previous chapters, environmental variations cause changes in the optical path. For example, an increase in temperature increases the optical path, while a decrease reduces it. We also observed that the optical path follows a trend of pressure. Now that we understand these disturbances, we can feed a receivable signal into our third control system as feedback to retrace the geometric path length. Studying the optical path length and maintaining a constant optical path throughout the setup will result in a more efficient spectrograph. Once we have the feedback signal, which we will explore in more detail in Chapter 4, we can use this signal to retrieve our optical path.

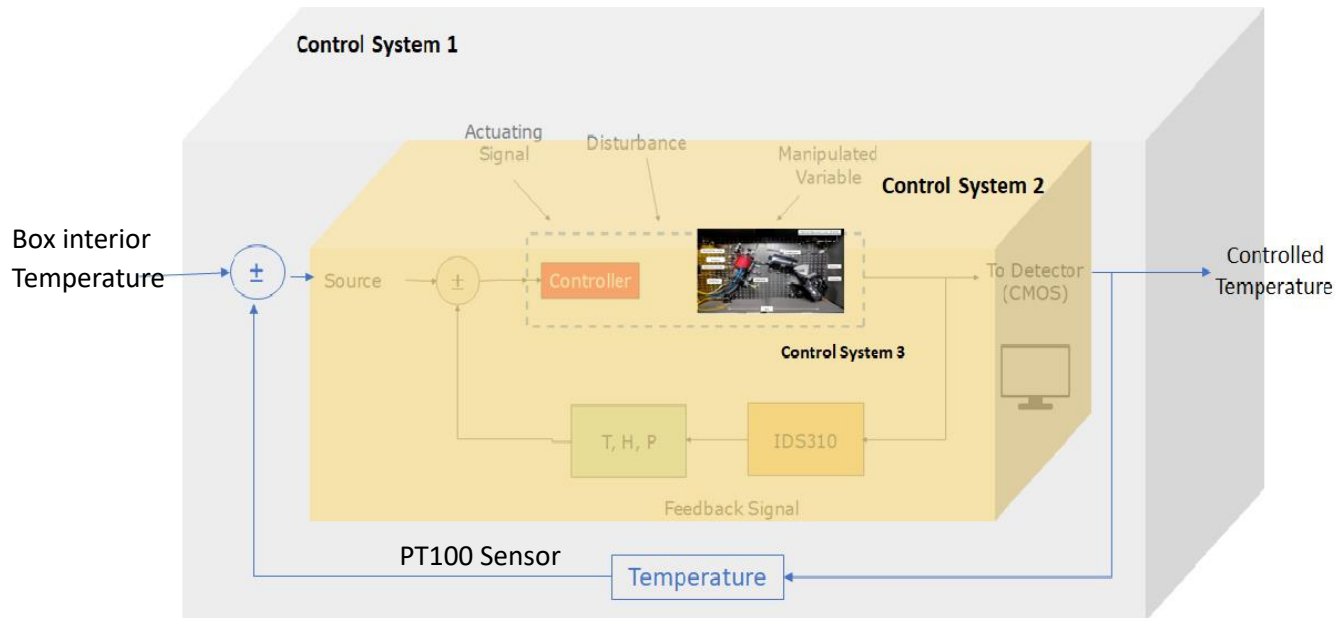


Fig. 3.2: Overview of the multi-layered control systems implemented in the project, emphasizing temperature stabilization, environmental isolation, and feedback mechanisms for maintaining optical path length stability.

3.2. Air Refraction Compensation

As previously discussed in Section 1.4, we will now delve deeper into the utilization of air refraction as a compensatory mechanism. The refractive index of air, denoted by η , has been the subject of extensive research and is a critical factor in our project. To elucidate the process, a flowchart will be provided in the subsequent sections. Our research project employs a variety of sensors and a laser interferometer to gather local values of temperature (in degrees Celsius), atmospheric pressure (in hPa), humidity (in percentage), and displacement measurement (Uncompensated, in picometers). The majority of environmental compensation units utilize a modified empirical equation to compensate for these factors. Using Equation 1, we calculate the refractive index (η). The next step involves the calculation of Lcompensated, which essentially represents the geometric optical path length. The formula for this calculation is as follows:

$$L_{\text{compensated}} = L_{\text{uncompensated}} \times \frac{\eta_{\text{standard air}}}{\eta_{\text{air}}} = L_{\text{uncompensated}} \times \frac{1.0002713938}{\eta_{\text{air}}}$$

CHAPTER 3: METHODOLOGY

This equation allows us to adjust the uncompensated displacement measurement (Uncompensated) based on the ratio of the refractive index of standard air to the refractive index of the local air (η_{air}).

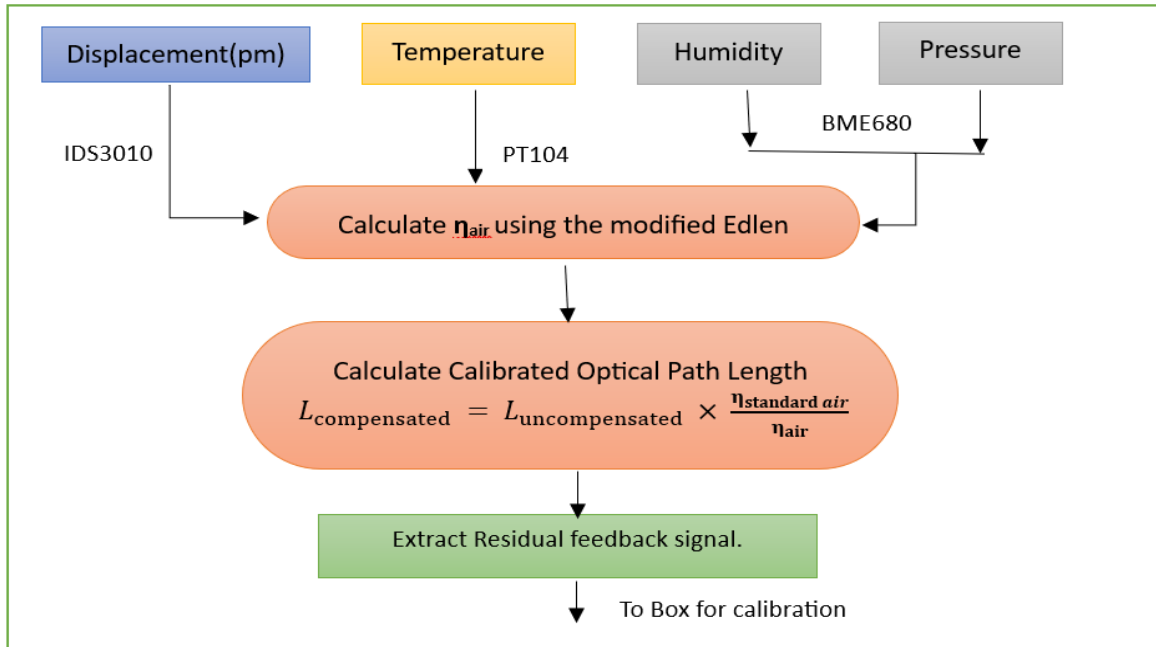


Fig. 3.3: Algorithm to extract the residual signal, which will be implemented as a feedback signal in the control system.

Following this, we extract the residual signal. The residual signal is essentially the difference between the measured value and the expected value. This difference serves as a feedback signal, providing us with valuable information about any discrepancies in our measurements. A comprehensive explanation of this process will be provided in Chapter 4.

By understanding and compensating for the effects of local environmental conditions on our measurements, we can significantly improve the accuracy and reliability of our research outcomes. This approach underscores the importance of considering environmental factors in scientific research and highlights the potential of using air refraction as a compensatory mechanism. In conclusion, this chapter provides a comprehensive overview of the nested control system, detailing the methods and mechanisms involved in maintaining the stability of our environmental control boxes. This understanding is crucial for the successful operation and efficiency of our spectrograph. The knowledge shared in this chapter is crucial for replicating our work, enhancing the system, or even applying these principles to other related fields. Stay tuned as we unravel the intricacies of our control systems and data collection methodologies.

Chapter 4

Experimental Data Analysis, Results and Discussion

In this chapter, we will discuss the key results obtained during our experiments and interpret the data. We focus on the role of the feedback signal in our closed-loop control system. This signal, representing the discrepancy between the measured and expected values of the geometric optical path length, is crucial for system accuracy. By adjusting the system input based on this feedback, we align the measured geometric path length closer to the expected optical path, enhancing the precision of our research outcomes. This feedback mechanism emphasizes the importance of feedback in scientific research and its potential in improving measurement accuracy. Further details will be discussed in the following sections.

In this section, we present the results of an experiment conducted in our laboratory to observe the behavior of our system over a duration of 1 hour. The experiment involved collecting temperature (T), humidity (H), and pressure (P) readings using the BME680 sensor. Subsequently, we applied a calibration technique to derive the expected geometric path length (GPL) from the measured Optical Path Length (OPL), also known as raw data or uncompensated data. The BME680 sensor operated at a sampling rate of 1 second, while the IDS operated at a sampling frequency of 1 KHz. Figure (a) illustrates the temporal evolution of temperature, humidity, and atmospheric pressure, while Figure (b) depicts the change in measured optical path length in picometres (pm) over time. Notably, the temperature and humidity remained relatively constant, indicating stable conditions maintained by the temperature controller in Box 1 prior to the experiment. However, a slight change of 1 hPa was observed in the pressure plot. The IDS and retroreflector were positioned at an approximate optical path length of 60 cm. Interestingly, the optical path length follows the trend of the pressure curve, indicating a correlation between pressure variations and changes in optical path length. Additionally, anomalies in the dataset, observed as rectangular box, were attributed to manual noise introduced as mechanical vibrations. Given the high-frequency operation of the IDS, such noise can be amplified. To mitigate this, a smoothing moving average technique with a window size of 100 was employed in the lower panel of Figure (b) to filter out high-frequency noise. Furthermore, a smaller window size of 30 was used in the upper panel to detect high-frequency noise caused by manual intervention during the experiment.

The subsequent plot illustrates the application of the calibration algorithm to determine the expected OPL or GPL over time. The calibration algorithm effectively compensates for air refraction, resulting in a nearly flat curve as expected. The variation in OPL was approximately 1.4 pm, while the GPL variation was around 0.5 pm.

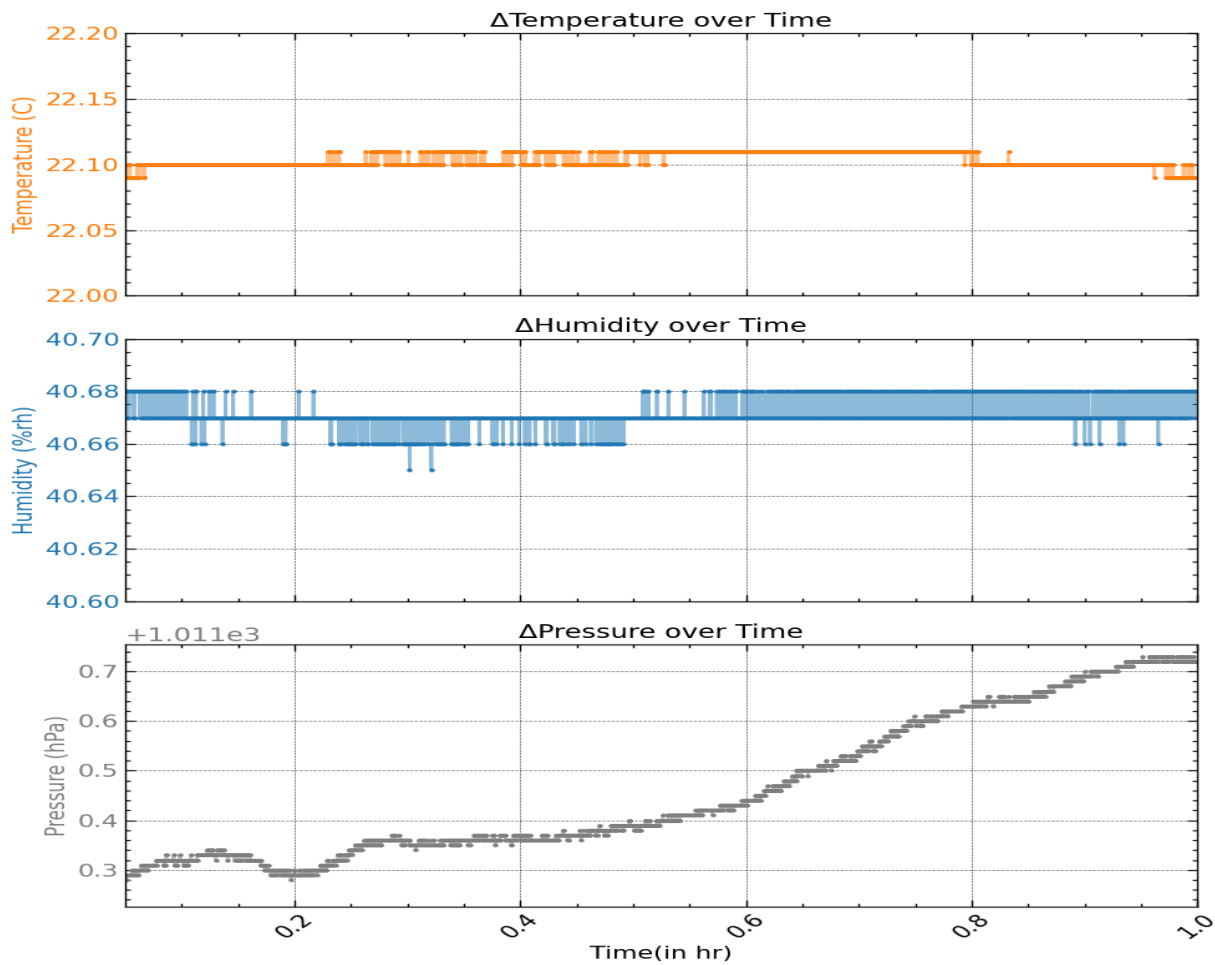


Fig. 4.1: Plot of T , H , P profile over time, highlighting constant temperature and humidity despite atmospheric pressure changes.

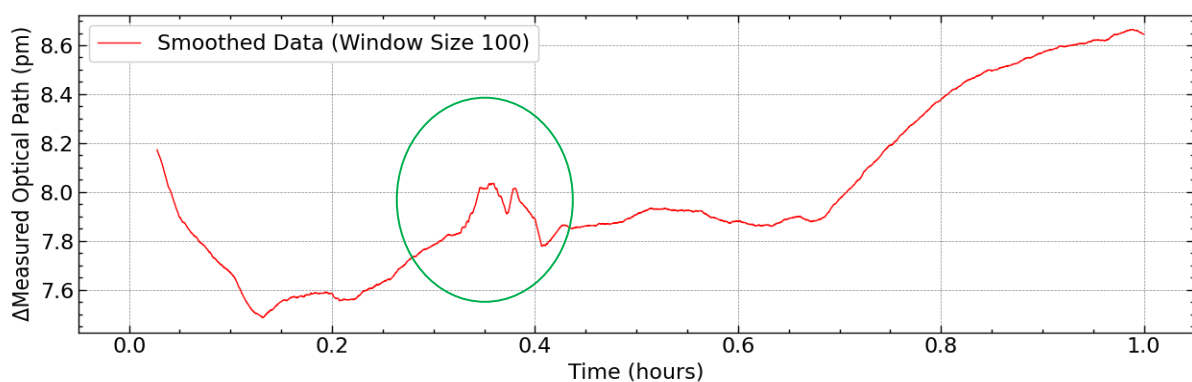
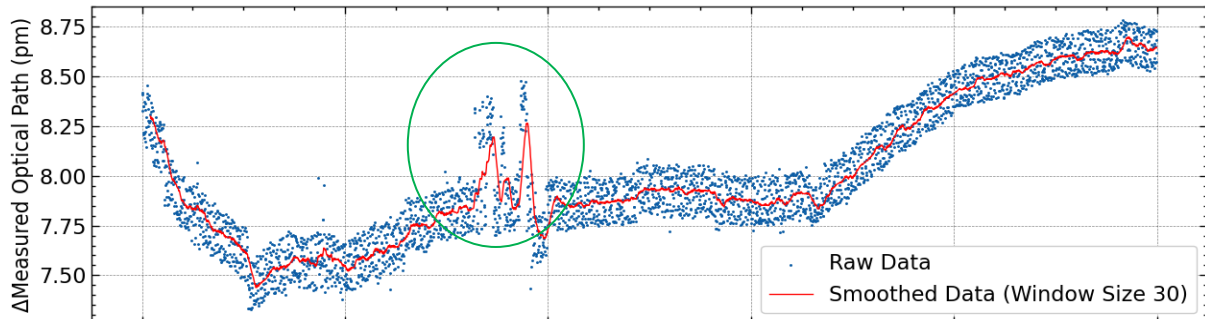


Fig. 4.2: Plot of Measured optical path length vs. time, showcasing its direct proportionality to pressure changes and noise reduction with moving average.

CHAPTER 4: EXPERIMENTAL RESULTS AND DISCUSSIONS

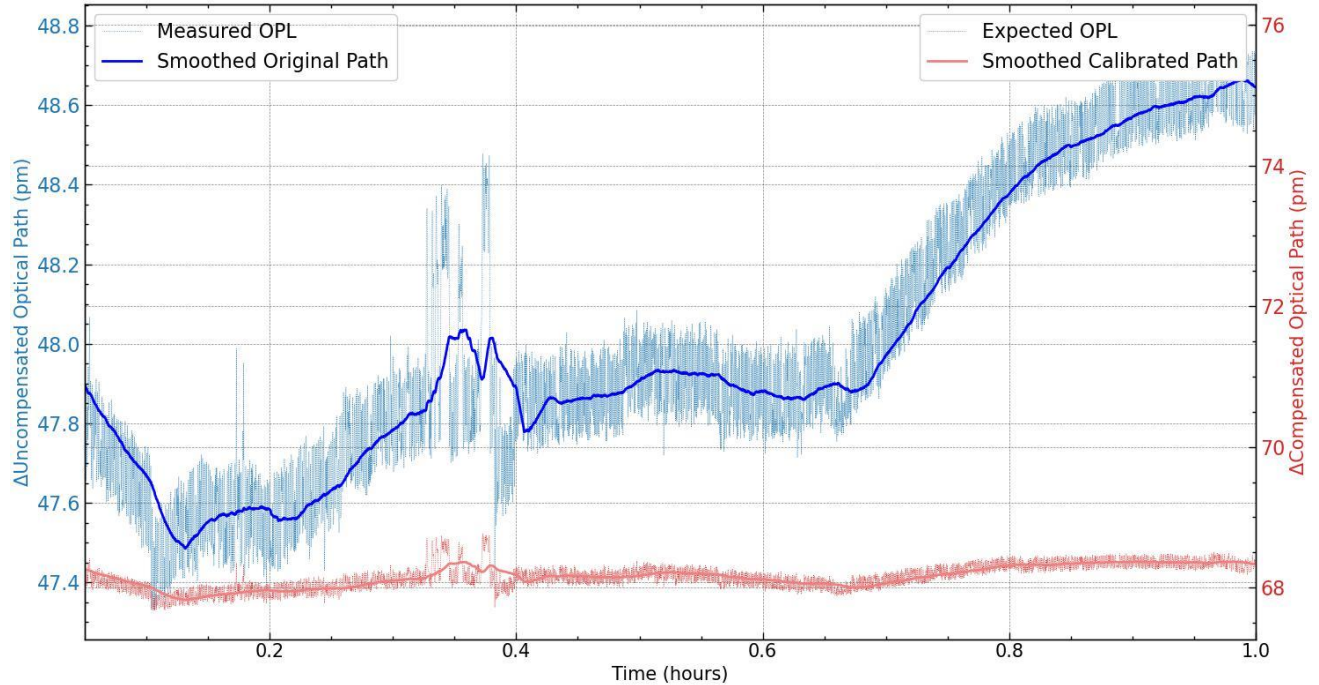


Fig. 4.3: Plot of Uncompensated path length and compensated path length with respect to time in hours, a smooth function of window size = 100 been used as a low pass filter, the compensated path is a flat getting rid of T,H,P components.

Moving on to the next section, we delve into another significant experiment conducted to gain further insights into the system and associated techniques. Building upon the discussion in Section 2.2.2 regarding the comparison between BME680 and ECU, we now focus on the optical path length. The plot in Figure () depicts the positional data collected during the experiment, which spanned over 160 hours within a confined space. Initially, for approximately 5 hours, the temperature control system in Box 1 was deactivated, resulting in a noticeable rise in optical path measurement due to a temperature increase of approximately 3.5 degrees Celsius. However, upon reactivating the temperature control, which took less than 2 hours to stabilize, the system exhibited a relatively constant temperature. From the dataset obtained, three key analyses can be conducted. Firstly, within the yellow shaded region, the thermal expansion of the carbon fiber breadboard, on which the instrument was placed, can be investigated in detail as discussed in Section 2.3.3. Secondly, focusing on the grey shaded region, it is observed that both the GPL and OPL remained constant for approximately 100 hours. Lastly, detailed modeling analysis can be performed to understand the relationship between the feedback signal, or residual signal, and its dependencies on the temperature, pressure, and humidity profiles.

CHAPTER 4: EXPERIMENTAL RESULTS AND DISCUSSIONS

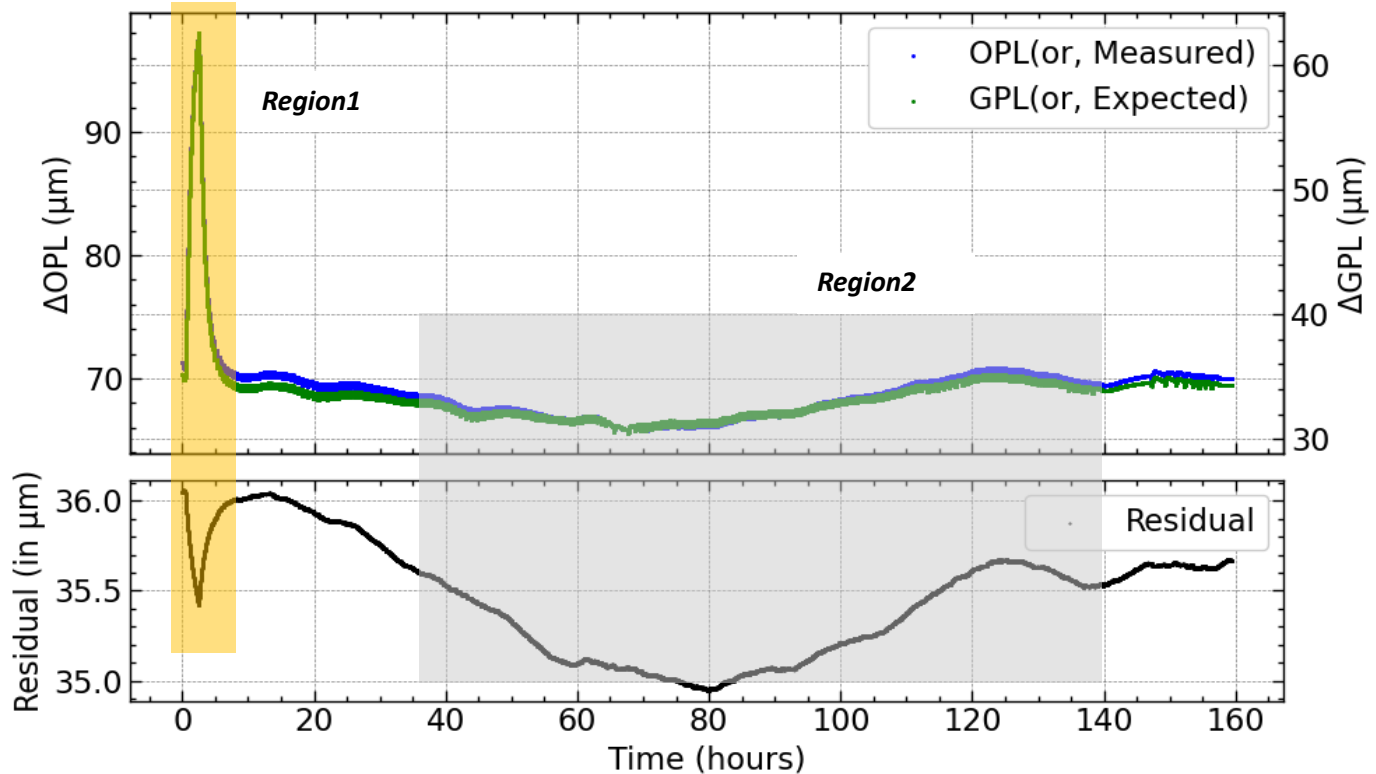


Fig. 4.4: Experiment conducted in Box1, plot is change in OPL and GPL with respect to house, lower panel is the residual signal, however the region of focus is region1 and region 2, suggests two different nature/ behaviour of the system.

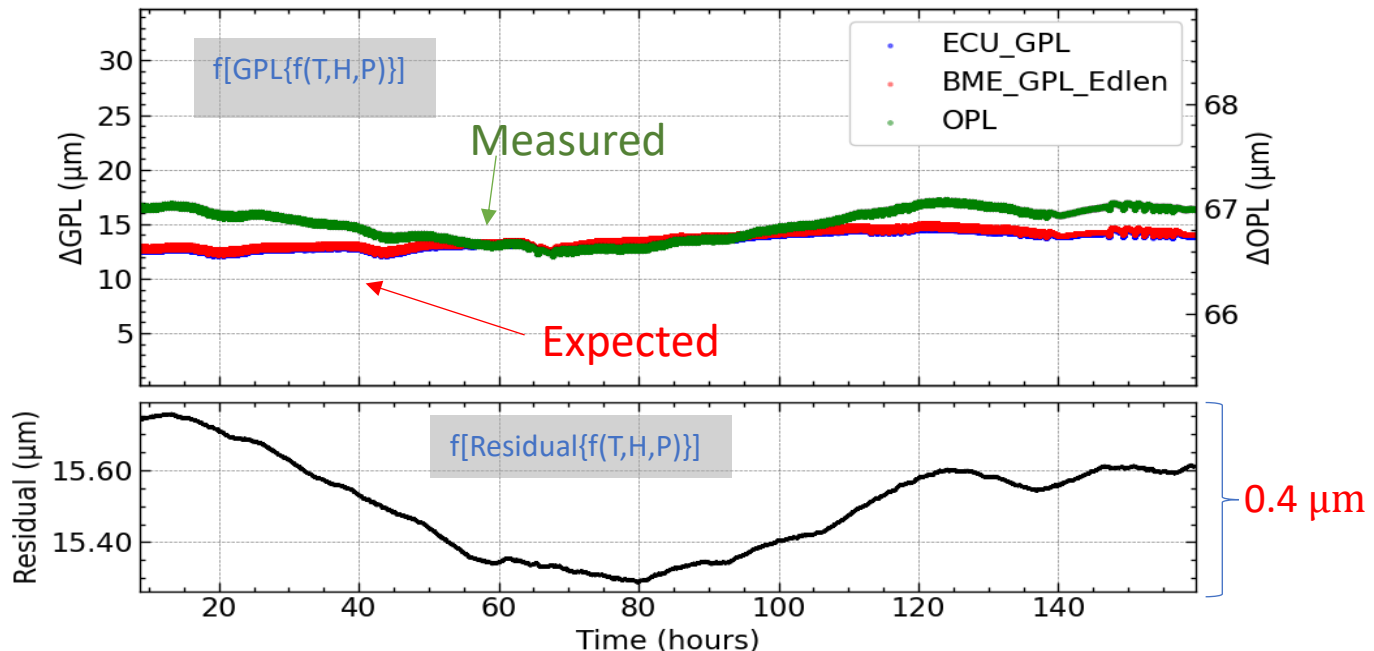


Fig. 4.5: Plot showing the the GPL vs OPL using the empirical model, has compensated the pressure term.

CHAPTER 4: EXPERIMENTAL RESULTS AND DISCUSSIONS

Transitioning, we introduce the residual analysis, beginning with the code snippet utilized to calculate the refractive index using the Ciddor-Edlen formula and subsequently determining the calibrated or compensated path. While the implementation of the reverse model yields results indicative of the system's behavior, it is noted that the algorithm may not be entirely accurate. For instance, a discrepancy arises when comparing the observed change in temperature resulting in a 20-micrometer change in OPL to the extracted values suggesting a 0.4-degree Celsius temperature change. However, this discrepancy is deemed reasonable considering the interdependence of temperature, pressure, and humidity on the optical path length.

Extracting Temperature, Pressure, and Humidity from Residuals:

In the research conducted, a unique approach was taken to understand the variations in temperature, pressure, and humidity. This was achieved by creating a residual signal, which is the difference between the measured and expected parameters. The residual signal, therefore, contains the negative values of these parameters.

```
# Function to calculate calibrated path (GPL)
def calculate_calibrated_path(OPL, refractive_index_standard, refractive_index_air):
    return OPL / refractive_index_air

# Function to calculate refractive index
def calculate_refractive_index(P, T, H):
    return 1 + (( 1.786e-4 * P * 0.1) / (273.5 + T)) - (1.5e-11 * H * (T ** 2 + 160)) # hPa to kPa: 1hPa = 0.1kPa
```

The concept of a reverse model was introduced, which essentially retraces the steps of the original model. This reverse model is instrumental in determining the specific changes in temperature, pressure, and humidity at any given time. These values, whether they exhibit a positive or negative gradient, can then be used as a feedback signal.

This feedback signal has the potential to be integrated into a control system to compensate for the path length. However, at this stage, this feedback signal has not been implemented into the control system. Despite this, there is a clear understanding of the steps that need to be taken based on the analysis conducted. The reverse model, therefore, serves as a tool for retracing the steps of the original model, using a set of different values to achieve a specific path length. This innovative approach opens up new possibilities for understanding and controlling changes in temperature, pressure, and humidity. It lays the groundwork for future research and potential applications in various fields. Using optimization techniques to minimize the difference between the observed residual and the residual calculated using the forward model with input parameters (T, P, H).

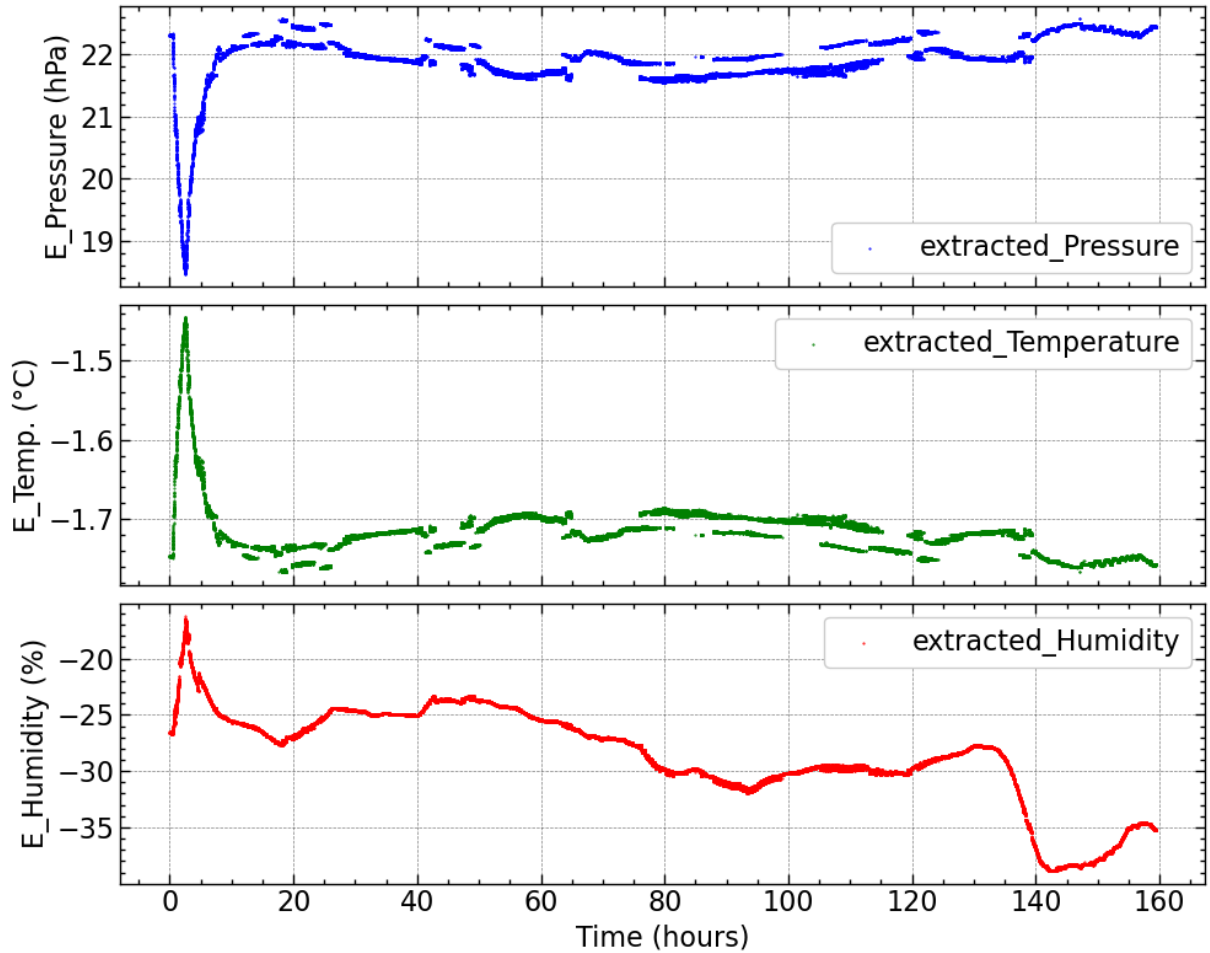


Fig. 4.6: Extracted T, H, P changes using reverse model, potential feedback signal for control system implementation.

Finding Relationships Between Parameters:

Investigating the relationships between pressure change, temperature change, and humidity change with respect to optical path length (OPL).

Temperature constant: $T = 20^\circ\text{C}$

CHAPTER 4: EXPERIMENTAL RESULTS AND DISCUSSIONS

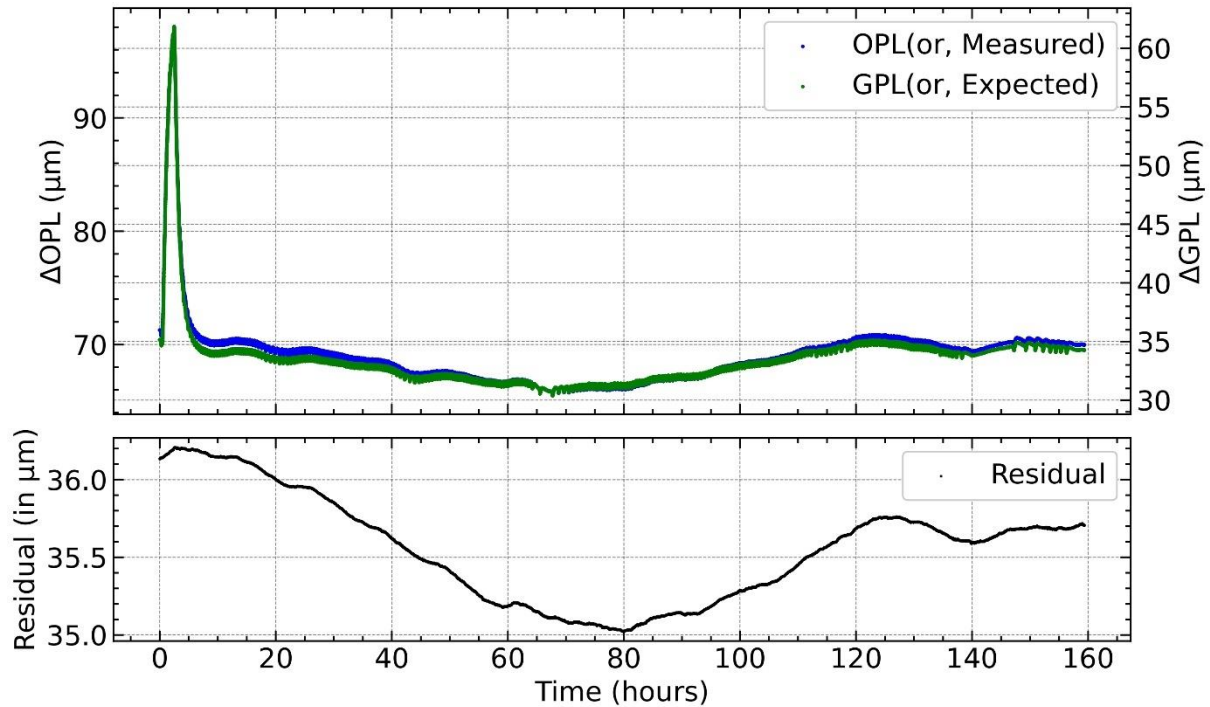


Fig. 4.7: Plot showing Pressure dominates when the temperature is kept constant

Temperature + pressure constant: $T = 20^\circ C$, $P = 1013.25 \text{ hPa}$

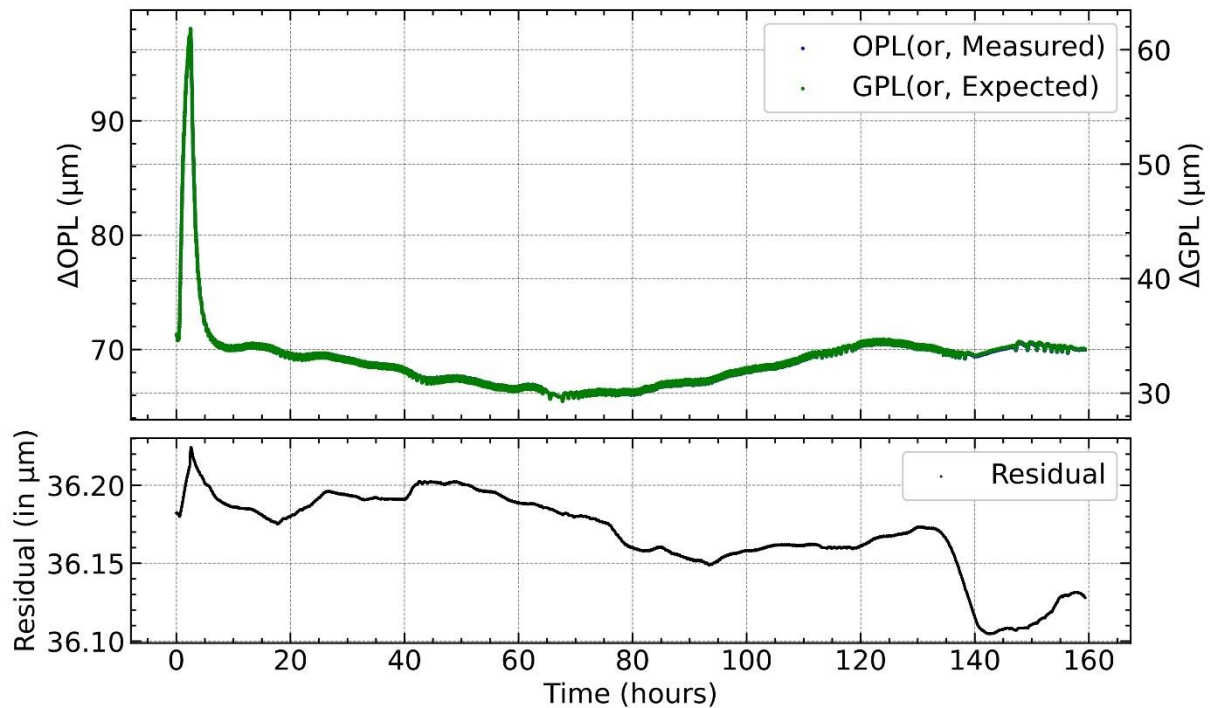


Fig. 4.8: Plot showing Humidity Dominates when the T and P is constant

CHAPTER 4: EXPERIMENTAL RESULTS AND DISCUSSIONS

Pressure Constant: $P = 1013.25 \text{ hPa}$

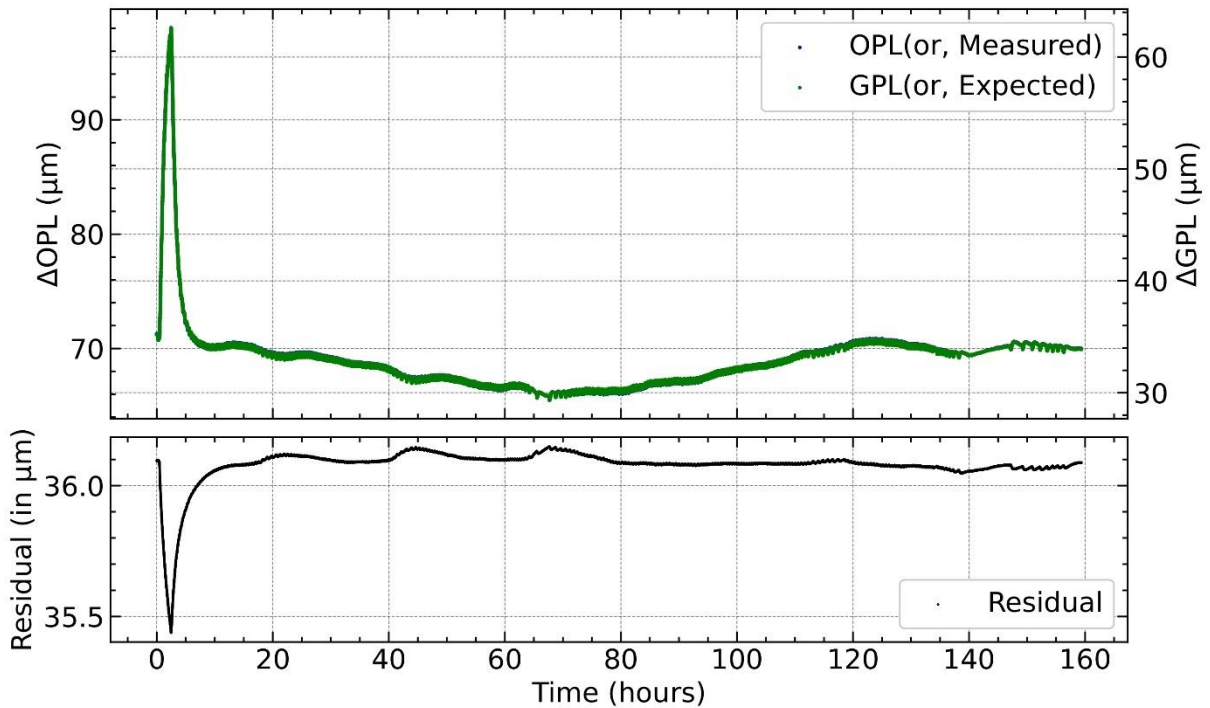


Fig. 4.9: Plot showing temperature dominates when pressure is constant

Humidity constant:

- i. 0%

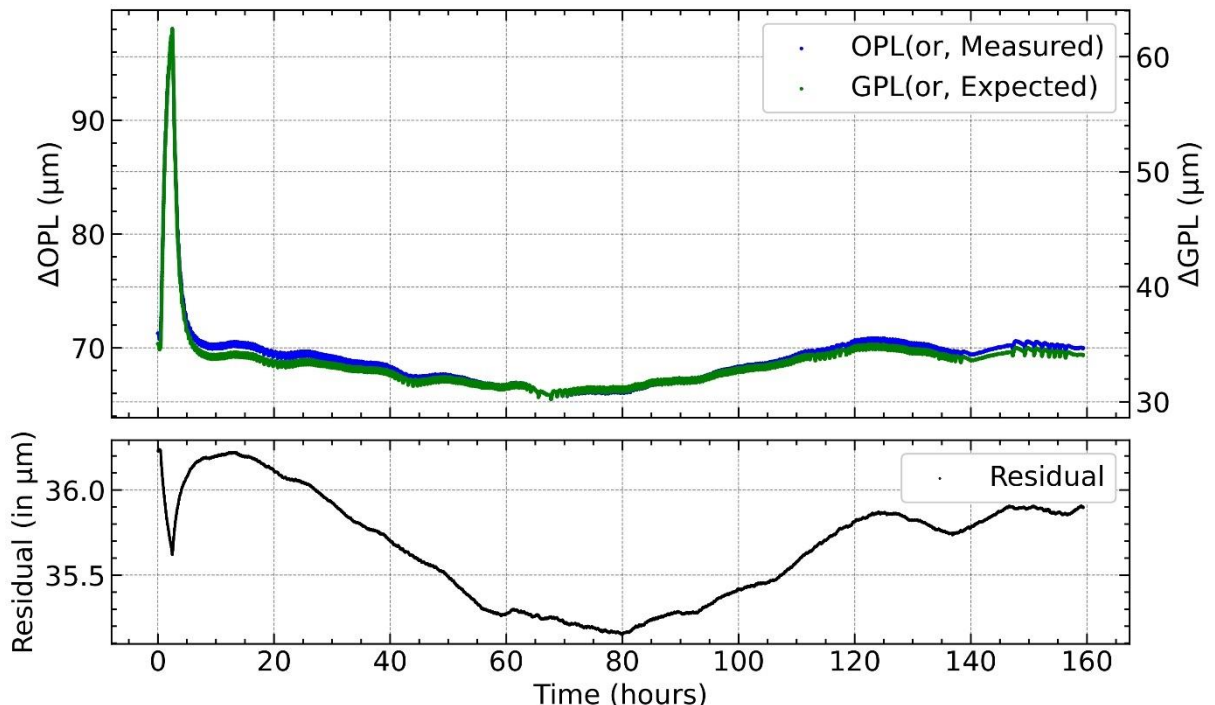
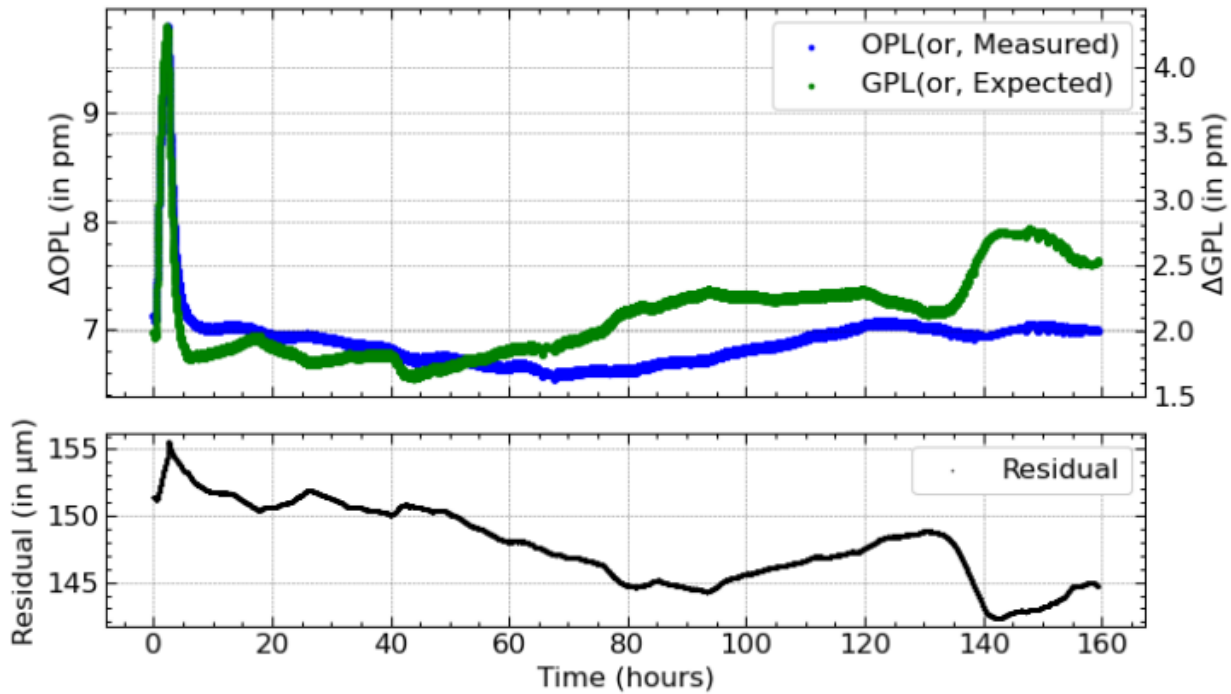


Fig. 4.10: Plot showing pressure dominates when humidity is at 0% while the T and P are varying.

CHAPTER 4: EXPERIMENTAL RESULTS AND DISCUSSIONS

ii. 50%



iii. 100%

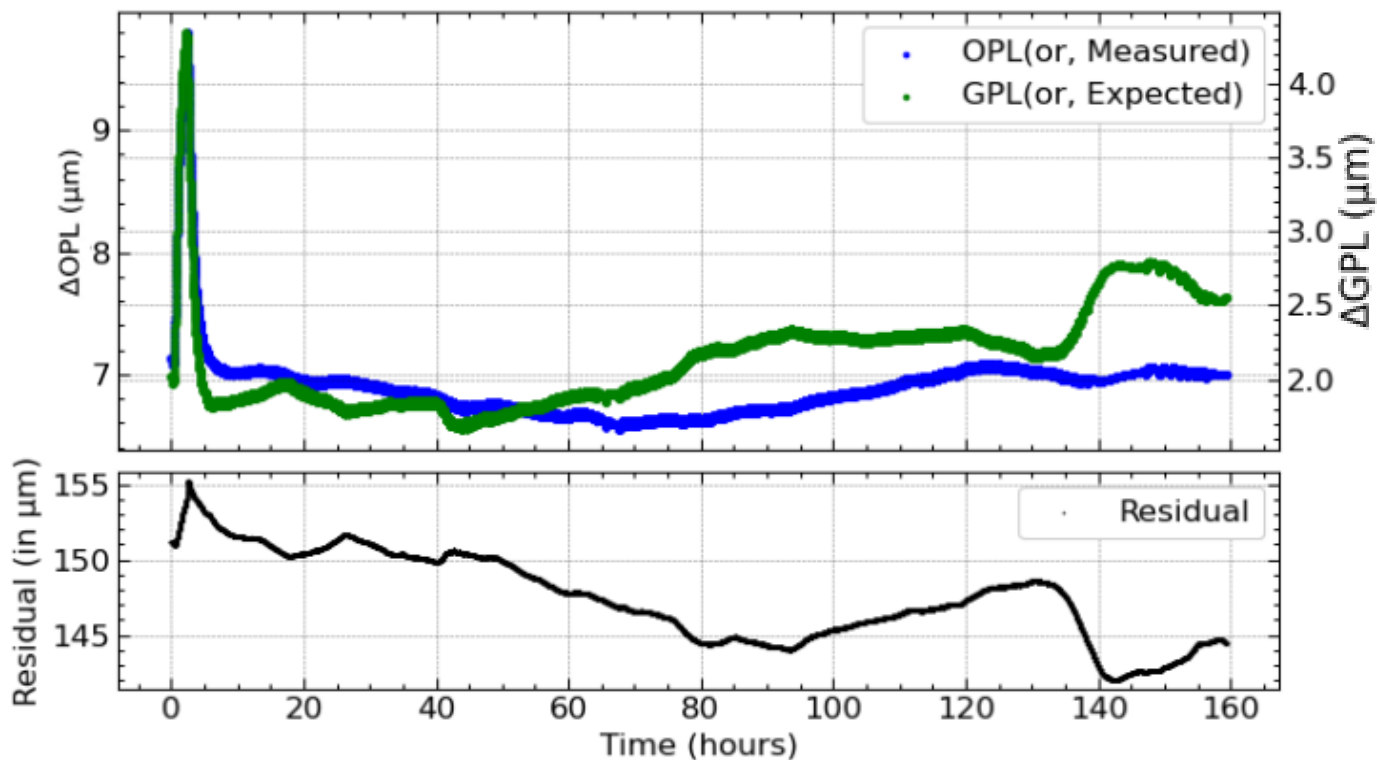


Fig. 4.11: Plot showing pressure dominates when humidity is at 50% while the T and P are varying, hence the Model is not appropriate for RH greater than 50%, the GPL increases

CHAPTER 4: EXPERIMENTAL RESULTS AND DISCUSSIONS

By analyzing the residual signal under various conditions, several key observations are made:

- Pressure variations dominate the residual signal when temperature remains constant.
- Humidity variations significantly influence the residual signal when temperature and pressure are constant.
- A constant pressure results in a nearly flat residual signal, indicating a tight correlation between OPL and GPL.
- Humidity variations exhibit distinct effects on the residual signal at different humidity levels, necessitating the consideration of alternative models for humidity levels exceeding 50%.

Region 2 Analysis

Now, let's delve into region 2 of the plot. In this timeframe, spanning from the 20th hour to the 140th hour, we observe minimal fluctuations in the path length measurements, indicating a high level of stability within the system. The upper panel (a) illustrates a variation in the Optical Path Length (OPL) of approximately 4 micrometers. However, the predicted Geometric Path Length (GPL) exhibits less variation, measuring less than 2 micrometers. The difference between the residual curves amounts to approximately 2 micrometers. During this period, the pressure experienced a nominal change of approximately 30 hPa, while the temperature remained constant at around 20.5 degrees Celsius. There was a slight fluctuation in humidity, around 20%.

This dynamic underscores the precision required for our system to maintain a flat curve of GPL. Despite minor adjustments necessary due to the thermal coefficient of expansion and contraction of materials, the overall impact on the scale from micrometers to picometers is negligible. Considering our long-term observational plan, akin to radial velocity observation, implementing a closed feedback loop utilizing these feedback signals ensures the stability of our system without the need for vacuum chambers. This approach safeguards the integrity of the high-resolution spectrum acquired for a given target, eliminating distortion.

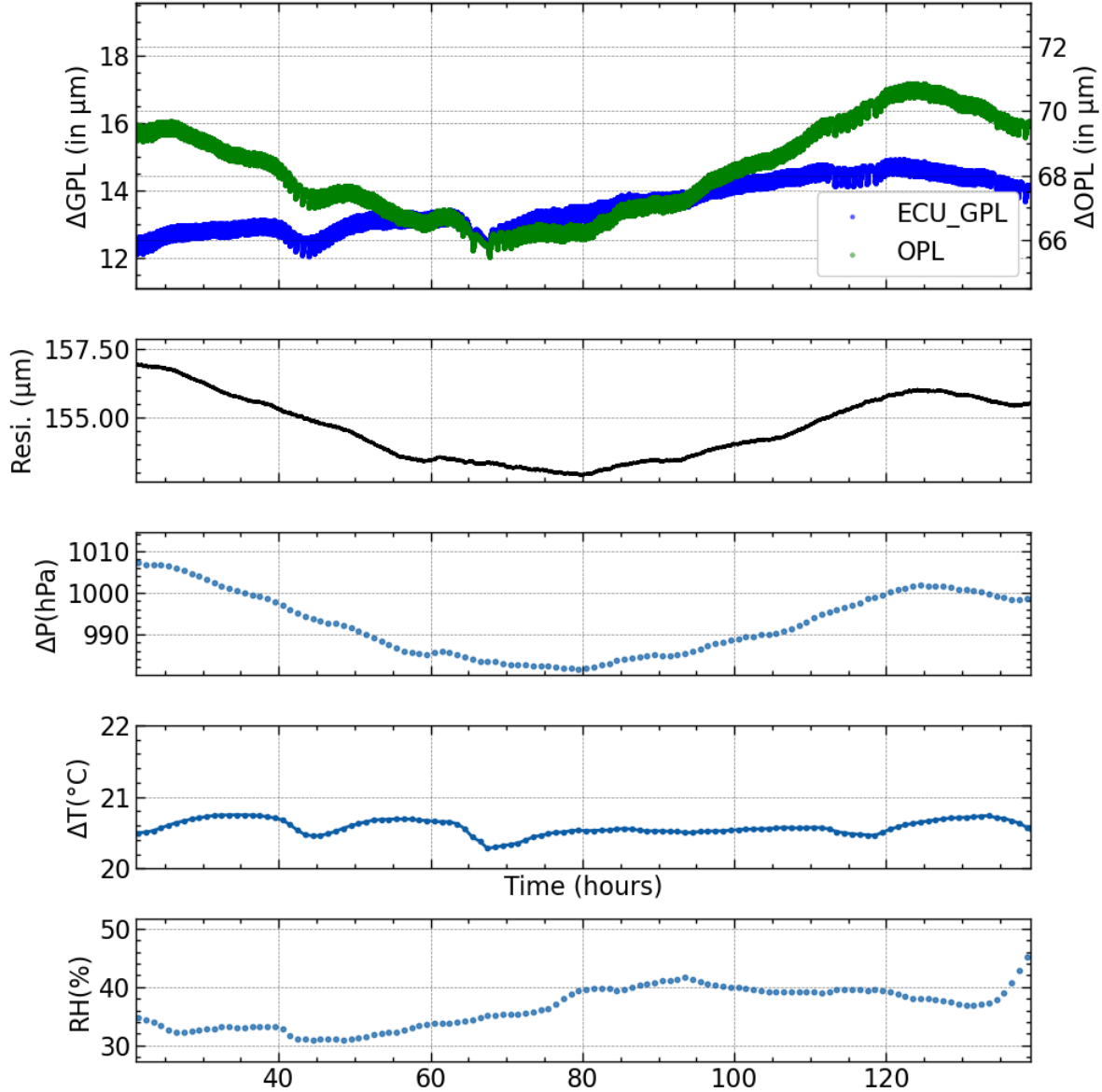


Fig. 4.12: In Region 2, spanning from the 20th to the 140th hour, minimal fluctuations in path length measurements reveal system stability. The upper panel shows Optical Path Length (OPL) variation of 4 micrometers, while the Geometric Path Length (GPL) remains under 2 micrometers. Pressure experienced nominal change (~30 hPa) with constant temperature (~ 20.5°C) and slight humidity fluctuation (~20%).

Chapter 5

Conclusion and Future Work

This section will summarize the key findings from the experimental analyses, draw conclusions regarding the performance of the closed-loop feedback control system, and propose avenues for future research and enhancements to EXOhSPEC.

In conclusion, the research project outlined in this report addresses the challenges associated with achieving high-resolution radial velocity spectroscopy, particularly in the quest for identifying habitable Earth-like exoplanets. The evolution of spectrographs for achieving a precision of 10cm/s, has been accompanied by numerous obstacles, ranging from instrument stability affected by environmental factors like temperature, pressure, and humidity, to challenges in wavelength calibrations and detector stability. To overcome these challenges, conventional approaches often resort to constructing vacuum environments in which the Rv spectrograph fits. However, our project proposes an alternative solution: the implementation of a closed-loop feedback control system. This system serves as an active self-stabilizing component, offering a viable alternative to vacuum chambers for HRVS.

5.1. Summary of Findings

Our research delves into the critical aspects of environmental stability, focusing on the refractive index of air as a tool for correcting optical path length variations. By leveraging the modified Edlen equation, we can accurately calculate the compensated path length, essential for precise measurements in our system.

Chapter 1 provided insights into the importance of closed-loop feedback control systems, followed by a detailed examination of refractive index properties and their impact on optical path length correction. In Chapter 2, we explored the various components utilized in our project, highlighting key insights gained from diagnostic experiments. Notably, our findings underscored the dominant influence of temperature, humidity, and pressure on optical path length variations, underscoring the necessity of a feedback control system.

Chapter 3 elucidated the methodology employed for data collection, with a particular focus on single and nested control systems. Additionally, we discussed the air refraction compensation technique used to determine the compensated optical path length, essential for precise measurements.

Finally, Chapter 4 presented crucial results gleaned from various experiments. Our analysis revealed that 1hpa change in atmospheric pressure corresponded to a 0.4 micrometer change in optical path length. Furthermore, we explored the efficacy of different models in predicting geometric path length and discussed the potential application of residual signals for feedback control.

5.2. Limitations and Areas of Improvement

Despite the significant progress made, several limitations and areas for improvement remain. Firstly, the implementation of the closed-loop feedback control system within Box 2 revealed challenges associated with air density gradients and temperature differentials within the enclosure. Future work should focus on mitigating these effects through the installation of low-noise fans or improvements to the PID loop. Additionally, while the current focus has been on temperature control, future developments should explore the integration of pressure stability mechanisms into the system. This will ensure consistent pressure levels within the enclosure, further enhancing measurement accuracy and system stability.

5.3. Future Developments and Enhancements

Moving forward, several avenues for future development and enhancements have been identified. Implementing the feedback signal derived from empirical formulas such as the Ciddor and Edlen equations will be crucial for refining the closed-loop control system. Integration of the system within Box 2 and assessing its stability with the developed algorithm represents a significant next step. Furthermore, the integration of a pressure valve mechanism into Box 2 will be essential for maintaining consistent pressure levels, thereby further enhancing measurement accuracy. Furthermore, the reference to web development in this context implies the incorporation of technology solutions for control or monitoring in real-time. A more dynamic and effective study environment may be ensured by implementing a web-based interface, which would also make the experiment more accessible and allow for remote monitoring. Essentially, the experiments lay the groundwork for future research and a better comprehension of complex systems and how they react to external inputs. It is hoped that the planned experiments with layered arrangements and smaller enclosures would reveal new aspects of the behavior of the system. Concurrently, the incorporation of web development elements emphasizes how crucial it is to integrate technical developments for faster data management and experimentation. In addition, implementation of ESP8266 NodeMCU⁶ which is an IOT (Internet of Things device) will help us to monitor the system in real-time. During the initial stages of the project, efforts were made towards designing a web page(Appendix D) for real-time monitoring, but completion was hindered by time constraints. However, this remains a critical aspect for future development, as real-time monitoring is essential for ensuring accurate feedback signals and responsive control.

In summary, the findings of this research project lay the groundwork for future advancements in high-resolution radial velocity Spectrograph. By addressing the limitations identified and pursuing avenues for enhancement with innovative approach, low cost, we can further improve the accuracy, stability, and adaptability of spectroscopic measurements, ultimately contributing to our understanding of the universe and the search for habitable exoplanets.

⁶ [NODEMCU ESP8266](#)

Bibliography

- Ciddor, P. E., 1996. Refractive index of air: new equations for the visible and near infrared. *Applied optics*, Volume 35, pp. 1566-1573.
- Edlen, B., 1966. The refractive index of air. *Metrologia*, Volume 2, p. 71.
- Ralph Elmer Wilson. “General catalogue of stellar radial velocities”, volume 601. Carnegie Institution of Washington Washington, DC, 1953.
- Debra A Fischer, Guillem Anglada-Escude, Pamela Arriagada, Roman V Baluev, Jacob L Bean, Francois Bouchy, Lars A Buchhave, Thorsten Carroll, Abhijit Chakraborty, Justin R Crepp, et al. “State of the field: extreme precision radial velocities”. *Publications of the Astronomical Society of the Pacific*, 128(964):066001, 2016.
- Otto Struve. Proposal for a project of high-precision stellar radial velocity work. *The Observatory*, Vol. 72, p. 199-200 (1952), 72:199–200, 1952.
- Michel Mayor and Didier Queloz. “A Jupiter-mass companion to a solar-type star”. *nature*, 378 (6555):355–359, 1995.
- Sbordone, L., Salaris, M., Weiss, A., and Cassisi, S. Photometric signatures of multiple stellar populations in galactic globular clusters. *AA*, 534:A9, 2011. doi: 10.1051/0004-6361/201116714. URL <https://doi.org/10.1051/0004-6361/201116714>.
- Sarah Logsdon, Marsha Wolf, Mark Everett, Qian Gong, Eli Golub, Jesus Valdenebro, Emily Hunting, Kurt Jaehnig, Jessica Klusmeyer, Dan Li, Ming Liang, Wilson Liu, William McBride, Michael McElwain, Jeffrey Percival, Jayadev Rajagopal, Susan Ridgway, Heidi Schweiker, Michael Smith, and Jason Wright. “The NEID precision radial velocity spectrometer: Commissioning of the port adapter”. 12 2020.
- C. Jurgenson, D. Fischer, T. McCracken, D. Sawyer, A. Szymkowiak, A. Davis, G. Muller, and F. Santoro. “Expres: a next-generation rv spectrograph in the search for earth-like worlds” . In Christopher J. Evans, Luc Simard, and Hideki Takami, editors, *Ground-based and Airborne Instrumentation for Astronomy VI*. SPIE, August 2016. doi: 10.1117/12.2233002. URL <http://dx.doi.org/10.1117/12.2233002>.
- Pepe, Stefano Cristiani, R Rebolo, NC Santos, H Dekker, A Cabral, Paolo Di Marcantonio, P Figueira, G Lo Curto, C Lovis, et al. Espresso at vlt-on-sky performance and first results. *Astronomy & Astrophysics*, 645:A96, 2021.
- R Paul Butler and Geoffrey W Marcy. “A planet orbiting 47 ursae majoris”. *The Astrophysical Journal*, 464(2):L153, 1996.
- Andreas Seifahrt, Julian Stürmer, Jacob L Bean, and Christian Schwab. “Maroon-x: a radial velocity spectrograph for the gemini observatory”. In *Ground-based and Airborne Instrumentation for Astronomy VII*, volume 10702, pages 1930–1939. SPIE, 2018.

Andrei Tokovinin, Debra A. Fischer, Marco Bonati, Matthew J. Giguere, Peter Moore, Christian Schwab, Julien F. P. Spronck, and Andrew Szymkowiak. Chiron—a fiber fed spectrometer for precise radial velocities. *Publications of the Astronomical Society of the Pacific*, 125(933):1336–1347, November 2013. ISSN 1538-3873. doi: 10.1086/674012. URL <http://dx.doi.org/10.1086/674012>.

Rosario Cosentino, Christophe Lovis, Francesco Pepe, Andrew Collier Cameron, David W Latham, Emilio Molinari, Stephane Udry, Naidu Bezawada, Martin Black, Andy Born, et al. Harps-n: the new planet hunter at tng. In *Ground-based and airborne instrumentation for astronomy iv*, volume 8446, pages 657–676. SPIE, 2012.

Christophe Lovis, Debra Fischer, et al. Radial velocity techniques for exoplanets. *Exoplanets*, pages 27–53, 2010.

Jonay I González Hernández, Francesco Pepe, Paolo Molaro, and Nuno Santos. Espresso on vlt: An instrument for exoplanet research. *arXiv preprint arXiv:1711.05250*, 2017

Andreas Quirrenbach, PJ Amado, H Mandel, JA Caballero, R Mundt, I Ribas, A Reiners, M Abril, J Aceituno, C Afonso, et al. Carmenes: Calar alto high-resolution search for m dwarfs with exoEarths with a near-infrared echelle spectrograph. In *Ground-based and Airborne Instrumentation for Astronomy III*, volume 7735, pages 455–468. SPIE, 2010.

GR Ricker, JN Winn, R Vanderspek, DW Latham, G ‘A Bakos, JL Bean, ZK Berta-Thompson, TM Brown, L Buchhave, and NR Butler. *Journal of astronomical telescopes, instruments, and systems*, 2015.

Paolo Di Marcantonio, Alessio Zanutta, Alessandro Marconi, Frédéric Baron, et al. Andes, the high resolution spectrograph for the elt: project management and system engineering approaches for mastering its preliminary design phase. In *Modeling, Systems Engineering, and Project Management for Astronomy X*, volume 12187, pages 9–23. SPIE, 2022.

Jones et. al., “A small actively controlled high-resolution spectrograph based on off-the-shelf components.” *Publications of the Astronomical Society of the Pacific*, 133(1020):025001, jan 2021. doi: 10.1088/1538-3873/abc7ee. URL <https://dx.doi.org/10.1088/1538-3873/abc7ee>.

Appendix

A. Arduino Code

```
#include <Wire.h>
#include <SPI.h>
#include <Adafruit_Sensor.h>
#include "Adafruit_BME680.h"
#define BME_SCK 13
#define BME_MISO 12
#define BME_MOSI 11
#define BME_CS 10

#define SEALEVELPRESSURE_HPA (1013.25)

Adafruit_BME680 bme; // I2C

const byte buffer_size = 64;
char received_chars[buffer_size];
char temp_chars[buffer_size];
char message_raw[buffer_size] = {0};
long integer_raw = 0;
boolean new_data = false;

void setup() {
    Serial.begin(9600);
    //Serial.println("BME680");
    while (!Serial);
    if (!bme.begin()) {
        Serial.println("Could not find a valid BME680 sensor, check wiring!");
        while (1);
    }
    // Set up oversampling and filter initialization
    bme.setTemperatureOversampling(BME680_OS_8X);
    bme.setHumidityOversampling(BME680_OS_8X);
    bme.setPressureOversampling(BME680_OS_16X);
    bme.setIIRFilterSize(BME680_FILTER_SIZE_3);
}

void loop() {
    receive_input();
    if (new_data == true) {
        strcpy(temp_chars, received_chars);
        parse_data();
        process_data();
        //print_input();
    }
}

void receive_input() {
    static byte index = 0;
    static boolean in_progress = false;
```

```

char start_char = '@';
char end_char = '#';
char raw;

while (Serial.available() > 0 && new_data == false) {
    raw = Serial.read();
    if (in_progress == true) {
        if (raw != end_char) {
            received_chars[index] = raw;
            index++;
            if (index >= buffer_size) {
                index = buffer_size - 1;
            }
        }
    } else {
        received_chars[index] = '\0';
        in_progress = false;
        index = 0;
        new_data = true;
    }
} else if (raw == start_char) {
    in_progress = true;
}
}

void parse_data() {
    char * strtok_index_;
    strtok_index_ = strtok(temp_chars, ":");
    strcpy(message_raw, strtok_index_);
    strtok_index_ = strtok(NULL, ":");
    integer_raw = atol(strtok_index_);
}

void process_data() {
    if (! bme.performReading()) {
        Serial.println("Failed to perform reading :(");
        return;
    }
    if (message_raw[0] == 'g') {
        Serial.print(bme.temperature);
        Serial.print(",");
        Serial.print(bme.humidity);
        Serial.print(",");
        Serial.println(bme.pressure/100.0);
    }
    new_data = false;
}

void print_input() {
    Serial.print("@");
    Serial.print(received_chars);
    Serial.println('#');
}

```

B. Python Code

<https://github.com/Biswajit1999/Master-Thesis-2024>

This github repositories comprise of all the codes used for the data analysis, however the data will be provided on request.

C. Experiment: IDS3010 + BME680 integrated in the box2

Aim: To check the environmental factors of the outer box.

Theory: (Relative Humidity and Temperature Relationship) As temperature increases, air can hold more moisture. If the amount of water vapor remains constant and temperature rises, relative humidity decreases. Conversely, as temperature decreases, relative humidity increases. The experiment was conducted for 60 hours. In the experiment the geometric optical length is kept being 1.0140260695880001 m.

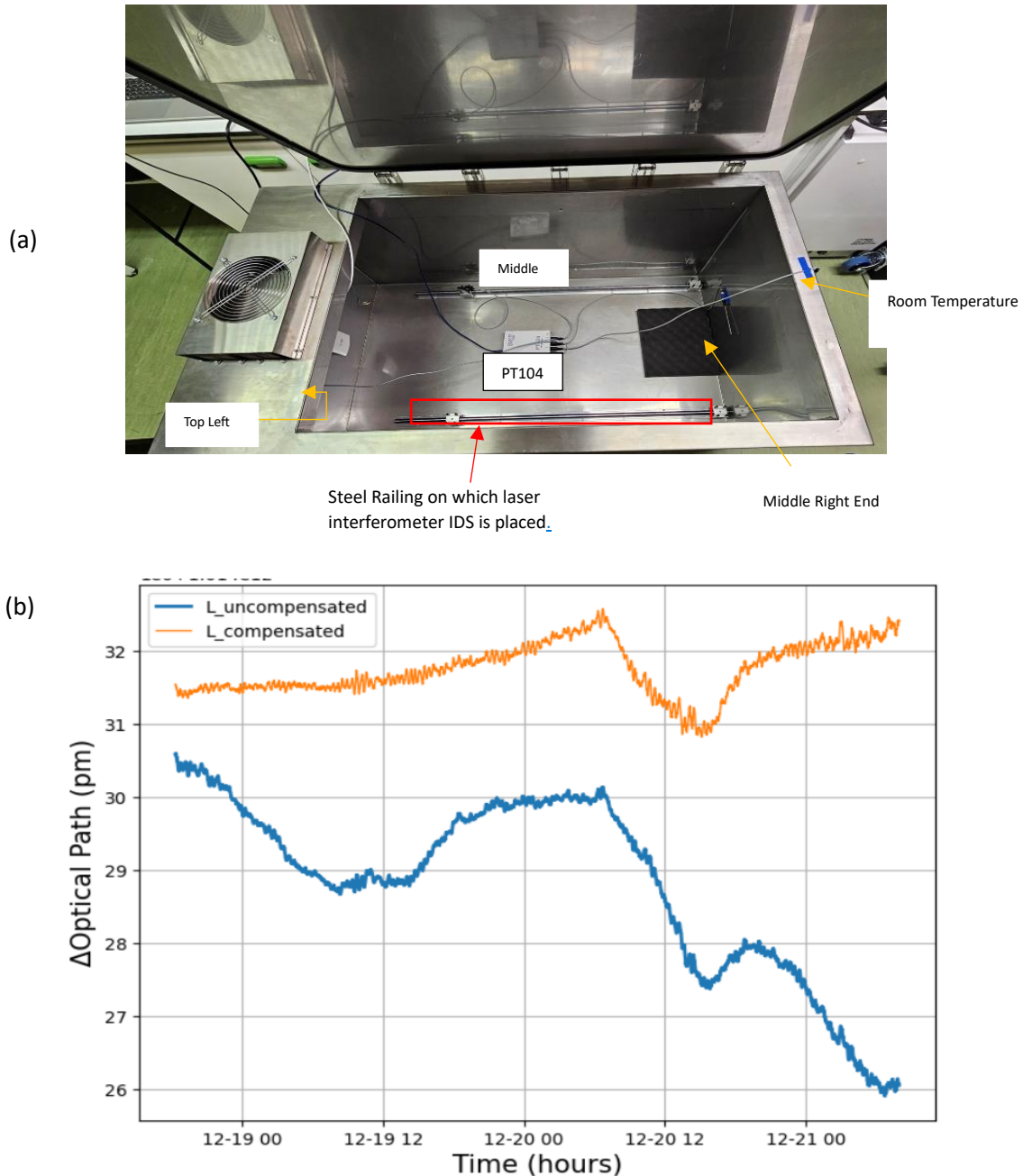
Result and Discussion: The principal aim of the experiment was to obtain a thorough understanding of the actions of a regulated environment, indicated by a specific box. In particular, the analysis of the long-term changes in the optical path was the main focus. A deliberate binning strategy was used in the first plot (a) to improve the visualisation of the data, with averaged points offering a more lucid depiction. This made it easier to see different patterns of temperature at different places both inside and outside the box. Interestingly, the temperature plot showed stable conditions inside the box with noticeable variations when the outside air conditioning was adjusted. One noteworthy finding was the delayed normalisation of temperature, which suggested possible problems with the values of the Proportional-Integral-Derivative (PID) loop that control the system's heat regulation.

Following shifting to plot (c), the investigation examined data on temperature, humidity, and pressure that were collected from the BME680 sensor. A contour map was created by strategically binning this dataset, which provided insightful information about the temporal and spatial distribution of humidity. The contour map that was created was essential in determining the system's physical state at particular points in time, and it made a substantial contribution to the improvement of the calibration procedures. Subsequent research concentrated on analysing the changes in the optical paths—both compensated and uncompensated—and brought attention to the significant effects of pressure and temperature. Although the corrected path was able to reduce the effects of changes in humidity and pressure, it was difficult to deal with changes in temperature. The possible mechanical flaws associated with the thermal expansion and contraction of the support railing under the laser interferometer were identified as the cause of this disparity. This mechanical problem, which was determined not to be immediately resolved, offered possible fixes that ranged from modifying the PID loop parameters to investigating structural changes, including switching to a carbon fibre board.

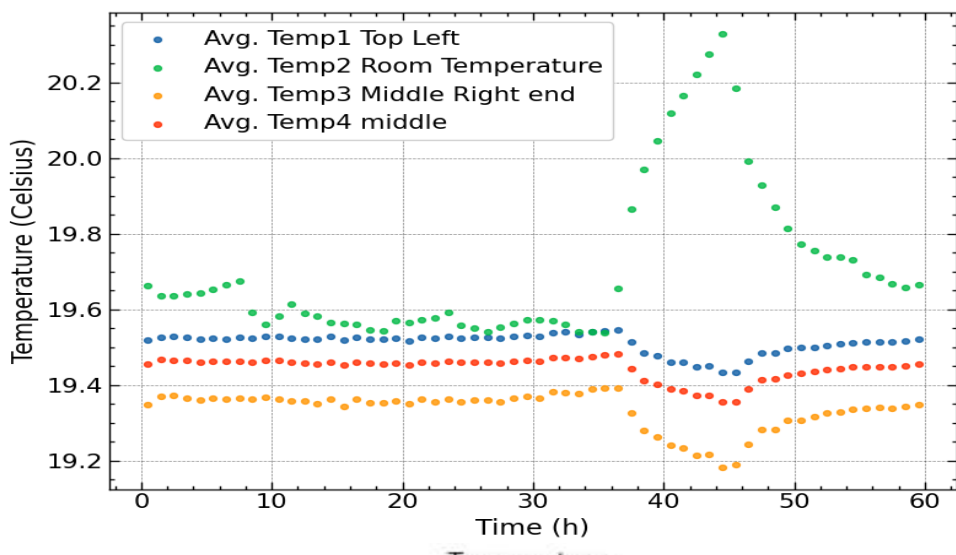
Equations essential to the calibration procedure were presented in Appendix B, highlighting the complex balancing needed to take a variety of environmental influences into consideration. A coefficient of thermal expansion that closely matched the material

composition of the box—Stainless Steel 304—was obtained by additional calculations in Appendix C. This alignment made the case stronger for comprehending and taking care of the mechanical factors influencing the accuracy of the experiment.

In conclusion, the experiment yielded important insights into the complex interactions between environmental variables in addition to accomplishing its main objective of determining how well the empirical formula calibrates. The results emphasised the necessity of all-encompassing remedies and the iterative nature of experimental refinement to guarantee the dependability of outcomes under various circumstances.



(c)



(d)

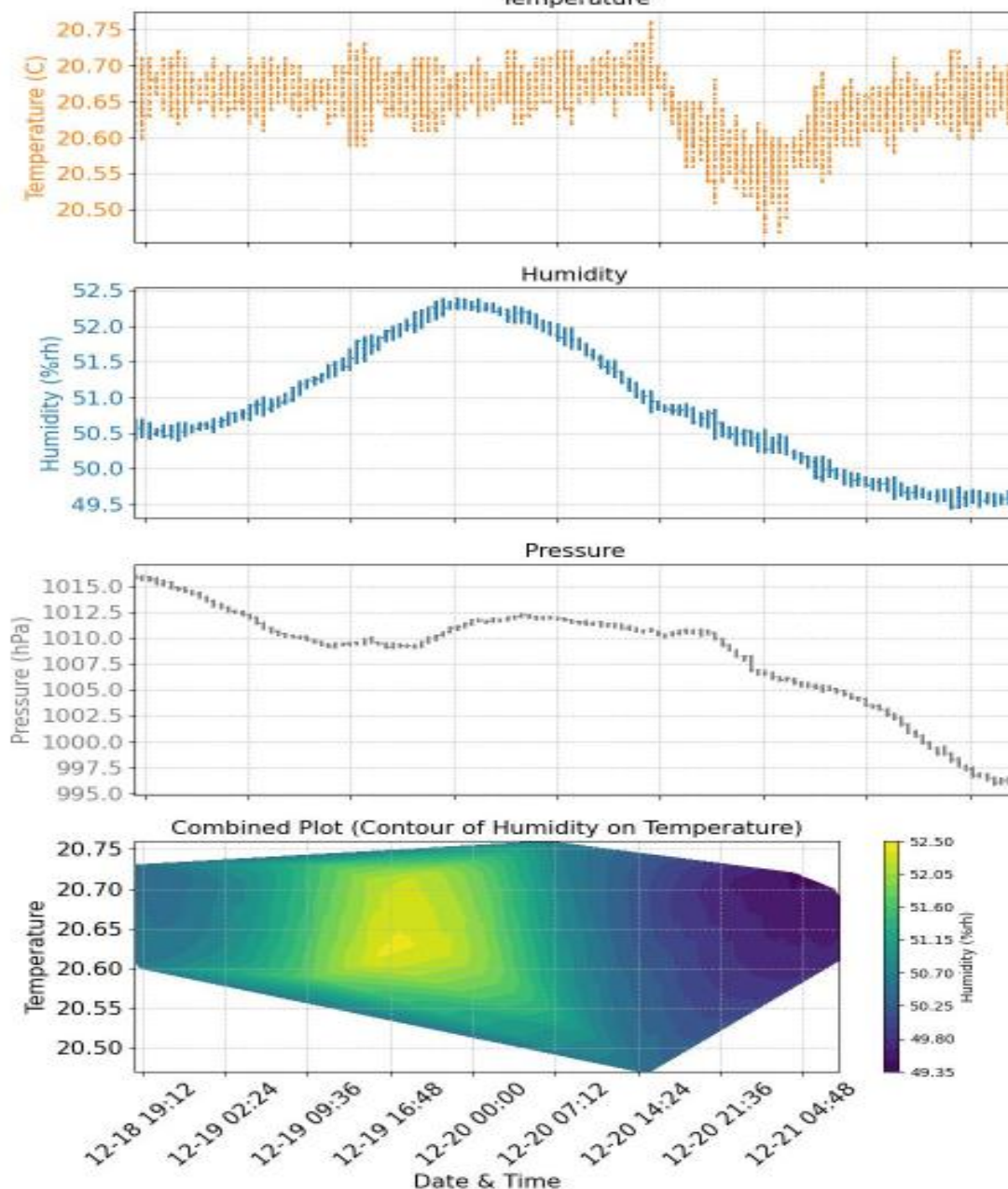


Figure 11. (a)Interior setup of Box2, (b)Temperature variation over time by PT104 sensor ,
(c)Change in optical path(pm) over time(d) Temperature, Pressure and Humidity variation over Time, and Contour plot of Temperature over Humidity

PID Values	Box 1(Fast Model)	Box 2 (Slow Model)
Kp (%/C)	1800	266.4335
Ti[s]	320	909.9076
Td	280	0
D Part Damping	0.001	0.3

Table: Recommended PID Values for Temperature Control in TEC software for Box 1 and Box 2.

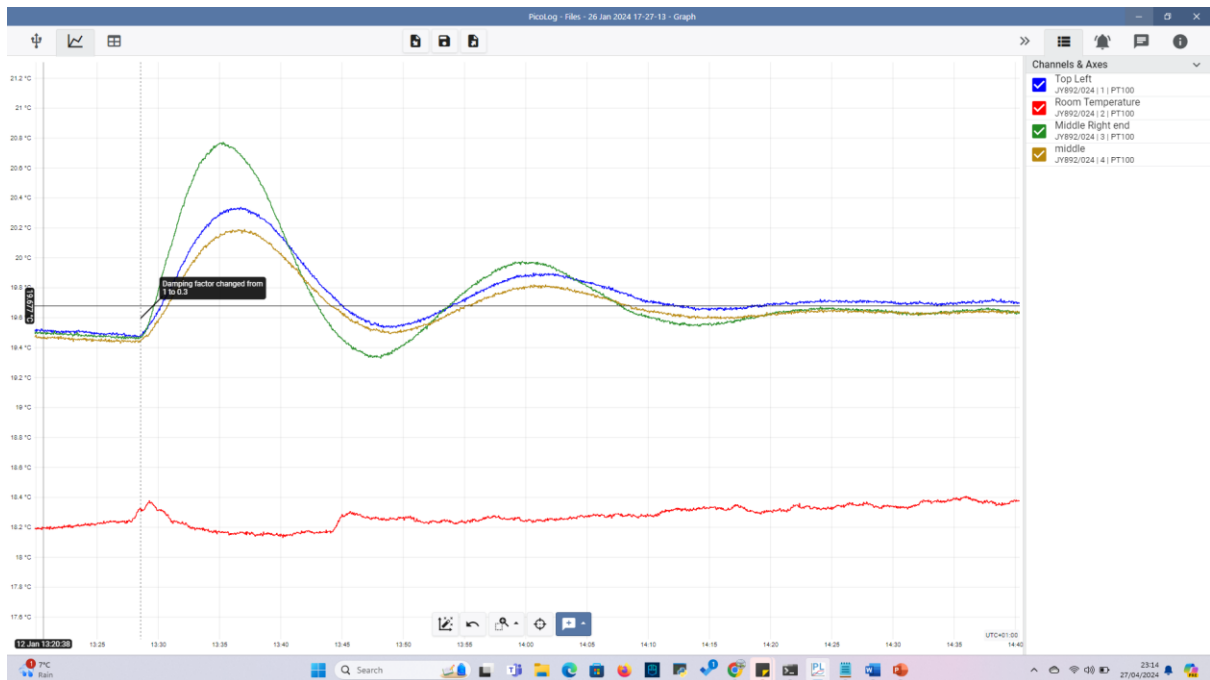


Fig. Plot of PID loop with damping factor 1 to 0.3, shows takes about 1hr to reach the constant desired set point temperature. Software – Picolog

D. Web Development

An effective way to keep an eye on spectrographs and manage sensors from anywhere is through remote access. Instant control is made possible by this feature, giving consumers the power to instantly optimise system performance. The web interface is made using python, javascript, HTML and CSS, currently under development. Quick adjustments are made easier by the web-based interface, which increases the system's overall robustness and adaptability to a range of difficulties. Users can effectively manage and adjust system parameters to meet unique needs with the flexibility of remote access, guaranteeing smooth operations and responsive control. There will be function which will allow user to choose between sensors and get particular reading, also allows to look at the present status of the system.

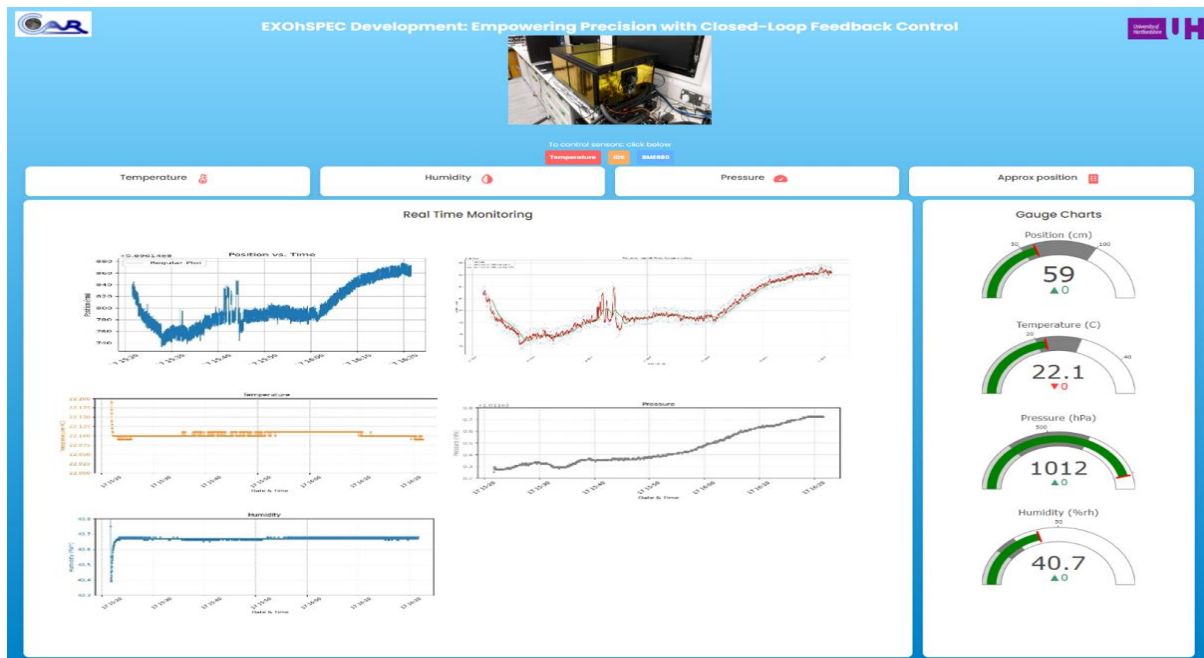


Fig: Real-time Monitoring Web Interface for Spectrograph Functionality and Sensor Control.